INTERNAL REPORT
HIP – 2006 – 09

ISBN 952-10-2962-5
ISSN 1455-0563
Espoo 2006

HELSINKI INSTITUTE OF PHYSICS

Emma Terämä: Transport Phenomena of Polar Biomolecules and Colloids, Perspectives Through Simulation 2006

Emma Terämä
Laboratory of Physics and Helsinki Institute of Physics,
Helsinki University of Technology, Espoo, Finland

Transport Phenomena of Polar Biomolecules and Colloids, Perspectives Through Simulation

Emma Marjut Terämä
* 26.12.1978

She was born in Helsinki, Finland where she has spent the most time so far. Her schooling started at Paradise Elementary in Las Vegas, NV in 1985. She received her secondary school IB-diploma from Helsingin suomalainen yhteiskoulu in 1997. The same year she started her studies towards a MSc degree at the University of Helsinki Theoretical Physics Department. In 1999 she studied as an Erasmus-scholar at the Freie Universität, Berlin and completed the degree in Helsinki in 2001. In the year 2000 she started working at Helsinki University of Technology (TKK) as a summer student.

Ever since she has worked towards the PhD degree, culminating in this manuscript. She spent the summer as a visiting scholar at UC Davis in 2004, and got married in the fall. In 2005 she was on maternity leave for six months and soon thereafter completed the Licentiate of Science degree in Technology.

HELSINKI INSTITUTE OF PHYSICS
INTERNAL REPORT

HIP – 2006 – 09

TRANSPORT PHENOMENA OF POLAR BIOMOLECULES AND COLLOIDS, PERSPECTIVES THROUGH SIMULATION

Emma Terämä

Laboratory of Physics and Helsinki Institute of Physics,
Helsinki University of Technology, Espoo, Finland

Academic Dissertation

Dissertation for the degree of Doctor of Science in Technology to be presented with due permission of the Department of Engineering Physics and Mathematics for public examination and debate in Auditorium E at Helsinki University of Technology on Jan 3rd, 2007 at noon.

ISBN 952-10-2962-5
ISBN 952-10-2963-3 (pdf)
ISSN 1455-0563
URL http://lib.tkk.fi/Diss/list.html#2007

To my family, Ville and Amos,
who provide the ultimate inspiration.

Abstract

The thesis focuses on the transport of polar biomolecules and colloid particles studied through atomistic and coarse-grained simulation techniques. The thesis is comprised of two themes complementing one another. First we concentrate on the structural and dynamical aspects of alcohol molecules in lipid bilayers with varying degree of unsaturation. Second, the thesis employs dielectrophoresis to elucidate the non-equilibrium transport phenomena of nano-sized colloidal particles. The former is an example of simulating a molecular system at the atomic level, providing insight into the mechanism of anesthetics such as alcohols. The latter topic exemplifies the more coarse grained approach of describing surface polarization effects of a colloid coupled to a varying external electric field and subsequent transport of the colloid.

In water solution the lipids self-organize into bilayer structures depicting biological membranes. The effect of ethanol and methanol solvents on the lipid bilayer structure and dynamics was investigated. Simulations show ethanol transport into and through the bilayer, results indicating an undisputable effect of alcohols, esp. ethanol, on membrane properties. Hydrogen bonding between lipid and alcohol molecules is observed, and lipid bilayer pressure profile changes due to alcohol are obtained.

For dielectrophoresis, novel computational models for the transport of (nano-sized) colloidal particles in non-homogeneous electric fields are developed. The model's coupling strength depends on field strength, colloid charge magnitude and charge distribution, which in real life also affect the general characteristics of (surface) conductivity and permittivity that evoke dielectrophoretic behavior of e.g. cells. The colloids in simulation are shown to be affected by their medium via Brownian motion and hydrodynamics. It is demonstrated that aggregation of nano-sized colloids can enhance their transport.

Preface

The work described in this thesis was carried out at the Helsinki University of Technology (TKK) Biological Physics and Soft Matter group led by Prof. Ilpo Vattulainen. The Laboratory of Physics (TKK) and Helsinki Institute of Physics (University of Helsinki) provided the main financial support. Excellent work conditions were provided by COMP and prof. Risto Nieminen, and supercomputing resources mainly by CSC. I would also like to thank the Magnus Ehrnrooth, Emil Aaltonen, Heikki and Hilma Honkanen, TES and Väisälä foundations for financially supporting the research and various trips abroad to conferences, summer schools and research visits.

I would like to thank the (theoretical physics) professors Keijo Kajantie and Jouni Niskanen at the University of Helsinki for scientific guidance and for enabling the inspiring Erasmus-student exchange to Freie Universität, Berlin in 1999. There I got the spark to start learning biophysics. Next in line are professors Tapio Ala-Nissilä and Matti Alatalo who interviewed me for a science summer job at the Laboratory of Physics, TKK, and accepted me to start working with the physics of foams and bubbles in the year 2000. Right after my graduation (MSc) in September 2001 Ilpo Vattulainen joined the TKK crowd starting novel research projects in computational biophysics. In this group I started work on the long and winding project called "my PhD". At this time many thanks are devoted to Ilpo, now professor at the Tampere University of Technology, and Mikko Karttunen, the biogroup leader at the Laboratory of Computational Engineerig, currently professor at the University of Western Ontario.

Support from the family and help with little Amos is sincerely appreciated: Anne Frank, Juha-Matti and Riitta Terämä, Kirsti Litja; friends for life: Amos' god-fathers; all the support in the world: Ville Terämä.

Figures of POPC, SM and cholesterol space-filling and molecular representations were provided by Jussi Aittoniemi and Perttu Niemelä.

Schematic representations and visual layout are the courtesy of Ville Terämä. Co-authors and office mates are acknowledged with grateful thanks. All of the friends of Ville and I attending our parties and get-togethers: many thank-yous are in place for providing me with life outside the office, delightful converstations and motivation on the path to the bright future.

At our home in Hakaniemi,
6 December, 2006

Abbreviations

AC – alternating current
DNA – deoxyribonucleic acid
DEP – dielectrophoresis
DSC – differential scanning calorimetry
DMPC – 1,2-dimyristoylphosphatidylcholine
DOPC – 1,2-dioleoylphosphatidylcholine
DPPC – 1,2-dipalmitoylphosphatidylcholine
DID – dipole–induced dipole
DC – direct current
ER – endoplasmic reticulum
GA – general anesthesia
HOESY – heteronuclear Overhauser enhancement spectroscopy
NOESY – homonuclear Overhauser enhancement spectroscopy
ITC – isothermal titration calorimetry
MAS – magic-angle spinning
MD – molecular dynamics
MAC – monitored anesthesia care
NMR – nuclear magnetic resonance
PDPC – 1-palmitoyl-docosahexaenoylphosphatidylcholine
POPC – 1-palmitoyl-2-oleoylphosphatidylcholine
PME – particle mesh Ewald
PBC – periodic boundary conditions
RDF – radial distribution function
SM – sphingomyelin
SOPC – 1-stearoyl-2-oleoylphosphatidylcholine
μTAS – micrototal analysis system

Table of Contents

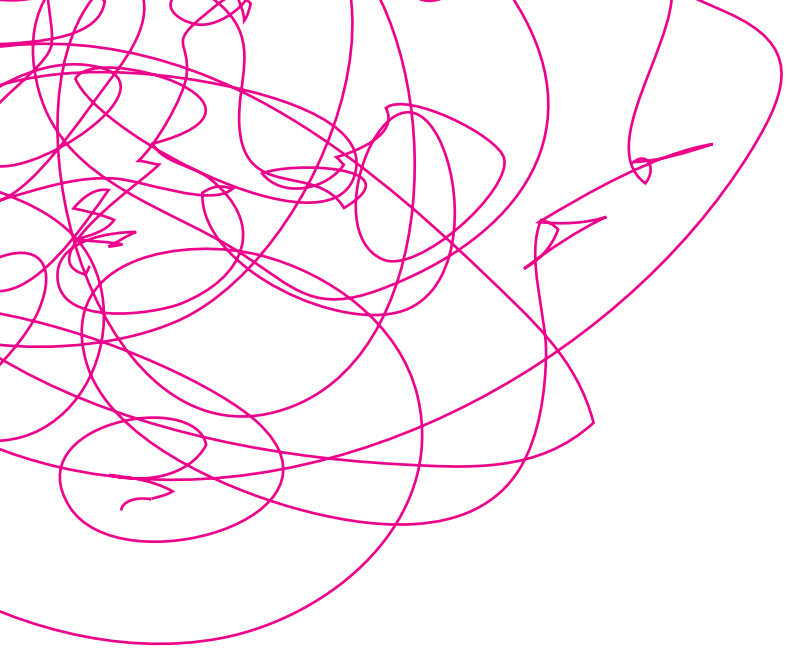

Outline

I would like to start this thesis by outlining the two main research topics. The fact that there are two is also the fundamental reason for deciding to describe them in a monograph-type manuscript instead of a combination of articles and a summary. Also, I find the monograph to bear closer resemblance to how I view the thesis: An ending of a PhD project that is to manifest the candidate's views and understanding of the underlying phenomena of her research, in addition to describing the novel scientific results and thorough explanations of the conclusions arrived at.

Common to the two research topics are the words in the title of this work, namely *transport* and *polar*. A setting comprising these both is the biological cell sketched in Fig. 1. The cell is an exemplar softmatter system that has abundant topics for a biophysicist to investigate. One of the cell's main organelles is its membrane. The membrane is important not only in function but also as a component largely determining the whole cell's response to outside stimuli such as electric
fields.

If we consider first the entire cell and appreciate it being a macroscopic object, its response to a hypothetical electric field would be given by its surface conductivity and permittivity. These are complex quantities that originate from explicit interactions of the surface elements; charges and partial charges, as well as their coupling to the external field. However, the gross behavior of the cell is what matters in life, and sometimes in experiments mimicking life. On the microscopic scale we can distinguish the detailed molecular structure of the membrane including lipids and proteins. The size, shape and electric characteristics of the membrane depend in the end on the molecular arrangement of the membrane constituents. Therefore it is intriguing to investigate the molecular interactions that can affect the structure of this complex cell boundary and subsequently the whole cell's electrical characteristics.

Figure 1. The cell.

The aim of this thesis is on one hand to better understand the complicated interplay of solutes and membranes, and on the other to investigate the properties of colloidal particles in external electric fields. Anesthesia and the fermentation process motivated the molecular dynamics study of alcohol and lipid membrane interactions studied first. The widely used experimental technique of dielectrophoresis provided the framework for the second computational study. The transport phenomena considered in both parts take place in a highly non-equilibrium state which provides a good challenge for any scientist. Part I contains four chapters. They describe the main aspects of the biological membrane and its interactions with the solute alcohol. An overview of the lipid bilayer structure and main research developments is given in Chapter 1. Chapter 2 is about the motivation to the research. The background for the research is explained with reference to anesthesia, and the molecular structure and functional importance of alcohols. Chapter 3 is concerned with techniques in membrane research. An overview of the experimental and computational methods that contribute to the study of membrane properties and interactions with solutes is given. Experimental high-lights are mentioned where appropriate, while the focus is on providing the reader with the background to the computational technique of molecular dynamics. Results of the computational study are given together with analysis in
Chapter 4.

The second part of the thesis comprises three chapters that describe work done on colloidal particles in external fields. The simulation method is Molecular Dynamics employed at a coarse-grained level (cf. atomistic MD). Chapter 5 gives an introduction into the topic of electromechanics and colloids. A more theoretical description can be found in Chapter 6. Detailed computational studies of nanoscale monomer and dimer transport are described in Chapter 7. Part II is thus concerned with a more approximative picture of the cell boundary whilst Part I describes the detailed structure of the membrane and its molecular interactions with solute particles. The last chapter concludes both Part I and Part II.

Part I

Chapter 1

Lipid Membranes

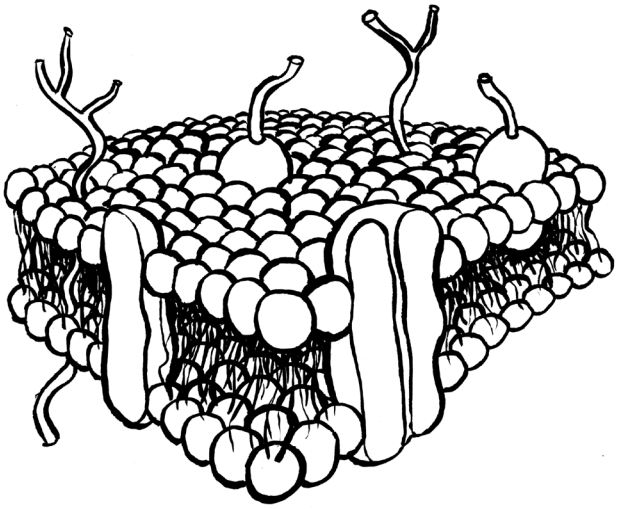

Figure 1.1. Schematic representation of the lipid membrane.

1.1 Introduction

The lipid bilayer, Fig. 1.1, is a structure persistent in all living animal cells. Cells use various lipid species to build these area dividing and function protecting structures. The bilayer enables cells to perform their vital functions, generate important products and transform substances into energy needed for transport and various other processes. In the process of cell division, the bilayer is particularly active. Substances produced inside cells are carried to other parts of the organ or body once they are securely manufactured inside this protective environment. This environment is kept separate from the surroundings by the biological membrane. For reviews on the topic, see references [1–7].

1.2 Models in time

The lipid-bilayer membrane was discovered by Gorter and Grendel in 1925. They were able to extract the area occupied by lipids in a known number of mammalian erythrocytes and concluded that these *fatty substances* covered the cells in a two molecule thick layer – the lipid bilayer [3]. However, their experiments were proven faulty and when corrected (in 1966), it was found that the amount of lipid was sufficient to span the area of the cell only in a monolayer configuration, or as a bilayer covering roughly half of the cell surface [8].

Already in 1959 the first arguments were heard in favor of a unified bilayer theory that all cell-organelle membranes had a common structure. From thereon it was the fluid mosaic model that gained strength. The bilayer lipids were shown through magnetic resonance methods to be flexing and diffusing in the plane of the membrane, that is, in constant motion [3]. Therefore it was concluded that the structure resembled more closely a fluid than a solid. An early version of the lipid-protein mosaic model was published in 1966 based on thermodynamic considerations of not only lipids but also proteins interacting in solution [8]. Proteins also took up space thus contributing to the overall area comprising the cell membrane.

The lipid-protein mosaic model was extended in 1970-1971 by Singer. He together with Nicolson produced the famous *Science* paper in 1972 which made the crucial distinction between integral and peripheral membrane proteins [9]. Proteins that are anchored in the plasma membrane of the cell are called integral membrane proteins. Proteins associated noncovalently, e.g. through hydrogen bonds with integral membrane proteins, are called peripheral membrane proteins. The model was designed to be thermodynamically feasible through maximizing hydrophobic and hydrophilic interactions [8]. The hydrophobic amino acid residues of the integral proteins are embedded in the bilayer hydrophobic core, and the polar, non-ionizable residues distributed between exterior and interior domains. The ionizable residues are essentially all in contact with water on the exterior, non-membrane embedded domains, and the ionic and polar moieties of the phospholipids are exposed to water on both sides of the membrane.

The lipid bilayer was now a pseudo two-dimensional liquid where both lipids and membrane associated proteins displayed a tendency towards lateral mobility [10]. This realization portrays quite well the currently accepted model for the biological membrane.

The section on membrane models would not be complete without considering rafts. The lipid raft hypothesis was proposed by Simons and Ikonen in 1997 [11]. Cholesterol plays an active role in this model, creating functional domains in cell membranes with sphingolipids and, to a lesser extent,

glycerophospholipids. These domains depict greater lateral ordering than the surrounding medium, and comes as no surprise that the raft regions have been proposed to form a liquid ordered phase while the neighboring domains with higher glycerophospholipid concentrations are in (less ordered) liquid disordered phase [2, 11]. The nature of the fore-mentioned phases is discussed in more detail in Sec. 1.5. Lipid rafts thus provide a mechanism for the lateral segregation of membrane components. The size of the rafts seems to vary a great deal, and there is an ongoing debate about the lifetime of these structures, which indicate that the field of study is still in its infancy.

The accompanying vesicle picture represents a lipid extract of lung surfactant including the protein SP-B and cholesterol. The liposome is approx. 40μm in diameter.[1] It is commonly considered that the ordered microstructures, rafts, serve as platforms for the attachment of proteins.

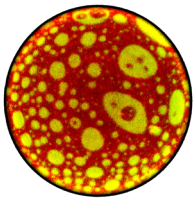

The intermolecular interactions of the membrane lipids with surrounding molecules involve peripheral as well as integral proteins [10]. Through proteins, rafts or membrane domains can function in various cellular processes (see next section). The incorporation of proteins in the raft domains brings forth another level of complexity in both structure and function of the biological membrane.

1.3 Biological function

Biological membranes entertain a plethora of lipids. The membranes in the brain and the eyes, for example, hold several lipids with four to six double bonds in one of the acyl chains. In fact most of the lipids in the membranes of these organs contain some number of double bonds. The surfactants in the lungs, then again, contain a high amount of fully saturated DPPC lipids with no double bonds. Table 1.1, modified from [1], summarizes the composition percentage of different phospholipids as well as cholesterol in different plasma and subcellular membranes.

Difference in composition can often be linked to functionality. Eucaryotic plasma membranes contain in addition to phospholipids an especially large amout of cholesterol, roughly 30% of the total lipid mass. Cholesterol is a steroid lipid with a fundamental ring system comprising of the perhydrogenated form of cyclopentanophenanthrene. The cholesterol molecules act to enhance the properties of the bilayer as a permeability barrier. Thus the composition is ideal for the plasma membrane whose function is first to provide a flexible yet stable boundary between the cell and its surroundings,

[1] http://scienceinyoureyes.memphys.sdu.dk/ Aug 11, 2006.

and second to regulate substance movement into and out of cells. Bacterial plasma membranes, on the other hand, are often composed of solely one type of phospholipid and no cholesterol. The mechanical properties of this type of a membrane are further enhanced by an overlying cell wall [12].

The cell organelles mitochondrion and *endoplasmic reticulum* (ER, also called sarcoplasmic reticulum in striated muscle) contain large membrane surfaces.

	Percentage of phospholipids					
	PC	PE	PS	SM	Phospholipids*	Cholesterol*
Plasma membrane	39	23	9	16	672	128
Mitochondria	40	35	1	1	175	3
Nuclear membrane	55	13	3	3	500	38
Sarcoplasmic reticulum	73	14	1	1	603	12

*µg/mg protein

PC = phosphatidylcholine
PE = phosphatidylethanolamine
PS = phosphatidylserine

Table 1.1. Lipid composition in some vital cell structures.

The composition of these membranes is very different from the regular plasma membrane depicted above. One indication of this is that they contain minute amounts of cholesterol. They also serve very specific functions in the cell, most of those functions taking place on their membranes. The ER is the site of production of most eucaryotic cell membranes. It is here that certain phospholipid translocators act in order to produce the specific phospholipid asymmetry of a membrane.

The human red blood cell is an example of such phospholipid asymmetry. It contains most of its choline head group containing lipids in the outer leaflet, and the negatively charged phosphatidylserine on the inside [12]. Thus, there is a major charge difference between the two halves of the red blood cell bilayer. One assumption is that certain membrane bound proteins require specific lipid headgroups in order to function. The detailed function of integral and peripheral proteins, however, is beyond the scope of this work. It can be stated that a significant function of the lipid bilayer is to accommodate these proteins.

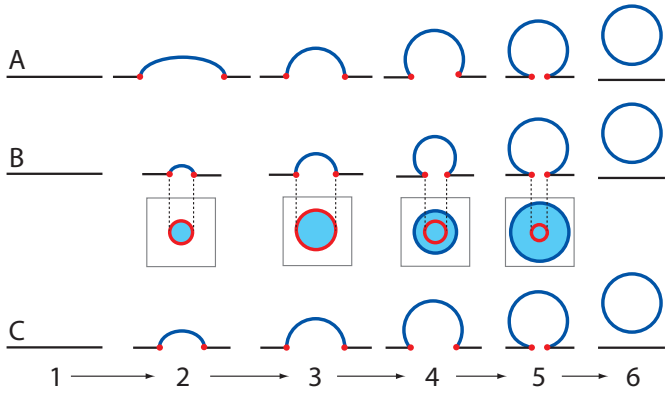

Figure 1.2. Three models for the budding of a presynaptic plasma membrane according to [13].

In accommodating proteins of different function, the lipid raft formation plays a key role. In forming differently composed domains at membrane outer leaflets, the lipids provide suitable environments for the attachment of various kinds of proteins. Rafts are thus expected to be involved in e.g. protein sorting, cell signalling, apoptosis and substance recognition [2, 5, 11, 14].

Biological membranes are actively participating in the life of a cell. Movement, division, the extension of neuronal arbors and vesicle trafficking are forms of cell activity involving membrane transformation. With the correct external or internal stimulus the membrane can fuse, bud or simply change its local curvature to accommodate the needs of the cell (see Fig. 1.2, modified from [13]). Subdomains of the membrane with their given curvature have been linked to precise biological functions. Regions in membranes may include specific proteins working together to promote membrane bending and nascent vesicle formation [15]. In endo– and exocytosis in general the membrane responds to a recognized transportable molecule by changing local curvature and allowing intermolecular interactions with the bilayer lipids to facilitate the transporting of the agent to the other side. Such processes are also accompanied by changes in the pressure profile across the membrane, which will be discussed later.

1.4 Chemical structure and composition

The membrane structure is most unique in that it does not merely exist as a physical barrier between cells, but serves as a two-dimensional matrix for a plethora of reactions and processes. These include ion transport, antigen–antibody binding and reduction–oxidation reactions, among others [16]. Because of these complex functions, it is not surprising that the biological membrane consists of many distinctly different classes of lipids, namely glycerophospholipids, sphingolipids and sterols, see Figs. 1.3– 1.5.

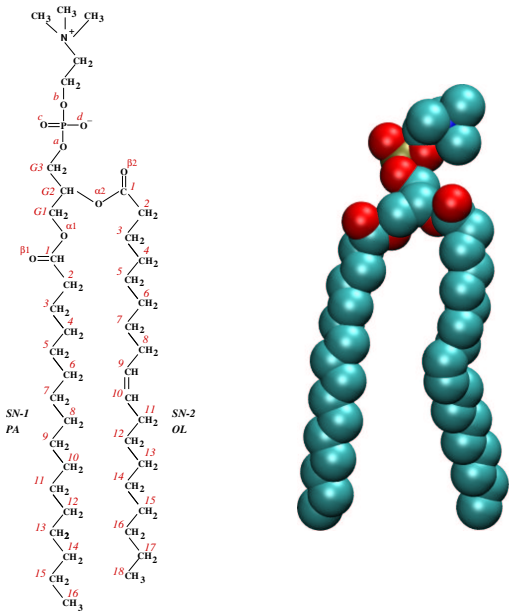

Figure 1.3. Palmitoyl-oleoyl phosphatidylcholine (POPC) structure.

A remarkable feature of membranes is the enormous diversity of lipids constituting them. The versatility of lipid species ranges from differences in the amount of double/single bonds, the length of the hydrocarbon chains, the difference in the *sn-1* vs. *sn-2* chains and the varying of the head group itself. Considering these possibilities we get a total amount of different lipids close to 1000. The most commonly found lipids in the biological membrane are glycerophospholipids with usually two fatty acids esterified in the *sn-1* and *sn-2* positions of the glycerol moiety. The aliphatic chains are saturated when they include only single bonds (e.g. *dipalmitoylphosphatidylcholine*, DPPC), or unsaturated when a single or multiple double bonds are included (e.g. monounsaturated *palmitoyloleoylphosphatidylcholine*, POPC).

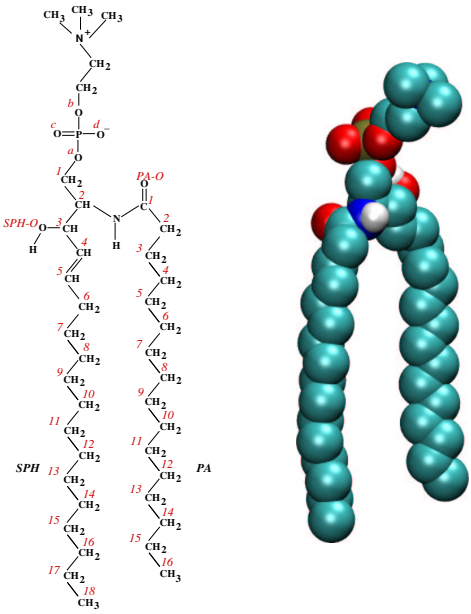

Figure 1.4. Sphingomyelin (SM) structure.

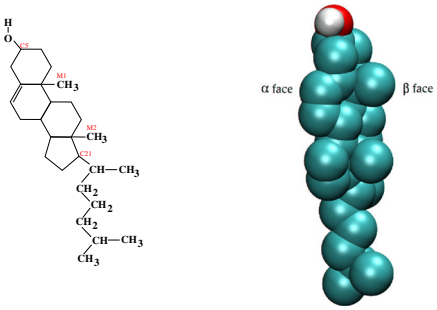

Figure 1.5. Cholesterol structure.

In addition to lipids, membranes include a variety of proteins and carbohydrates. Measured by weight, the ratio between membraneassociated proteins to lipids varies from about 1 to 3 [8], carbohydrates contributing in addition approximately 10 percent [1]. Some proteins are connected to the membrane only through electrostatic interactions. Mere environmental changes in pH, ionic strength or buffer composition may cause these proteins to be dislocated from the bilayer. Thus the protein–lipid weight ratio is susceptible to large fluctuations.

The composition of the bilayer also changes with function. Different organelles in the body have different membrane compositions ranging from

different lipid species to difference in protein and carbohydrate content. Myelin, for example shows a marked difference to the general membrane composition with protein to lipid ratio at only 0.23 [8]. This represents myelin's function, since it acts more like an insulating than a conducting medium. Hauser and Poupart describe lipid variation with respect to membrane type in a recently published book [1].

1.5 Phase behavior

To start a more detailed discussion on the biological membrane let us begin with considering how this self-assembling structure depends on temperature and the species comprising it. The two main phases of one-component bilayers are the gel, and liquid disordered phases schematically represented in Fig. 1.6 and 1.7 respectively. An index to currently available temperature–composition phase diagrams is given in [17]. The reader is invited to view this source for detailed information on few- as well as multi-component membrane phase behavior.

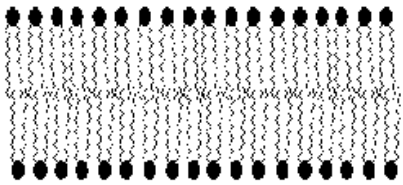

Figure 1.6. Lipids in gel state.

Figure 1.7. Lipids in liquid disordered state.

1.5.1 One-component membranes

Two phases are known for unilamellar liposomes, the fluid (or liquid disordered, l_d) and the gel (or solid ordered, s_o) phases [2, 6]. These are separated by the main transition temperature, T_m, which varies from one lipid species to another depending on e.g. level of saturation. Essentially all lipids have a different Tm, the value being typically around 300 K.

In the fluid, or liquid disordered phase, the acyl chains of the lipid molecules are only weakly ordered. The same applies to the headgroup translational ordering – it is minimal. The gel phase, on the other hand, involves highly ordered chains. A tilt is common along the length of the chain with respect to the bilayer normal. The surface depicts typically a hexagonal packing of the lipids. In addition, the case of a multilamellar liposome differs from the above in that there also exists the so-called ripple phase between the two fore-mentioned phases at temperatures $T < T_m$ [18].The ripple phase spans from the interactions of two lamellar membranes close to one another. Scanning calorimetric studies [19] have shown for the lipid DPPC three endothermic phase transitions. These are the subtransition at 291 K, pretransition at 308 K and the main phase transition gel to liquid crystal at about 314 K. For POPC the main phase transition temperature T_m is 268 K [20].

1.5.2 Two-component membranes

A two-component membrane system is best described through an example. Let us consider first the pure DPPC bilayer in more detail. At low temperatures these systems are in the gel phase characterized by all-trans hydrocarbon chains and the hexagonal packing of the head groups. At temperatures higher than the transition temperature (DPPC T_m = 314.5 K), the structure is in the liquid state with certain gauche defects to be found in the chain region, and no headgroup ordering. The main phase transition is thus characterized by two simultaneous order-disorder transitions. A translational one in the head group and chain regions, and an additional orientational transition in the chain region. Now adding the effect of another component, e.g. cholesterol, the main effect is the decoupling of these two transitions. A new phase, the liquid ordered, l_o phase will be formed. This phase is characterized by the absence of the head group hexagonal ordering with a prevailing high degree of order in the chain region. There is currently strong agreement that the l_o and l_d domains can coexist [2]. A typical phase diagram of a two-component membrane is shown in Fig. 1.8 (Nota bene: l_d-s_o coexistence region not shown very well).

1.5.3 Multi-component membranes

In addition to several lipid species, bilayers can contain proteins. Proteins bring another variable into bilayer construction and phase behavior. Bilayer structures with multiple components are poorly known to date. Interesting questions to pose are: How do the various components interact and what is the result of the possible interaction on the physical and dynamic properties of the membrane? Some phase diagrams have been introduced recently in literature [2, 22].

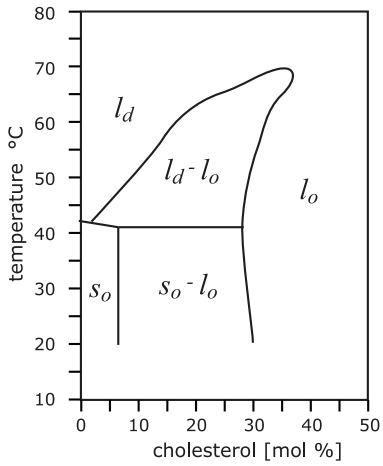

Figure 1.8. Schematic phase diagram of DPPC–cholesterol system [21].

Better understanding of multi-component bilayers will bring us closer to a detailed description of more complex, and thus more realistic biological membranes. Consider a typical mammalian cell membrane with approximately 100 different lipid species each having their own T_m. There simply is no straight-forward way to classify the overall phase transitions of a structure of such complexity. Instead, the local arrangement and domain formation of the lipids can play a crucial role in determining the interesting qualities and dynamic behaviour of the membrane if not actual phase behavior. In the end, the study of lipid rafts attempts to give answers to the above questions (Figure 1.9 by Perttu Niemelä).

1.6 Physical characteristics

Physical consideration of the biological membrane includes determining elastic properties, phase existence and order parameters but also the dynamics, i.e. the motion inherent in the membrane structure. The dynamic degrees of freedom of the lipid molecule are inherently linked to the elasticity of the membrane. Let us first consider the acyl chain moiety of the lipid molecule. The hydrocarbon chains comprise about half of the total bilayer volume and serve as a major structure defining quantity for the whole membrane.

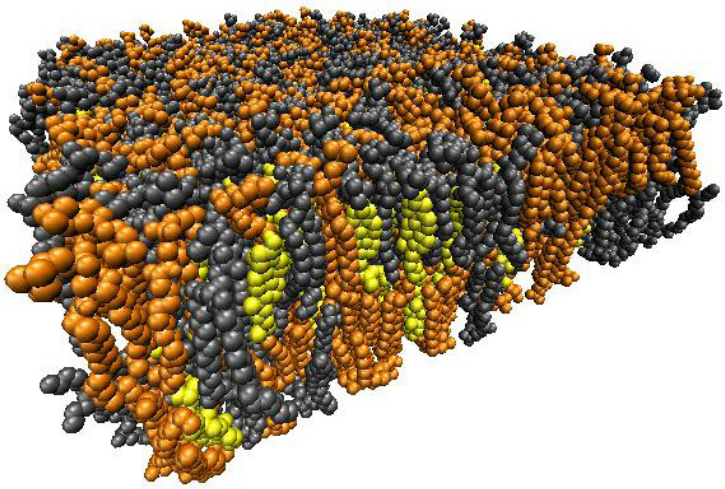

Figure 1.9. MD simulation snapshot of a membrane with lipids SM (orange), PC (gray) and cholesterol (yellow). Water molecules suppressed for clarity.

1.6.1 Lipid order

The first of two principal orderings is the lipid *conformational* order. It is described through the order parameter [23]

$$S_i = \frac{1}{2}(3\cos^2(\theta_i) - 1), \tag{1.1}$$

where θ_i is the angle between the frame of reference, i.e. bilayer normal and a chemical bond labeled i. The convention is that for an instantaneous, immobilized stiff bond the order parameter is highest $S = 1$.

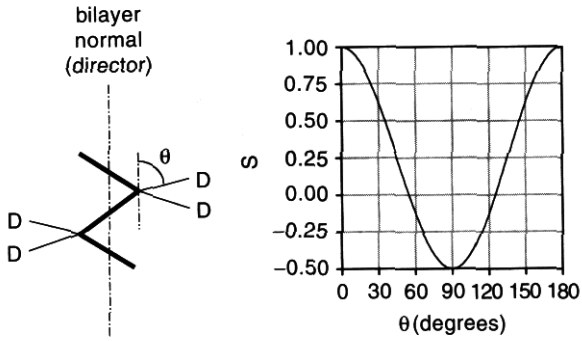

Figure 1.10. Angular dependence of the bond order parameter [23].

Then the deuterium order parameter $S_{CD} = {}^{2}/_{3}S_{xx} + {}^{1}/_{3}S_{yy}$ indicates the average orientation of the C–D bond vector with respect to the bilayer normal with the molecular axes defined as [24] z: vector from C_{n-1} to C_{n+1}, y: vector perpendicular to z and in the plane through C_{n-1}, C_n and C_{n+1} and x: perpendicular to y and z. Measurements of the S_{CD} by nuclear magnetic resonance, ^{2}H NMR have revealed the existence of a distinct order profile for lipid hydrocarbon chains [23, 25, 26]. Chains tend to have higher order near the lipid/water interface due to being anchored to the rigid glycerol headgroup. The methyl end of the flexible hydrocarbon chain is free to move facing the hydrophobic bilayer center.

For saturated chains the order profiles are similar in all model and biomembranes [23]. When fully extended, the acyl chain adopts sp3 hybridized geometry of the CH2 groups, and the angle between successive C–C bonds is approximately 109. This is called the *trans* configuration and results in the chain order parameter $SCD = -0.5$ with C–^{2}H bonds oriented perpendicular to the bilayer normal, cf. Fig. 1.10. The negative sign of S_{CD} is often not quoted because it cannot be determined from the symmetric ^{2}H NMR spectra.

The order parameter is known to reflect properties of the membrane, such as area per lipid, membrane thickness [6] and lateral diffusion [27]. Order parameters are rather routinely determined for lipid molecules by spectroscopic approaches with atomistic resolution. Computation of the order parameter from simulation studies is equally feasible.

Lipid *translational* symmetry is defined in the plane of the membrane. It is the other important component in defining the membrane geometry and lipid ordering. Order on the surface can be compared to two-dimensional solid state systems. Crystal order is characterized through primitive lattice vectors spanning a Bravais lattice [28]. In the case of gel phase lipids, these

vectors depict typically hexagonal ordering, at least over rather long (quasi) scales. The primitive vectors in the 2-D simple hexagonal Bravais configuration are $\mathbf{a}_1 = a\hat{\mathbf{x}}$ and $\mathbf{a}_2 = \frac{a}{2}\hat{\mathbf{x}} + \frac{\sqrt{3}a}{2}\hat{\mathbf{y}}$, where $|\mathbf{a}_1| = |\mathbf{a}_2|$.

1.6.2 Flexible interface

Biological membranes, due to their liquid nature in physiological conditions, are highly deformable with relatively small area compressibility [29]. This area incompressibility is determined by the ratio of the elastic modulus that characterizes area compression and expansion K_a, to the shear modulus. Evans et al. showed already in 1976 that the elastic (area compressibility) modulus to shear modulus ratio was a very large number, proving the membrane to behave in a twodimensional, incompressible manner under shear and elongation [29].

Also thickness compressibility can be obtained from the area expansion elastic modulus. Results show that the bilayer is at least 300-fold less compressible than a gas-like substance but 10 to 100 times more compressible than an ordinary liquid [6]. Membranes can thus be further considered as soft, condensed surfaces, in another word *flexible*.

The elasticity theory for curved surfaces can be applied to the case of membranes through e.g. the introduction of the radius of curvature, R_0, the bending rigidity κ, and the saddle-splay modulus, $\bar{\kappa}$ [30]. For small local curvatures of surface S the free energy can be defined as

$$H = \int dS[\sigma + \lambda_s H + 2\kappa H^2 + \bar{\kappa}K], \tag{1.2}$$

where $H = (c_1 + c_2)/2$ is the mean curvature, and the gaussian curvature is given by $K = c_1 c_2$. Then R_i are the principal radii of curvature with $c_i = 1/R_i$, $i = 1, 2$ [30].

The bending elastic modulus has been predicted to be proportional to molecular area compressibility. For simple elastic models holds $\kappa/K_a \approx d^2/b$, where d is membrane thickness and b a constant depending on the distribution of lateral pressure across the bilayer [6]. In terms of thermal energy $k_B T$, the typical values of these elastomechanical modules for bilayers are around 10 $k_B T$, which is the κ value for DMPC [10]. E. Evans and W. Rawicz give examples of bending, κ and stretching, $\bar{K}$ elastic constants for real membranes around room temperature [31], where $\bar{K}$ stands

for the surface expansion modulus derived through the elastic moduli for bending and direct area expansion. See Table 1.2.

Lipid	$(10^{-19}\ \mathrm{J})$	$\bar{K}(N/m)$
DMPC at 29°C	0.56	0.145
SOPC at 18°C	0.9	0.190

Table 1.2. Elastic moduli of bilayers, modified from [31].

Typical bilayer dynamics involves undulations. The persistence length ξ is defined through the normal-normal correlation function, which becomes decorrelated at ξ due to thermal undulations. For length scales below the persistence length, the membrane is locally flat [32]. Biological membranes are thus very stiff and their persistence length is much larger than any other typical length scale [30].

1.6.3 Describing dynamics

Dynamics of molecules inside the membrane is a challenging subject. Quantifying motion is readily done by parameterizing, e.g. obtaining diffusion coefficients, but what information do we gain from these?

There exists a great variety of lateral diffusion coefficients. Their values range from zero to about $10^{-10}m^2/s$ [33]. Consider a molecule diffusing at a rate of $10\text{-}11m^2/s$ for a period of 10 s, it will have travelled on average a distance of about 20 μm, equalling the diameter of an animal cell. The motion being diffusive, of course means that the molecule will not have travelled that far, but zig-zagged along its way according to the definition of Brownian motion.

A particle of mass m and velocity vx in the x-direction has an average kinetic energy proportional to thermal energy $\langle \frac{1}{2} m v_x^2 \rangle = \frac{1}{2} k_B T$ to spend on both translational and rotational motion [34]. Considering molecular motions inside larger structures or domains and quantifying their typical length and time scales provides us with a means to estimate changes in structure and possible interaction mechanisms.

Flip-flop

The so-called flip-flop is a rare event taking place when a bilayer lipid molecule changes leaflets, i.e. moves from the top bilayer part to the bottom one or vice versa. They are often facilitated by other than lipid molecules in the membrane, such as special integral proteins, flippases [8]. These events are related mainly to the location of socalled *transition state*s of a system [35]. The flip-flop transition of a lipid is accompanied by an increase in potential energy of about 15 kJ/mol [36] casting a barrier for these processes. Indeed, flip-flops are rare events and usually take place with rates of the order of 1 per second or less. The relevant time scale of this process is thus much longer than that of the traditional diffusing, i.e. lateral diffusion along the same leaflet of the membrane. The system makes a collective effort of structural reorganization in order to accommodate the flip-flop. The amount of lipids on each leaflet stays, however, approximately constant, for the flip-flops occur at an approximately steady rate in both directions. The photoreceptor disc membranes in retinal rods [37] and the human erythrocyte membrane are examples of biochemically interesting systems where flip-flop has been observed to take place [36].

Lateral diffusion

The current understanding is that lipids perform two types of translational motion inside the membrane: continuous diffusion and jump diffusion (see e.g. [38]). Simulation studies are expected to bring insight into the two regimes of lipid dynamics. In this study, focus is set on the diffusive regime. The lateral tracer diffusion coefficient is given by

$$D_T = \lim_{t\to\infty} \frac{1}{2dt} \langle [\mathbf{r}(t)]^2 \rangle \tag{1.3}$$

where d is the dimension of the system and $\langle [\mathrm{r}(t)]^2 \rangle$ is the mean squared displacement of the center of mass of a tagged molecule, averaged over all molecules.

Lipid lateral diffusion has been extensively studied in the past [26, 39–42]. It has been suggested that membrane lipid hydrogen bonding and electrostatic interactions are the main modulators of the slow lateral diffusion [26]. Our diffusion analysis results are given in Section 4.3.4.

Rotational diffusion

The amount of kinetic energy a particle has to perform translational motion, it also has to perform rotational motion, if this degree of freedom is not hindered (e.g. by structure). Rotational diffusion gives information

about the available space and possible mechanisms of action of solutes with the membrane. Hydrogen bonding of the headgroups may hinder lipid rotation inside the bilayer. The mere inclusion of solutes in the membrane with or without bonding may cause steric hindrance.

The second rank reorientational autocorrelation function $C_2(t)$ is given by [43]

$$C_2(t) = \frac{1}{2}\langle 3[\mu(t)\cdot\mu(0)]^2 - 1\rangle, \tag{1.4}$$

where μ(t) is a unit vector that defines the chosen rotational mode. Two different rotational modes are relevant for this study. These are obtained through the rotational autocorrelation functions for the lipid P–N vector, and the interfacial vector, i.e. the vector defined by the carbon atoms sn-1 and sn-3 of the lipid head group. The P–N vector is that pointing from the headgroup phosphorous, P to nitrogen, N, see e.g. Fig 1.3.

Typical results are shown in Sec. 4.3.5. Although valuable information has been gathered using this method, it should be noted that the molecules in membranes change their shape in time [33]. Approximating the shape and size of these molecules as fixed cylinders produces a source of error.

Permeation and partitioning

Permeation has relevance from several ordinary cell functions to medically very complex ones [44, 45]. It is a process by which solutes that don't require active transport enter the cell. Thus permeation means the entering or diffusing of a substance, gas, vapor, liquid, or solid through a barrier without physically or chemically affecting it. Many drug molecules, for example, interact directly with cell membranes [46]. A closely related topic is that of partitioning, and this is very relevant to simulation studies, where the surrounding space is limited and permeation, or the passing through of substances is more difficult to examine.

The currently accepted picture of the cell membrane is the distribution of proteins in a lipid matrix with varying concentration and respective phases. Most drug molecules undergo membrane permeation at one time or another. Some enter the target cell solely by passive permeation, without the help of transmembrane proteins. The study of membrane permeability is crucial for developing an understanding of general drug delivery, as passive transportation mechanisms are not well understood.

The study of general anesthetic interactions with membranes serves as a small solute permeation and dynamics study. Permeation and partitioning

of small molecules has been widely investigated both experimentally and computationally [45, 47–53]. Membrane permeability values of short chain alcohols are given for the first time in the micropipette aspiration study of Ly and Longo [54].

Chapter 2

Motivation

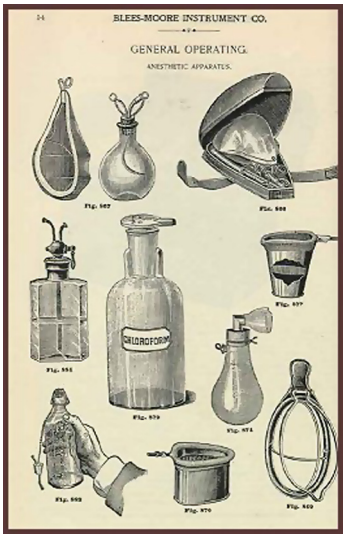

Figure 2.1. Historical anesthetic equipment.[2]

Pain has an element of blank;
It cannot recollect
Where it began, or if there were
A day when it was not.

– Emily Dickinson

2.1 Anesthesia history

As early as the 12th century, mandragora, hashish, opium, alcohol, etc. were used to relieve pain during simple surgical procedures [1]. For some reason, this practice was discontinued during the Middle Ages with the result that many patients died. In 1844 the dentist Horace Wells became the first man to successfully use nitrous oxide as an anesthetic [2]. The problem with nitrous oxide was that its effect was not long enough for lengthy medical operations.

[1] http://www.oyston.com/history/ Aug 11, 2006
[2] http://www.anes.uab.edu/aneshist/aneshist.htm Aug 11, 2006

I also attended on two occasions the operating theatre in the hospital at Edinburgh, and saw two very bad operations, one on a child, but I rushed away before they were completed. Nor did I ever attend again, for hardly any inducement would have been strong enough to make me do so; this being long before the blessed days of chloroform. The two cases fairly haunted me for many a long year.

– Charles Darwin *(1809-1882), Autobiography*

Chloroform was invented in Britain in 1847, a year after the introduction of ether in America [55]. Anesthesia made surgery easier but not necessarily safer. Dr. Morton, former partner of Dr. Wells, was the first to use ether as an anesthetic. The public demonstration took place on October 16th, 1846 at Massachusetts General Hospital. A man was anesthetized by Dr. Morton so that a tumor could be painlessly removed from his jaw-neck area. This marked the beginning of modern anesthesia. Said the patient: "*I did not experience pain at any time, though I knew that the operation was proceeding,*" to which Dr. Warren stated the famous line: "*Gentlemen, this is no humbug*" [3]. The timeline of anesthesia–related inventions with respect to the discovery of the lipid membrane is depicted in Fig. 2.2.

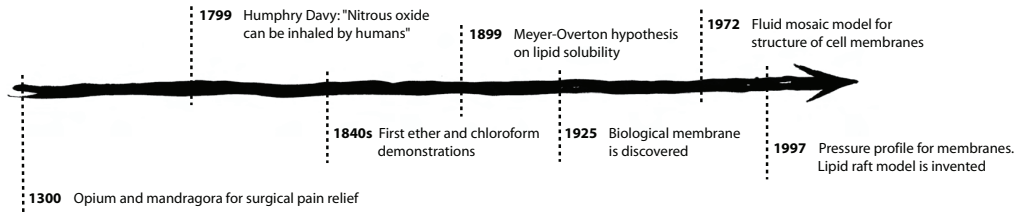

Figure 2.2. Timeline.

2.1.1 Towards general anesthesia

In 1899 the Meyer-Overton hypothesis on lipid solubility was established [56]. This was brought further in 1906 by Meyer's model for anesthetic-lipid action. It stated that the potencies of anesthetic drugs were directly proportional to their lipid solubilities. This is true for the alcohols also. Later

[3] http://www.general-anaesthesia.com/ Aug 11, 2006

Mullins (1954) pointed out that better correlations with potency could be had if molecular volumes were taken into account, i.e. the amount of space taken up by the compound within the membrane [57]. If a compound were taking up space within a membrane, then it would be expected that the volume of the membrane should be greater with the compound than without. Seeman [58] was able to demonstrate this in 1974 with the effect of ethanol on blood cell membranes. Higher concentrations of ethanol would be expected to occupy more space than lower concentrations and have a greater effect, which was observed.

The cell membrane can be conceptualized as a fluid structure in which proteins can move about due to the fluid nature of the surrounding lipid structure. In a fluid membrane one protein can change place with another or move to attach to another, thus facilitating function. Clearly the degree of fluidity of the membrane influences this functioning. Diminishing the fluidity decreases the ability of the proteins to move and interact, while enhancing the fluidity may lead to a disordered mess or a rupture in the membrane structure. In the studies by Chin and Goldstein [59] ethanol was shown to fluidize the membrane thus providing a possible basis for altered protein function.

Anesthetic substances produce a state that can be characterized by the following five requirements: unconsciousness, amnesia, analgesia, immobility or muscle relaxation, and the attenuation of autonomic responses. A whole spectrum of techniques is available today, including Monitored Anesthesia Care (MAC), General Anesthesia (GA), regional anesthesia (spinal, epidural) and nerve blocks among others [60]. People in the medical profession as well as patients require better, more specific and safer anesthetic agents. Research is trying to achieve these standards but also develop anesthetic substances with high potency, that are undamaging, and goes without saying, nonlethal.

2.2 Alcohol

Already the ancient Romans knew how to utilize the physiological effects of alcohol. Bibamus, moriendum est. Let us drink, death is inevitable – goes the Roman aphorism. As we all know, only ethanol produces these desired anesthetic-like effects whereas methanol, for instance, is poisonous if consumed in similar quantities. We ask, what is the difference between these molecules that explains this difference in behavior and what might cause the desired qualities of ethanol? The following sections provide further insight.

2.2.1 Structure and bonding

Hydrocarbons are compounds which contain hydrogen (H) and carbon (C) only. Alcohol is a generic name for a large group of organic chemical compounds that are derivatives of hydrocarbons in which one or more of the hydrogen atoms has been replaced by a hydroxyl –OH functional group. The hydroxyl group imparts particular properties to the radical to which it is attached.

Alcohols are named according to the radical to which the –OH group is attached. For example, if the –OH group is attached to the methyl radical CH_3, the name of the compound CH_3OH is methyl alcohol or methanol. If it is attached to the ethyl (C_2H_5) radical then one has ethyl alcohol or ethanol (CH_3CH_2–OH). The general formula for alcohol is ROH, where R signifies a hydrocarbon radical attached to an –OH group.

The main characteristic of alcohols is the presence of the hydroxyl group –OH. Alcohols can be classified according to the number of hydrocarbon fragments bonded to the –OH group, and this thesis is only concerned with the two simplest members from the group of primary alcohols.

2.2.2 Hydrogen bonding and polarity

The presence of the –OH group gives the molecule special characteristics. The molecule is polar due to the partial charge separation between the hydroxyl oxygen and hydrogen. This holds a significant biological importance, for the polarity of the –OH group makes it possible for the molecule to create hydrogen bonds. For instance, the hydrogen of the –OH group on the alcohol may hydrogen bond to an oxygen of a water molecule or to an oxygen of another alcohol, or any other hydrogen bonding polar species.

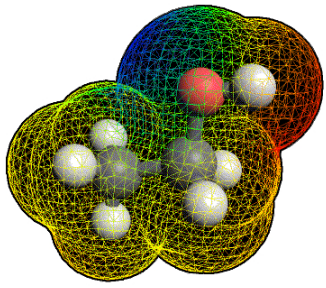

Figure 2.3. Molecular image of ethanol.[4]

[4] http://www.strw.leidenuniv.nl/astrochem/molecules.html Oct 10, 2006

Ethanol (see Fig. 2.3), be it in physiological context, inside a simulation or in an alcoholic beverage, is surrounded by water. Therefore it is of interest to observe characteristics of both water and alcohol. The most studied liquid, water, obtains several of its unique qualities through hydrogen bonding. The hydrogen bond is in part electrostatic and in part covalent, roughly 90%–10% respectively. When a hydrogen bond forms between two water molecules, the redistribution of electrons changes the ability of the molecules to hydrogen bond further. Accepting one hydrogen bond encourages the donation of another, for an accepting water molecule has reduced electron density centered on its hydrogen atoms and its remaining "lone pair" region[5]. Thus water's ability to hydrogen bond is immense, and is not comparable to that of any other polar molecule. This is nicely demonstrated in the difference of the dielectric constant: ~80 for water, 24 for ethanol. Due to its high dielectric constant water also screens electric interactions unlike other solvents.

The centers of positive and negative charge are separated in polar molecules. They possess a dipole moment, meaning that in an applied electric field, the molecules align themselves with the field. The degree to which a substance opposes this alignment is called its dielectric constant or permittivity and, because water is exceptionally cohesive, it has a high dielectric constant. This allows it to act as a solvent for ionic compounds: the attractive electric field between the oppositely charged ions is reduced by about 80-fold due to the water screening, allowing thermal motion to separate the ions into solution.[5] The hydrogen bond network of water thus plays an important role in many properties, such as density, heat capacity, permittivity and water's ability to dissolve compounds [61].

The polarity of ethanol and water are quite close. Polarity can be measured through the dielectric constant or the dipole moment of a compound. For water, the dipole moment in bulk liquid phase is approximately 3.0 D and for ethanol 1.7 D [62]. The polarity of a solvent determines what type of compounds it is able to dissolve and with what other solvents or liquid compounds it is miscible with. Polar solvents can be further subdivided into polar protic and polar aprotic solvents. Water and ethanol both belong to the class of polar protic solvents, which in chemical reactions favor the use of the $SN1$ reaction mechanism [63].

[5] http://www.lsbu.ac.uk/water/ Aug 8, 2006

2.2.3 Commercial importance

The two simplest alcohols, methanol and ethanol, have the greatest commercial importance. Both are widely used as solvents in industry. Methanol is also used as a starting material for the synthesis of acetic acid, adhesives, fibers and plastics. It is produced through hydrogenation of carbon monoxide

$$CO + 2H_2 \longrightarrow CH_3OH \tag{2.1}$$

in the presence of ZnO/Cr_2O_3 catalyst and high temperature (400 °C) [64].

The commercial use of ethanol is more widely known. It is perhaps best known as the end product of fermentation of glucose in the presence of yeast

$$C_6H_{12}O_6 \longrightarrow 2CH_3CH_2OH + 2CO_2, \tag{2.2}$$

producing ethanol alcohol. The reaction is catalysed by the enzymes in yeast. Once the fermentation mixture reaches an alcohol content of about 13 Vol-% the yeast is no longer viable. Further production may involve distillation.

There cannot be enough snacks,
There can only be not enough vodka.
There can be no silly jokes,
There can only be not enough vodka.
There can be no ugly women,
There can only be not enough vodka.
There cannot be too much vodka,
There can only be not enough vodka.

– Russian saying

Distillation also produces vodka and other hard spirits. Mendeleev (1834–1907) discovered in the late 19th Century that combining volumes of water and alcohol, the resulting mixture is of less volume than the initial two put together. Alcohol is aggregated due to molecular interactions. Measured by weight, Mendeleev discovered that one molecule of ethyl alcohol diluted with two molecules of water gives an ideal mixing ratio of roughly 40 percent [65]. He was awarded his doctorate for the dissertation titled *On the Combinations of Water with Alcohol.*

Both ethanol and methanol can be used in internal combustion engines of vehicles. Grain-derived fuels, such as these, are a popular concept because they do not deplete the world's oil reserves. At present, ethanol is added to traditional gasoline to produce gasohol. It is also predicted that in the future, ethanol could be a means of adding hydrogen to a storage tank to power the fuel cell that will, hopefully, replace the currently used combustion engines [66].

2.2.4 Specific action

The specific action that raised our interest in ethanol is its ability to create anesthesia. Ethanol is well known as an intoxicating substance. Save for the long-term effects or hang-over, which are a result of slightly toxic metabolism byproducts, there is evidence of ethanol action as an anesthetic that could provide useful knowledge on anesthetic and small solute action in general. Ethanol and other alcohols influence the membranes surrounding certain cells in the body and thus cause changes in brain and other organ function.

Low molecular weight alcohols such as methanol and ethanol mix freely with water. This is due to the two nearly equal-size moieties, namely –OH, and C_2H_5 in ethanol. The solutions, however, are microheterogeneous, which could also account for their preferential alignment inside membranes.

In dilute alcohol aqueous solution, studies have shown that hydrophobic hydration induces a surface excess of alcohol at the air-water interface [67]. (Hydrophobic hydration is the increased ordering of liquid water around a hydrophobic solute particle.) The alcohols tend to form linear hydrogen-bonded chains, increasingly so with increasing alcohol hydrophobicity, that is, increasing the length of the hydrocarbon chain on the alcohol. Water, on the other hand, forms tetrahedral clusters [68]. The hydrogen bonded chains are seen in both methanol– and ethanol–water systems [68]. In line with their hydrophobic nature (hydrocarbon moiety), the alcohols preferentially occupy surface sites, up to maximum values equivalent to about a monolayer [67]. Comparing to our simulations [69, 70] this seems like a logical explanation to why both ethanol and methanol are witnessed to align right below the lipid headgroups despite their different physiological effect. Both molecule types simply prefer the lipid-water interface to the bulk-like solvent outside the membrane where water forms its typical strong hydrogen bond network.

At higher alcohol concentrations (molar $[alcohol] : [water] > 0.1$),

microaggregation of alcohol occurs and the bulk solution starts to loose ideality. The aggregate solute molecules destroy water's elaborate hydrogen bond network and the molecular interactions in bulk decrease [67]. Consequently, the surface excess of solute decreases as alcohol concentration in the bulk increases. In simulations this could be manifested as more alcohol in water after "monolayer" is formed at the lipid-water interface. However, molecular interactions in simulated water are not as strong as in real life. Recent studies have also suggested that with a small hydrophobic molecule, the water ordering due to the hydrophobic hydration may not be significant [71]. Clearly the final word on this issue has yet to be spoken.

The affinity of ethanol for both water and fat is a result of its hydrogen bonding ability and alkyl group. This dual affinity manifests itself in the presence of membranes and water as alcohol's preference to align itself at the interface of the two. This particular tendency to attach itself right below the lipid head-groups is supported by several studies and is suggested to alter the fluidity of the membrane. This in turn changes the ability of other constituents of the membranes such as proteins, to function properly. These modifications may influence overall cellular function in the brain and body, and eventually lead to the various manifestations of alcohol action.

The polarity of ethanol and its ability to make hydrogen bonds proves to be a means of interacting with the lipid bilayer. Hydrogen bonding and polarity also enable solubility in water which makes it an interesting player in the biological context. Details about the mechanism of anesthetic action are mostly unknown. Through consideration of the dynamics of these molecules in the lipid bilayer mainframe we wish to create some hypotheses and further discussion.

2.2.5 Alcohol affects membrane lipids and proteins

Fermentation is an example of a natural process where the system comprises alcohol and living cells. In normal fermentation as the ethanol concentration rises, the yeast cells experience decreased nutrient uptake, inhibition of cell growth, loss of cell viability and otherwise impaired fermentation performance [72]. It can be said, in other words, that the yeast cells become intoxicated, and as a result the fermentation process is halted. The site for this ethanol toxicity in yeast has been proposed to be the plasma membrane, i.e. the interaction site of alcohol and lipid molecules.

Other toxic effects of ethanol have been observed in mice: Chronic exposure of mice to ethanol reduces the ability of ethanol to fluidize membranes [59]. This data therefore suggests a mechanism accounting for toler-

ance: Ethanol molecules have on one hand a specific effect on the cell/organism, but on the other this function depends on saturation, i.e. too much ethanol will cause negative feedback in the cell.

The cell/organism becomes tolerant to ethanol intake. If the levels are toxic, the object dies, as is the case with yeast cells.

Alcohols have been shown to interact with the hydrophobic regions of proteins [73]. In integral membrane proteins these are the regions embedded inside the membrane close to the carbohydrate chains of the lipids. Protein side chain mobility was enhanced by ethanol in a study by Abadji and coworkers [74]. Also the protein conformation itself is subject to influence: Ethanol changes membrane protein conformation through dehydration [75]. In a study by Cartwright et al. ethanol inhibited non-competitively the protein ATPase activity in plasma membranes. The data indicate that inhibition of plasma-membrane ATPase activity by ethanol could account for the inhibition of glycine accumulation by ethanol [76]. This is an example of ethanol affecting the membrane through specific sites / specific binding to proteins.

An example of indirect or nonspecific influence is given by K. Tu et al. who observe subtle structural changes in membranes with halothane, but discover no evidence for preferential orientation of the halothane molecules [77]. L. Koubi et al. also study halothane and this time note preferred positioning in upper parts of lipid acyl chains [78]. The following year they are not able to observe membrane potential changes associated to the addition of non-immobilizer, in contrast to the halothane case [79]. In 1997 Ho and Stubbs receive fluorescence spectroscopy evidence of ethanol participating in the interlipid hydrogen bond network [80]. S. E. Feller et al. in 2002 support this with their findings, that ethanol interacts with POPC lipid primarily via hydrophilic interactions [81].

Starting in 1997, Cantor comes up with an interesting hypothesis: Anesthetics induce changes in the lateral pressure profile. This affects the embedded protein conformation and thus influences protein function. A protein favors a closed state conformational equilibrium [82–84]. This is depicted schematically in Fig. 2.4, where h is the membrane thickness in z-dimension and $A(z)$ depicts the protein cross-sectional area as a function of z.

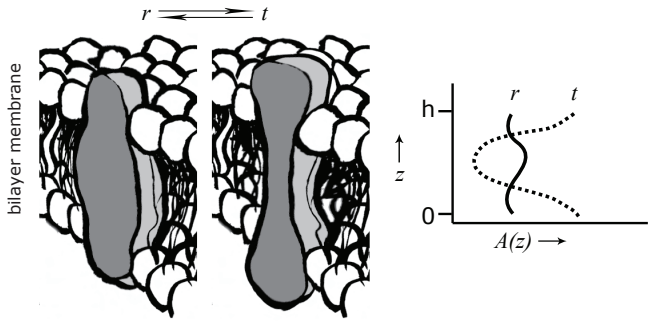

Figure 2.4. An intrinsic membrane protein in two conformational states, r and t.

Changes in membrane pressure profiles in response to addition of alcohol are thoroughly discussed in Section 4.3.7.

To summarize, the proposed effects of small solutes on the biological membrane are:

1. **Direct influence on membrane channel functions** [85]
2. **Specific binding to membrane receptors** [76, 86]
3. **Specific sites of interaction at lipid/protein interface** [76]
4. **Indirect or nonspecific influence** [77]
5. **Membrane partitioning** [78]
6. **Changes in membrane dipole potential** [79]
7. **Changes in lateral pressure profile** [82]

In conclusion it can be said that ethanol interacts with the lipid–water interface in many ways. In the presence of alcohol, membranes seem to become more fluid-like and permeable to small solutes. Ethanol can penetrate through the lipid network of the biological membrane, and interact with the membrane structural components in various ways.

Chapter 3

Methods

3.1 Introduction

The study of biological systems is based on experimental research, as are all natural sciences. Nature provides us with the framework, and experiments *in vivo* as well as *in vitro* a controlled way of observing those phenomena in more detail. In the formulation of a theoretical description the rise of computational science is of great help. Models of the systems studied through experiments can be built and tested without the difficulty of the experimental setup.

The behavior of biological systems can vary depending on time scale. Conformational changes, translational and other forms of movement, not to mention structural changes all have characteristic time scales. It is rarely possible to simulate nor experiment on all relevant time scales in one go. This has to be taken into account when choosing the method and setting up the research configuation. This is also the case in the so-called multiscale problem, where different simulation techniques have to be employed to study a given system over different scales in time and space. Similar questions determine the choice of an experimental setup.

3.2 Experimental consideration

A wide range of experimental techniques is available in biophysical research. The following examples have been chosen because of their distinct value-adding quality to membrane research. Here we briefly outline some of the relevant techniques and results.

3.2.1 Structural analysis

Spectroscopic methods are powerful in giving information about structure. Characteristic changes in structure often go hand in hand with function. Experimental structure resolving methods involve X-rays [87], Fourier trans-

form infrared [75], fluorescence studies [88] and *nuclear magnetic resonance* (NMR) of which more details follow. Another calorimetric method, *differential scanning calorimetry* (DSC) is useful in determining thermodynamic characteristics of phase transitions [19, 87]. Both titration calorimetry and DSC have been used to study the influence of alcohols on phosphatidylcholine phase behavior [89]. Structure-defining methods are thus useful in determining changes due to permeating solutes such as alcohol.

NMR

NMR is a method based on the magnetic properties of atomic nuclei. It is one of the most powerful structure determining methods available. Advanced NMR methods can be used for biomolecules such as proteins to discern distances between pairs of atoms within the molecule. However, in contrast to X-ray crystallography, NMR can only be used for relatively small biomolecules, e.g. very complex and heavy proteins are outside the scope of NMR. *Magic-angle spinning* (MAS) yields improved ^{1}H NMR spectra for liquid crystalline phosphatidylcholines, resolving the isotropic chemical shifts of all protons in the polar headgroup and the glycerol backbone of the lipid [90]. Zhou and co-workers use ^{1}H MAS NMR to investigate lipid hydration and the arrangement at the membrane/water interface. MAS-assisted two-dimensional Overhauser effects (NOESY and HOESY)[1] are used to determine the locations of the water molecules [90].

Several NMR studies suggest that ethanol favors the lipid/water interface in the presence of a bilayer [81, 91–93]. Feller and co-workers use 1H MAS NOESY NMR and molecular dynamics simulations to study ethanol distribution across membranes [81]. Their results confirm the ethanol preferential interfacial alignment, but show in addition that ethanols can penetrate into the region of lipid upper chain segments.

Koenig and Gawrisch use NMR to analyze ethanol orientation and motions when bound to a bicelle membrane [94]. They observe lipid and ethanol associations in a geometry supported by our findings.

3.2.2 Mechanical and viscous properties

A range of techniques are applicable to the study of mechanical stretch and viscous properties. These include photon correlation spectros– copy [95], dynamic light scattering [96] as well as NMR and X-ray diffraction studies [97]. Atomic force microscopy and micropipette aspiration are also possible choices for methods, as follows.

[1] Utilize the Nuclear Overhauser effect and dipolar coupling to create a twodimensional NMR spectrum.

Micropipette aspiration

Hung Ly described in his PhD thesis the method of micropipette aspiration in the study of short chain alcohol effects on biological membranes [98]. In this technique, a small diameter glass pipet is brought into contact with the target, e.g. vesicle. A known suction pressure is applied within the pipette, causing an aspiration of the vesicle into the pipette (see Fig. 3.1). The length of aspiration ΔL gives a measure of several important mechanical properties. It has proven to be an effective way to study membrane systems [31, 99, 100]. The advantage of micropipette aspiration is that it provides a unique way to directly probe the structural and mechanical properties of single giant unilamellar vesicles.

Ly's study includes determination of the area expansion modulus, bending modulus, lysis tension and lateral area expansion of fluid and gel phase phosphatidylcholine vesicles, mostly SOPC and DPPC. He further considers permeation of alcohols into the membrane. In short, Ly et al. observe that ethanol toxicity may be caused by ethanol's ability to alter mechanical and structural properties of the bilayer [101]. This is evident from the changes observed, namely decrease in bending modulus, area compressibility modulus, lysis tension and lysis area strain. They also note an increase in area per lipid and a consecutive decrease in bilayer thickness [101]. In another study they observe that lipid bilayers obey Traube's rule, i.e. that for every addition of a CH_2 group an alcohol becomes more effective in decreasing interfacial tension of the bilayer [54].

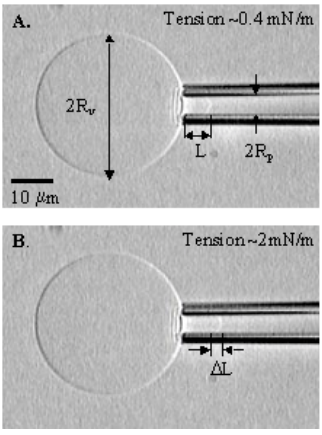

Figure 3.1. Micropipette snapshot showing L in response to tension [101].

Interfacial tension is directly related to mechanoelastic properties and thus serves as an approximation for their behaviour as well.

In a recent publication by the same group, giant vesicle studies involving

various sterols were carried out in several water/ethanol solution concentrations producing so-called elasticity/phase diagrams [102].

3.2.3 Dynamic properties

Thermodynamic considerations bring another insight into the study of solute–membrane interactions. Thermodynamic parameters are derivatives of the Gibbs energy. Volume, V and partial molar volume, V_a are given by

$$V = \left(\frac{\partial G}{\partial p}\right)_T \tag{3.1}$$

$$V_a = \left(\frac{\partial V}{\partial n_a}\right)_{p,T}. \tag{3.2}$$

The latter expresses how molecular volume changes with composition in an aqueous solution.

Enthalpy is a measure of a molecule's internal energy, and is also derived from the Gibbs energy

$$H = \left(\frac{\partial G}{\partial T}\right)_{p,n_a}. \tag{3.3}$$

These are important observables in the technique introduced next.

Titration calorimetry

Titration calorimetry is essentially the study of enthalpic interaction responses. The method *isothermal titration calorimetry* (ITC) allows for determining enthalpy changes associated with the transfer of substances from one solution to another. The titration calorimetry methodology is thoroughly described in a study of saturable highaffinity binding of ligands to proteins by Wiseman et al. [103].

For analyzing, the solvent-null method provides a means of determining from the titration results the partition coefficients of the studied substance. Amy Rowat and co-workers have employed this method in the study of lipid saturation and ethanol effects [70]. The method was also used to look at thermal fluctuations of unilamellar DMPC vesicles in the presence of non-ionic and ionic surfactants [104] and farnesylated peptides in model membranes [105].

The method provides insight into solute partitioning [89] but in defining the partition coefficients one must be cautious. ITC, fluorescence spectroscopy and equilibrium dialysis measurements all rely on small amounts of salt or organic solvent to be added into the aqueous phase. These produce a significant source of error in the determination of the partition coefficient, for salt screens electrostatic interactions, and organic solvents (e.g. alcohol) partition into membranes themselves [105].

Fluorescence spectroscopy

Fluorescence spectroscopy is based on the electronic transitions of molecules, as depicted in Fig. 3.3 by Alakoskela [61].

Figure 3.2. Cartoon of fluorescence spectroscopy.[2]

The oscillating transition dipole interacts with the oscillating electric field of light. The advantages of the method include low cost, easy and sensitive measurements and small sample size. It can be used to study dynamics of the order of nanoseconds. The strength as well as weakness of the method lies in the fact that it is based on the use of probes. The fluorescent probes make the method easy to use but results complicated to analyze, for the characteristics of the probe and its interactions need to be fully understood [61].

[2] http://www.vias.org/science cartoons/ Oct 10, 2006

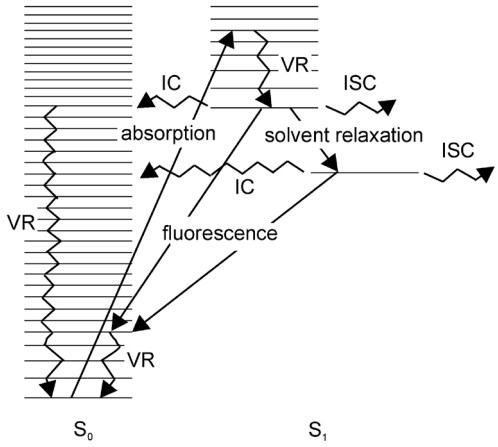

Figure 3.3. Molecular excitation from singlet S_0 ground state to the first excited state S_1 in biological fluorescence spectroscopy. VR stands for vibrational relaxation, IC for internal conversion and ISC for intersystem crossing between a singlet and a triplet state (not shown).

The dipole potential of the membrane can be expected to alter the binding of dipoles to membranes. However, the naturally complex environment of the bilayer lipids ensures this to be a more complicated problem. It has been shown that for the association of ions with membranes the contributions of the hydrophobic, dispersion and electrostatic interactions can be predicted and an effect of membrane dipole potential can be seen [106, 107]. Alakoskela and co-workers have observed a definite impact of the membrane dipole potential on the association of pregnanolone, another anesthetic, with monolayers of different lipid composition [61].

3.3 Molecular dynamics – The computational approach

The challenge in describing the bilayer through computational models lies in the numerous length and time scales present. Model building starts from the need to understand *the bigger picture*. It follows essentially the same steps as an experimental procedure, namely preparing the sample, connecting to a measuring instrument and measuring the property of interest. If (or more often, when) the measurements are subject to statistical noise, they will have to be averaged over time. The longer you average, the more accurate the measurement output. The measurements can be designed to mimic

experimental studies or provide comparison to a theoretical hypothesis. Once a computational model is constructed, it can be applied to a variety of systems and problems with minor adjustments. Model systems can thus provide a reference frame for experimental and theoretical studies alike.

The method of *molecular dynamics* (MD) can be employed at a variety of length and time scales. This method is best used when both static and dynamic quantities are of interest at the atomic level. A great amount of detail is achieved through atomic molecular dynamics simulations, whereas a number of coarse graining steps can be taken if less detailed descriptions suffice. This simulation method is designed for computing equilibrium and transport properties of classical manybody systems [108]. By classical it is here meant that the nuclear motion of the particles obeys the laws of classical, or *Newtonian* mechanics. Solving Newton's equations of motion on the ground state electronic surface obtained from a "first principles" calculation yields the so-called *ab initio* [109] -method. On the other hand, the underlying quantum effects are implicit in the inter- and intramolecular interactions manifested in the simulation through applied force field or potential energy terms, as used here.

Molecular dynamics involves solving the Newtonian equations of motion

$$m_i \frac{\partial^2 \mathbf{r}_i}{\partial t^2} = \mathbf{F}_i, \qquad i = 1 \ldots N \tag{3.4}$$

of individual species, atoms, molecules or other structures [110]. Their positions $\mathbf{r}_i(t)$ and velocities $\mathbf{v}_i(t)$ are defined at each timestep and the trajectories for N particles are generated iteratively using e.g. the following algorithm:

$$\mathbf{r}_i(t+\delta t) = \mathbf{r}_i(t) + \delta t \mathbf{v}_i(t) + \frac{(\delta t)^2}{2m_i}\mathbf{F}_i(t) \tag{3.5}$$

$$\mathbf{v}_i(t+\delta t) = \mathbf{v}_i(t) + \frac{\delta t}{2m_i}[\mathbf{F}_i(t) + \mathbf{F}_i(t+\delta t)] \tag{3.6}$$

where $\mathbf{F}_i(t)$ is the total force on particle i at time t, and is calculated from the potential energy function. This is the most time consuming part in the whole iterative process. The method being purely classical does not cause problems at normal temperatures, although very light hydrogen atoms can have characteristic quantum mechanical behaviour.

The force is calculated from the potential energy. The potential energy can be separated into two parts, the internal and external,

$$V = V_{int} + V_{ext}, \tag{3.7}$$

where the internal part consist of summed terms for bonds, angles and dihedrals, and the external part accounts for the nonbonded interactions of the molecules [111].

3.3.1 Empirical force fields

While the choice of simulation methodology plays an important role in comparison between theory and experiment, the choice of force field plays a crucial role in determining the quality of the simulation. The development of force field parameters and choice of force field to use for a particular system is by no means trivial. Parametrizing a certain molecule or group starts by considering intramolecular potential energies and atomic partial charges through quantum chemical calculations. These are then held fixed while determining non-bonded Lennard-Jones interaction potentials. Results are compared to experimental data and the potential is adjusted accordingly. Therefore the emphasis on "empirical" in the title.

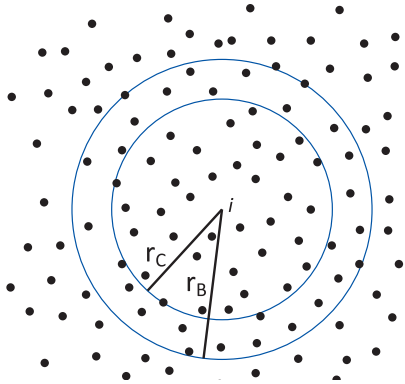

Figure 3.4. The neighbor list of particle i contains particles within the radius $r_C < r < r_B$.

The potentials can be divided into non-bonded, bonded and special interactions. In the *non-bonded* are included the Lennard-Jones, Coulomb and modified Coulomb interactions which are computed based on a neighbor list, see Fig. 3.4. *Bonded* stands for the covalent bond streching, angle bending, proper and improper dihedrals, computed based on fixed lists (bonded interactions do not change, after all, in the course of the simulation un-

less chemical reactions take place, which normally do not). *Special* potential functions are reserved for additional position and distance restraints, and are based on fixed lists. Further insight can be found in e.g. Ref. [112].

A typical force field for biologically relevant molecules could be

$$V = \sum_{bonds} \frac{k_i^b}{2}(l_i - l_i^{ref})^2 + \sum_{angles} \frac{k_i^a}{2}(\theta_i - \theta_i^{ref})^2 + \sum_{torsions} \frac{V_T}{2}[1 + \cos(n\omega - \gamma)] \sum_{i=1}^{N-1} \sum_{j=i+1}^{N} \left\{ 4\varepsilon_{ij} \left[\left(\frac{\sigma_{ij}}{r_{ij}} \right)^{12} - \left(\frac{\sigma_{ij}}{r_{ij}} \right)^{6} \right] + \frac{q_i q_j}{4\pi\varepsilon_0 r_{ij}} \right\}. \quad (3.8)$$

Here the first term is a harmonic potential that results from the bond stretching of a pair of bonded particles with a reference distance l_i^{ref}. Deviations from this distance, which the particles adopt in the absence of other interactions, result in an increase of energy defined by the spring constant k_i^b. The second term in (3.8) is likewise harmonic but characterizes the bending with respect to the reference angle θ^{ref} of three particles "chained" together (see Fig. 3.5 (b)). Torsions are rotations of a 4-atom configuration about their center longitudinal axis, V_T quantifying the energy barrier associated with the rotation. The second last term of (3.8) is the short-range Lennard–Jones potential. This can be associated with the repulsion caused by the Pauli exclusion principle and the van der Waals interactions resulting from dispersion forces. Finally, the last term describes the Coulomb interaction between charges q_i and q_j.

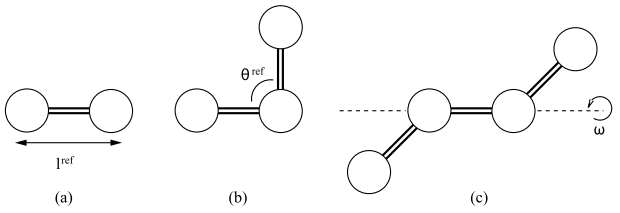

Figure 3.5. Reference length and angles in bond stretching (a), bending (b) and torsion (c).

The so-called *united atom* or extended atom description requires less computational intensity than an *all-atom* description [111]. United atom force fields are generated by uniting each carbon atom and its bonded hydrogens

into a single interaction site, which leads to the introduction of pseudo-atoms such as CH_2. Essentially it is the hydrogen atoms that are included implicitly. The procedure is illustrated schematically in Fig. 3.6. This is particularly feasible when simulating large systems such as proteins, lipid membranes or both.

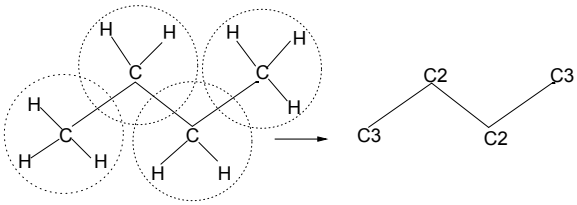

Figure 3.6. United atom description for butane with C3 indicating a methyl and C2 a methylene group.

In simulations of model systems that differ from previously studied structures only slightly, minor parameter adjustment is often done without the thorough force-field development operation, such as the quantum chemical considerations. Small study-systems are often implemented and tested against known experimental data in order to verify the chosen parameters. However, sometimes a set of parameters works only for a given system for a given purpose. Khare et al. [113] describe refining force field parameters for primary alcohols in order to capture the correct vapor–liquid equilibria behaviour. Previously parameters in an all-atom force field had been adjusted to capture the behavior of the shortest alkanol member, methanol, as it differed from the other primary alcohols [114]. Examples such as these show that a given parameter set is intended for a given system *for a given purpose*. There is no such thing as a generic set of force field parameters.

3.3.2 Ensemble

Before the simulation is complete, certain technical aspects need to be considered. These include the coupling of temperature and pressure.

Processes causing temperature deviations include system drift during equilibration, drift due to force truncation and errors in integration and frictional forces causing the system to heat up. Either a weak or a strong coupling scheme can be implemented in order to minimize these effects. The weak coupling scheme of Berendsen [115] utilizes first-order kinetics to couple the temperature to an external heat bath of temperature T_0. This is very efficient for relaxing the system to the target temperature T_0. But

in order to sample a correct canonical ensemble, the extended ensemble approach, or Nos´e-Hoover coupling, needs to be used [116, 117]. In this approach, the system Hamiltonian is extended by introducing a thermal reservoir and a friction term.

In addition to temperature, pressure is as likely to deviate from the desired value. Therefore it also needs a coupling algorithm, also called a pressure *bath*. Again two approaches are commonly employed at constant pressure, the Berendsen [115] or an extended ensemble approach called Parrinello-Rahman [118]. Given a constant particle number N, one has the most common ensemble used in membrane simulations, namely the NpT or isothermal-isobaric ensemble [119].

The coupling algorithms are best implemented separately for groups of atoms alike. This is called group coupling. The reason for this is that during the simulation, the energy change between different components is not perfect, and thus one part (typically the solvent) may require higher energies and correspondingly higher temperatures than the rest of the system, causing the other part to cool below the desired temperature. The parameters, temperature and time constant, for the temperature coupling in groups are given before the start of the simulation.

3.3.3 GROMACS

The GROMACS package [120, 121] is an engine to promote molecular dynamics and energy minimization employed at the atomic level. It is suitable for a wide range of applications where high structural accuracy is required. This type of modeling aims at predicting macroscopic properties based on a detailed atomic description. Using more minute details ensures greater predictive power but also more computational strain.

The force field provides the simulation with a description of forces acting on a body. These include all possible interactions between the atoms within a molecule and neighboring molecules, except for polarizabilities (although these too are taken into account in some very recently implemented force fields but not thoroughly tested as of yet). However, the force fields are never as accurate as a quantum description. Also, the bonds and bond angles are usually handled as constraints in the GROMACS engine in order to increase the efficiency of the MD simulations. Vibrating bonds or quantum oscillators in their ground state resemble more closely constrained bonds than classical oscillators. Therefore the error produced by the use of force-fields is deemed small to the overall system description and dynamics. The simulation of bulk phases is done through implementing so-called periodic

boundary conditions (PBC) [122]. There the N-particle model system is surrounded by similar volumes side by side creating a bulklike environment, see Fig. 3.7. Any given particle then interacts with all the particles in this infinite periodic system. The force fields used in the system are pair-additive for all interactions except for the longrange Coulomb interactions. This means that all non-bonded forces result from effective pair potentials. Thus the pair interactions are not valid for isolated pairs or even for systems that differ substantially from the test/model case for which the parametrization was carried out. Polarizabilities being omitted, cases that require correct dielectric behavior may be biased. For example, in the case of liquid alkanes the simulations may exaggerate the long-range electrostatic interactions between the partial charges. Then again, the long-range interactions, especially Lennard-Jones, are cutoff. Due to the minimum-image convention, this means that the cutoff range is always half a box size or less, depicted in Fig. 3.7 as the area enclosed by the red circle. In large systems and systems containing other than partial charges, long-range electrostatic algorithms such as Ewald sums need to be implemented.

The reliability of the method of heavy, iterative atomic molecular simulation is based on the fact that macroscopic properties are ensemble averages. This means that each simulation run produces a kind of example of the system behaviour that contributes to the representative statistical ensemble created in the end. An ensemble can be generated in several ways, either by repeating a simulation several times with a different starting configuration, or, as is more common in the case of the membrane simulations, taking all the molecules of a kind and averaging over time.

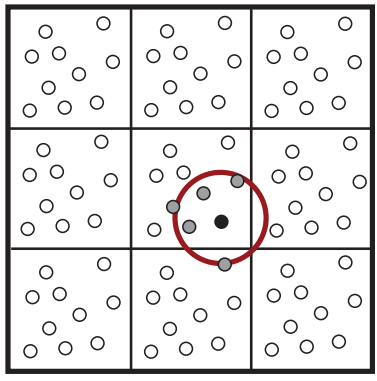

Figure 3.7. Periodic boundary conditions.

3.3.4 Limitations of MD

One of the main limitations especially affecting atomic GROMACS simulations is the empirical nature of the force field. Limitation, here, refers to the use of force fields in general, as they replace exact theoretical descriptions where such are not available. The parameters required for a given system range from describing partial charges of atoms to bond length and angle specifications. The empirical or *ab initio* (quantum) method used for the parameter determination is carried out without solvent for crystallized structures or in vacuum, as is mostly the case in quantum chemical calculations. These cause definite uncertainties in the resulting force field, mostly in the form of the force field capturing average effects rather than a detailed description of the forces acting at the atomic level. In addition, uncertainty due to the challenge of determining the energy parameters related to the van der Waals interactions and the dihedral potentials is transferred onto the thermodynamic and statistical properties of the system. Attempts to overcome some of these limitations have been proposed, including the MD package Amber where quantum mechanics based semi-empirical methods are implemented in addition to the classical molecular dynamics [123].

A second limitation of MD in general is the integration time step. In order to investigate dynamics of, say protein structures, the total simulation time should preferably be of the order of a microsecond, μs. The currently available computer efficiency is not enough to sustain μs long simulations for a typical integration time step of 2 fs, which limits feasible simulations to a maximum time of a few hundred nanoseconds [124]. The integration time step is chosen according to the time scale of fastest motion in the system, i.e. bond oscillations. Thus the recent advances in lengthening simulation times are due to faster computers and development of coarse-graining methodology.

Chapter 4

Alcohol-Membrane Study

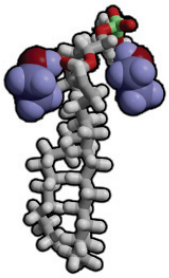

Figure 4.1. Ethanol molecules hydrogen bonded to a lipid molecule.

4.1 Introduction

It is a well-known fact that hang-over results from toxic products of alcohol metabolism in our bodies. However, we are at a loss when trying to describe the molecular scale mechanisms of the interaction of alcohols with (macro)molecules and cell structures in our bodies. The same goes for the mechanisms of general anesthetic action. Both alcohols and anesthetics have been widely studied experimentally, but computationally only selected species have received attention. Also, comparison to experimental studies has driven the computational observations to include static quantities more than dynamic ones. The introduction of dynamics into simulations is crucial in developing the overall understanding of molecular interaction.

The implementation of lipid molecules onto coarse grained simulation platforms is an attempt to better describe the large scale phenomena of lipid phase behavior as well as long time scale dynamics. This does not compete with the current atomic modeling, for the gain from these two approaches is very different. One aims at simulating large scale phenomena while the other aims at unveiling processes over atomic and molecular scales.

The influence of general anesthetic and alcohol on membrane dynamics is vital in developing an understanding for the underlying molecular interaction mechanisms. The molecular scale mechanism of alcohol and other anesthetics is still rather poorly understood, despite more than 100 years of clinical use. The challenge in simulations is to obtain dynamic quantities with

reliable statistics and couple the results to existing experimental observations in order to formulate a hypothesis of alcohol effects on membranes. Information about single molecule dynamics as well as collective effects can be obtained with good time resolution by computational methods. The limiting factors in computer simulations have been the system size and simulation duration. Structure and dynamic considerations of fully hydrated 128-molecule lipid bilayers with added alcohol are presented for the first time. The simulation time of each system was 50 nanoseconds.

Here is introduced a dynamical analysis pertaining to both lipid molecules in membrane structures as well as solute molecules penetrating the bilayer. The permeation of ethanol and methanol in di-palmitoylphosphatidylcholine (DPPC), palmitoyl-oleoyl-phosphatidylcholine (POPC) and ethanol in palmitoyl-docosa-hexaenoyl-phosphatidylcholine (PDPC) bilayers is discussed as well as suggestions for the mechanisms by which the partitioning is achieved. Estimates of partition coefficients are given and qualitatively discussed with experimental results. In addition to permeation and partitioning we present dynamics through diffusion studies. Figure 4.2 shows typical trajectories of four different ethanol molecules, indicated by four different colors, with respect to the bilayer frame of reference (z-coordinate is parallel to the bilayer normal). Diffusion of lipids and alcohols is considered in the plane of the membrane (translational), and the rotational diffusion of lipids is discussed. The concept of membrane lateral pressure profile is revisited.

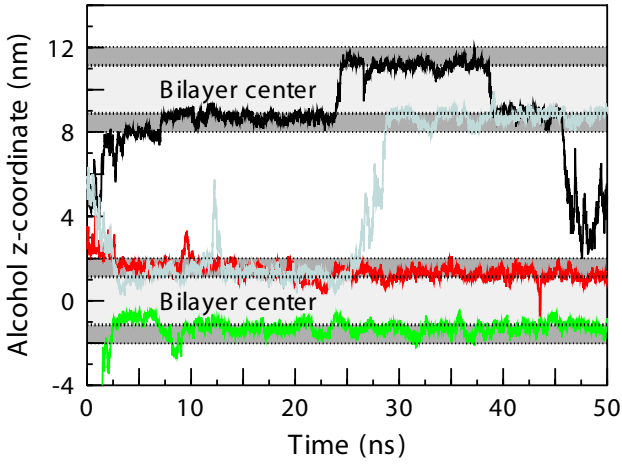

Figure 4.2. Characteristic trajectories of four different alcohol molecules.

This chapter is based on publications I and II (see p. 135) with research performed together with Samuli Ollila, Emppu Salonen, Ilpo Vattulainen and Mikko Karttunen. Collaboration with Michael Patra, Amy Rowat and co-workers as well as Roland Faller and his group is thankfully acknowledged.

4.2 System setup

The three simulated lipid structures are depicted in Fig. 4.3. Each forms a stable bilayer through self-assembly at 323 K where the lipids are in liquid-crystalline (liquid-disordered) state. The temperature is higher than room temperature due to DPPC's high transition temperature, below which it tends toward the undesired gel state. The same temperature was used for all the systems in order to allow for full comparison of structural as well as dynamic quantities.

The starting point of the simulations was a fully hydrated system of 128 lipid molecules. The selected lipids were PDPC, POPC and DPPC (cf. Fig. 4.3) in order of increasing saturation. 90 alcohol molecules, ethanol or methanol were added resulting in a total system size of roughly 35 000 atoms.

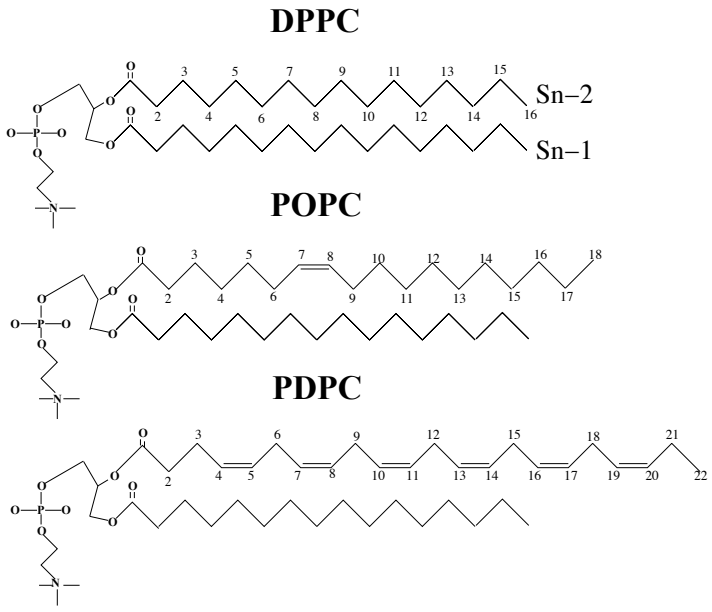

Figure 4.3. Phospholipid structures.

Each simulation was run for a duration of 50 nanoseconds. The DPPC system was based on a previous 100 ns simulation of pure DPPC, and a further 50 ns completed for the studies described in [125, 126]. For POPC a ten nanosecond equilibration simulation was carried out. The pure PDPC structure had been simulated for 50 ns [127]. The fully hydrophobic sections of the lipids were described using the united atom model described in the previous section. The polar groups of lipids as well as alcohol and water molecules whose hydrogen bonding nature cannot be lost, were described by force fields described in [121]. Force field parameters for bonded interactions were taken from Berger et al. [128]. Partial charges were from Tieleman and Berendsen [129]. For water particles, the simple point charge (SPC) model [130] was used. The ethanol and methanol force fields were taken from Lindahl et al. [121].

All simulations were carried out using the GROMACS package. The long range electrostatic interactions of the charged groups were handled by the PME (Particle Mesh Ewald) method [125, 131, 132]. Temperature of the NpT–ensemble was kept at 323K by the Berendsen thermostat and normal pressure by the Berendsen barostat [115]. The latter implies that the simulation box was allowed to fluctuate. The temperature was chosen such, that the lipids were well above the melting temperature, which is T_m = 315K for DPPC and lower for the unsaturated lipid species. The coupling time constant for the thermostat was 0.1 ps.

4.3 Results of computational modeling

Out of the 50 ns simulation time roughly 30 ns were used for analysis. This ensured that all systems had equilibrated fully and the alcohol molecules had acquired a steady-state distribution in the system according to their natural partitioning. In the following paragraphs the focus is on ethanol–lipid systems due to higher value of interest. Methanol results are mentioned where appropriate.

4.3.1 Area per lipid

Average area per lipid shows an effect of the alcohols. The fluctuations in the measured area per lipid are visible from Fig. 4.4 which depicts the evolution of the area per lipid over time. Averaged results give e.g. for DPPC

(pure): $\langle A \rangle$ = 0.655 nm^2, and DPPC with ethanol: $\langle A \rangle$ = 0.699 nm2. These agree well with previous simulations and experiments (see e.g. [132] and references therein). Further results are given in Table 4.1. The pure POPC result is in agreement with previous computational studies [133, 134] and slightly larger than the results from x-ray diffraction studies [135, 136].

As seen from Table 4.1, the presence of alcohol at this concentration has a small but nonvanishing effect on the area per lipid. Further analysis shows that the addition of alcohol expands the bilayer surface slightly, and the thickness decreases rendering the volume per lipid largely unchanged. This is expected, since the main effect of the addition of alcohol seems to be a reduction of the water surface tension. This is in agreement with observations of a DPPC-halothane system, halothane being another anesthetic [77].

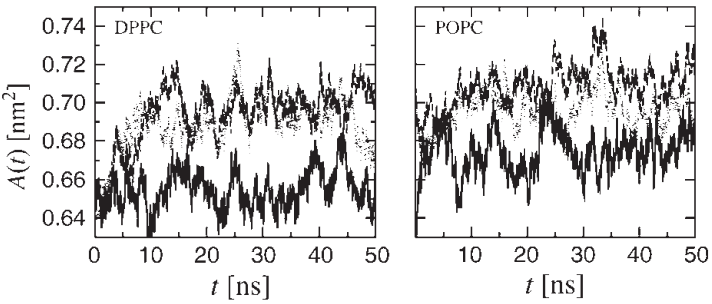

Figure 4.4. Time evolution of area per lipid for DPPC (left) and POPC (right) bilayers (solid line), and for added solute methanol (dotted) or ethanol (dashed).

System	Average area per lipid
DPPC (pure)	0.655 ± 0.002 nm2
DPPC + ethanol	0.699 ± 0.002 nm2
DPPC + methanol	0.693 ± 0.004 nm2
POPC (pure)	0.677 ± 0.003 nm2
POPC + ethanol	0.699 ± 0.003 nm2
POPC + methanol	0.693 ± 0.003 nm2

Table 4.1. Average area per lipid.

The area per lipid was also investigated by varying ethanol concentration. Results are shown in Fig. 4.5 where alcohol concentration is given as mass (alcohol) per mass (solution). Error estimates for this plot are, however, quite large but the qualitative result remains, namely that the bilayer area expands significantly on introducing more alcohol into the system. This behavior is

in agreement with recent coarse-grained simulation studies of Dickey et al. [137] as well as micropipette aspiration experiments [54, 101].

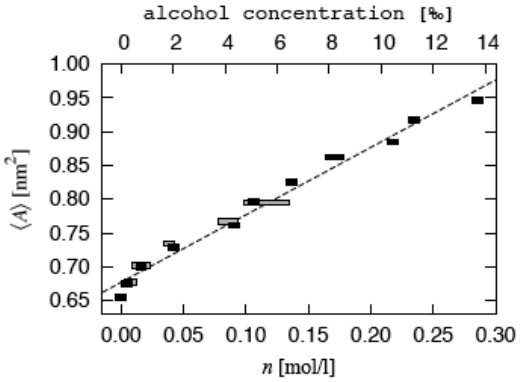

Figure 4.5. Area per lipid for DPPC with increasing alcohol concentration.

4.3.2 Mass density and hydrogen bonding

Alcohol molecules have a tendency to penetrate the lipid/water interface. This is confirmed by mass density studies. The effect is stronger for ethanol than methanol. The alcohol molecules are not located directly at the interface but slightly deeper inside the bilayer. Figure 4.6 shows the overall picture of DPPC and POPC bilayer mass densities, with separate data for the upper and lower leaflet lipids as well as total lipid density. Water molecules reside mainly against the polar lipid head groups and outside the bilayer. The center of the bilayer is altogether void of water molecules. This general picture is very much the same for the bilayer with or without alcohol in the system. The alcohol component is shown in Fig. 4.7. The data shows the lower lipid leaflet, water and alcohol mass densities. The color coding for all the following is: *red* for systems containing ethanol, *green* for systems containing methanol and *blue* for pure lipid systems. The lipid mass density curve can be further divided into the phosphate (P) and choline (N) residues of the headgroup (not shown). Comparing to the alcohol curve it is then clearly visible that the ethanol molecules preferentially locate themselves right below the lipid headgroup region. This finding is in line with experimental studies by Gawrisch et al. [93] who find through MAS-NOESY spectral analysis that despite varying the ethanol concentration between 0.1 to 1 ethanol/lipid the highest probability for ethanol location is near the upper portion of the acyl chains and glycerol backbone.

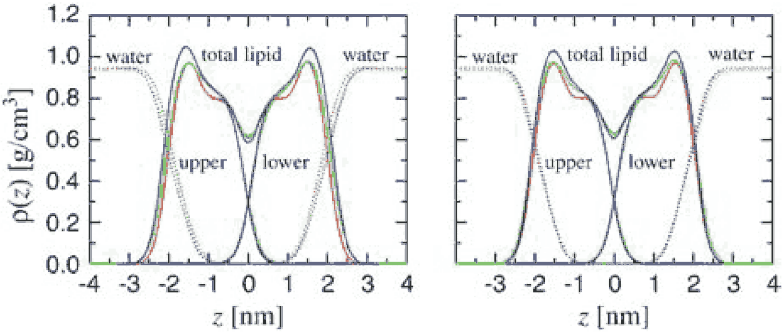

Figure 4.6. Mass density profiles across the bilayer for DPPC (left) and POPC (right) with z = 0 indicating bilayer center.

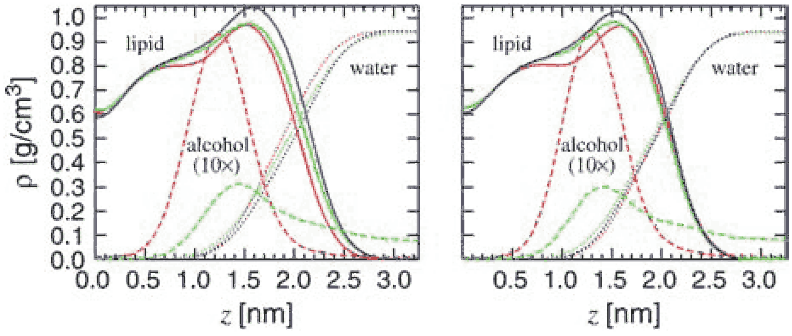

Figure 4.7. Mass density profiles of one bilayer leaflet for DPPC (left) and POPC (right) with alcohol profile emphasized.

Visualization of the atom positions shows that ethanol molecules are located close to the ester oxygens of the lipids (cf. Fig. 4.1). This result is confirmed by hydrogen bonding analysis, where possible donors and acceptors are identified by their chemical properties, and a hydrogen bond is then assumed to exist whenever two such atoms and an additional hydrogen atom fulfill certain geometric conditions. (The distance between a hydrogen and an acceptor has to be smaller than 0.25 nm, and the angle between the acceptor, hydrogen, and donor has to be smaller than 60 degrees.) The results (not shown) confirm that a majority of the ethanols are involved in hydrogen bonds with lipids, whereas not a single hydrogen bond between a methanol and a lipid molecule was found. Many lipids are involved in more than one hydrogen bond, not surprising considering they possess an ester oxygen in each of the two hydrocarbon chains. The lifetime of these hydrogen bond interactions is very short, of the order of 1 ns, which is in agreement with experimental observations [93].

The concentration effects on the mass density profiles are interesting. Through varying the ethanol concentration of a DPPC-water system the effects of the alcohol on the lipid bilayer structure became more evident. Figure 4.8 shows the results. The increase in ethanol concentration shows the expected increase in ethanol mass density inside the bilayer (bottom). However, in addition it seems the bilayer becomes slightly *thinner* in response to accommodating more alcohols (top). This is surprising, since it would seem more natural for the bilayer to expand in the z-direction in order to accommodate an increasing amount of alcohol. The thinning effect goes hand in hand with the observation that the water density slightly increases closer to the lipid headgroup region (center). If one looks more closely at the lipid mass density profile one notices the vanishing of the so-called methyl trough as alcohol concentration is increased (cf. x-axis).

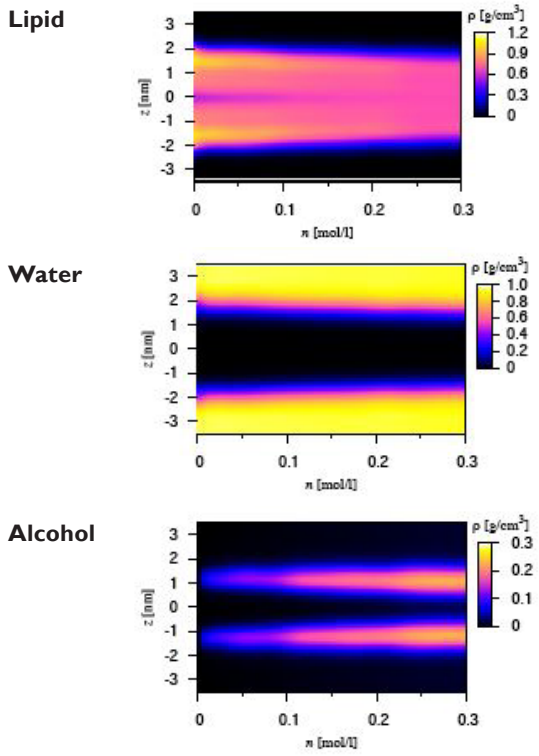

Figure 4.8. Mass density profiles across the bilayer for DPPC with increasing alcohol concentration.

The trough, visible in the range of about $0 \leq [\mathrm{EtOH}] \leq 0.1$, is indicative of the small void in the center of the bilayer when no or low amounts of solute are present. Vanishing of the trough can be explained through the increase in area per lipid with simultaneously maintaining the overall volume. Clearly

this calls for thinning of the bilayer in the direction normal to the surface which can only be achieved through compression and subsequent vanishing of the empty space in the bilayer center.

These results are corroborated by the work of Koubi et al. [78]. They find that anesthetics (halothane) collect in DPPC upper chain segments, right below the headgroups, expanding the bilayer area significantly and decreasing lamellar spacing rendering the volume unchanged.

4.3.3 Order parameter

The deuterium order parameter $S_{CD} = {}^{2}/_{3}S_{xx} + {}^{1}/_{3}S_{yy}$ (see Sec. 1.6.1) is an experimentally relevant observable characterizing the ordering of lipid acyl chains. Due to the bilayer being symmetric with respect to rotations around the z-axis (normal to the surface) we can write $S_{xx} = S_{yy}$ and $S_{xx} + S_{yy} + S_{zz} = 0$ rendering S_{CD} = -½S_{zz}.

Figure 4.9 shows the results of our computational studies in the form of $|S_{CD}|$ for all cases, ethanol, methanol and pure (lowest plots indicate pure lipids).

The order parameter analysis shows that both ethanol and methanol slightly enhance, at first, the ordering of the lipid acyl chains. Methanol increases ordering close to the glycerol group, whereas the effect of ethanol is strongest below the glycerol group, around the center of the hydrocarbon chains. This is fully consistent with the mass density profile data. This result is contradictory to the evidence in the study by Feller and co-workers [81]. Also earlier experimental studies suggest that for pure lipid bilayers the order parameter value decreases with increasing carbon atom ordinal, see e.g. [138] (cf. Fig. 4.3 for carbon atom numbering). Another view can be obtained looking at Fig. 4.10 which shows the explicit effect of ethanol, data given separately for $s_n{-}1$ and $s_n{-}2$ for the DPPC case. Hydrogen bonding to an ethanol molecule results in a smaller order parameter value, i.e. decreased order of the lipid chain in our simulations.

We propose that the order parameter is changed by two separate contributions – a local effect that is due to the proximity of alcohol molecules to the lipids and is monotonic with alcohol concentration and a more general effect that is due to the surface tension of the water-alcohol mixture and is highly nonmonotonic. Simulations reported here are in the regime of the second effect which changes with increasing alcohol concentration. Compared to our case, Feller et al. have a higher alcohol concentration and a lower hydration level and observe a decrease in the order parameter.

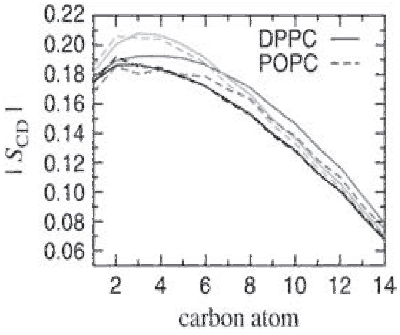

Figure 4.9. Deuterium order parameters. Data shown for two chains in the case of DPPC, and $s_n - 1$ only for POPC.

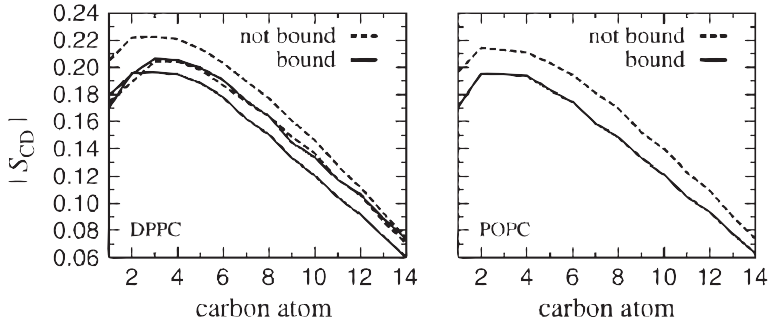

Figure 4.10. Order parameters in the presence of ethanol. Distinction is made between lipids that are bound to those that are not bound to ethanol.

Aratono et al. [139] provide support to the above scenario. They studied the effect of ethanol in water solutions in the presence of an air/water interface. The surface tension is modified by the presence of ethanol. Aratono et al. showed that the density of ethanol at the surface is not a monotonous function of the ethanol mole fraction but has a sharp maximum. They observed that at lower mole fractions there were large effects at the surface, whereas at larger mole fractions the effects were smaller and in the opposite direction.

To obtain further proof, we simulated the system with different alcohol concentrations. The number of alcohol molecules was varied between 45 and 450. We obtain a steady decrease of the order parameter for higher ethanol concentrations as can be seen from Fig. 4.11. The $|S_{CD}|$ order parameter profiles determined for DPPC and POPC clearly show, that the maximum value, corresponding to a position near the ester group, depends on ethanol concentration in a nonmonotonous fashion rising slightly for low $[\mathrm{EtOH}]$ and then decreasing. The minimum $|S_{CD}|$ values of the same graph

are obtained for chain segments close to the bilayer center. This behavior is in full qualitative agreement with the experimental findings of Aratono et al. The results in Fig. 4.11 also explain the discrepancy between our earlier results and those reported by Feller et al. [81]. They essentially considered a different regime with a resulting decrease of the order parameter with increasing concentration of ethanol.

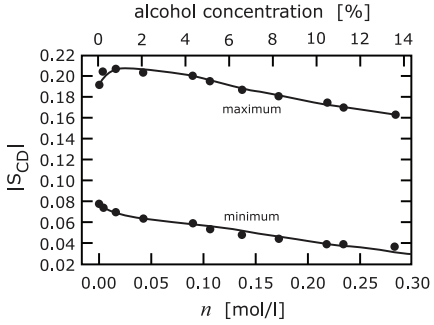

Figure 4.11. Dependence of $|S_{CD}|$ on ethanol concentration.

4.3.4 Lateral diffusion

Lateral diffusion can give insight into the differences in mobility and possible mechanisms of alcohol interaction with membranes. What we wish to accomplish, is to compare our results to lipid studies with other solutes or anesthetics, also to pure lipid simulation without solutes. The information we can gain from this is directly related to alcohol influence on the lipid membrane. Interactions of lipids with alcohols through e.g. bonding would lead to decreased lipid lateral movement since bond breaking requires energy. Ethanol, an anesthetic readily permeating into the bilayer, is expected to show different dynamic behavior than methanol.

Our studies show that ethanol molecules are indeed mobile in the bilayer and readily bound to the lipid head groups. Ethanol molecules are more mobile in the z-direction equal to the bilayer normal in the sense that they are able to penetrate through the bilayer. Subsequently they tend to have lower lateral diffusion rates than methanols as indicated by the mean squared displacements depicted in Figure 4.12. Methanol molecules spend more time solvated in the water phase and thus are more mobile in the lateral diffusion respect than ethanols, indicated by the results of Fig. 4.12 where data is averaged over all simulated alcohol molecules, whether in the bilayer or in solution. Hence the results are affected by the partitioning of the alcohols in the bilayer. Lipid saturation does not play a role in alcohol

lateral diffusion since both DPPC and POPC systems gave almost identical alcohol mean squared displacement results.

The lateral diffusion coefficients acquired for the different lipids in the presence of alcohol at 323K are shown in Table 4.2. The results have been determined from the mean squared displacement data over 10-50 ns (possible small variations for separate systems). However, error estimates for these values are quite high (of order 20%), due to the lipid mean squared displacement not having reached its saturation point and remaining fluctuations due to incomplete sampling. Therefore the determination of the diffusion coefficients is suggestive at this time. Longer simulations and more detailed analysis on alcohol concentration effects are needed.

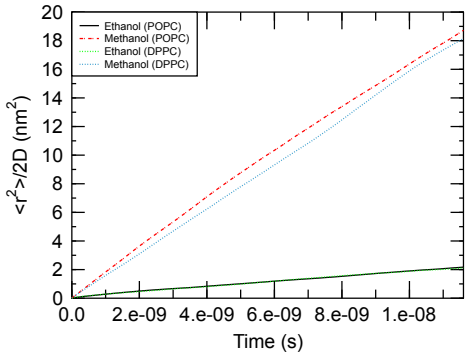

Figure 4.12. Mean squared displacements for alcohols.

	DPPC D (10^{-7} cm^2/s)	**POPC** D (10^{-7} cm^2/s)	**PDPC** D (10^{-7} cm^2/s)
pure	1.2 ± 0.3	2.0 ± 0.3	2.3 ± 0.3
EtOH	1.3 ± 0.3	2.3 ± 0.3	N/A
MeOH	1.2 ± 0.3	2.5 ± 0.3	N/A

Table 4.2. Lateral diffusion coefficients of DPPC and POPC lipids with ethanol/methanol and PDPC where available.

Comparing to other studies, it can be seen that the lateral diffusion coefficients of DPPC with solute ethanol remains the same order of magnitude as for pure DPPC. Experimental evidence gives a range from 0.97 × 10^{-7} cm^2/s to 1.5 × 10^{-7} cm^2/s [140]. Hofsäss et al. report for pure DPPC a diffusion coefficient value as high as 3.9 × 10^{-7} cm^2/s [39]. Similar values are reported by Essmann and Berkowitz [141]. It should, however be noted, that the simulation time in the preceding two studies was 10 ns

which does not give reliable statistic for the determination of the diffusion coefficient. For POPC Filippov et al. (2003) [40, 41] found through pulsed field gradient NMR the lateral diffusion coefficient at 323K to lie around 2×10^{-7} cm^2/s. The lipid PDPC is usually not simulated at this high temperature, therefore comparison to our results is difficult to find. However, the trend visible in Table 4.2 is plausible and trustworthy within the denoted error margins.

Briefly, the lateral diffusion is enhanced for increasing unsaturation. This is in line with the observed increase in the average area per lipid for increasing unsaturation. In addition, ethanol seems to increase the lateral diffusion rate as it also increases the area per lipid. Qualitatively, these findings are in agreement with so-called free area theories, which predict an increase in D for increasing free area (per lipid) in the bilayer plane, see e.g. [142, 143] and references therein. While we have not quantified the magnitude of free area here, it is likely that it increases together with the average area per lipid. Long range effects can be argued to be visible in diffusion studies of simulations of several tens of nanoseconds. Böckmann et al. 2003 [144] report 100 ns simulations with diffusion studies and also compare their results to short time scale (10 ns) simulations, where the diffusion results can be estimated to depict roughly the "rattling in a cage" –type short range movement of the lipid molecules. The relevant point to note is that the lateral diffusion coefficient over short times is larger than the one determined from the long-time (hydrodynamic) simulation regime. A long-time translational diffusion coefficient value of 1.2×10^{-7} cm2/s is obtained by Lindahl and Edholm for DPPC through performing a 100 ns molecular dynamics simulation [42]. Our results lie nicely in between those obtained by the long and short simulation times summarized above.

4.3.5 Rotational diffusion

Rotational diffusion gives information about bound alcohol effects on lipid headgroup mobility. Hydrogen bonding of the ethanols to lipid headgroups may hinder lipid rotation inside the bilayer. The mere inclusion of alcohol molecules in the membrane with or without bonding may cause steric hindrance.

Two different rotational modes were selected for analysis. The rotational autocorrelation functions $C_2(t)$'s are analyzed for the lipid P–N

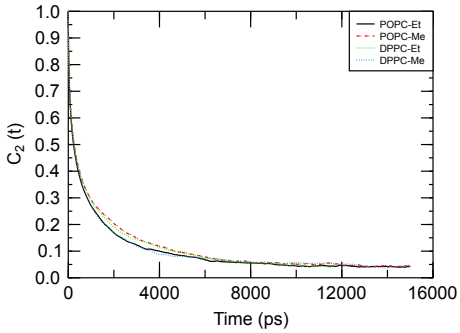

Figure 4.13. C2(t) for the P–N vector.

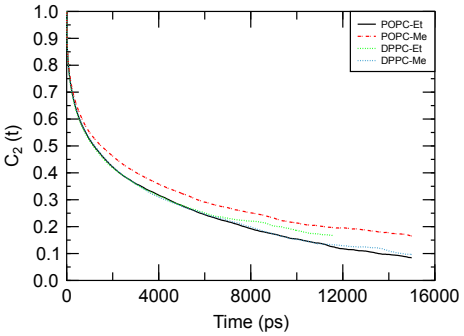

Figure 4.14. C2(t) for sn-1–sn-3.

vector as well as the interfacial vector. After measuring, the results of the autocorrelation function are fitted to a decaying exponential, whose decay rate yields the rotational relaxation rate. This, in turn, is proportional to D_R, the rotational diffusion coefficient [33].

The results indicate, that the P–N vector relaxes readily with a decay half-time comparable to the pure lipid (DPPC) case (not shown). The interfacial vector, on the other hand, shows slower relaxation as was expected based on earlier results (DPPC pure, PSM) [43]. Further reference can be found in Moore et al. [145]. Perhaps surprisingly the rotational diffusion of these groups in lipids is only weakly affected by binding of alcohols. In part this is likely due to the short lifetime of the alcohol hydrogen bonding with the lipid head groups, approximately 1 ns. The autocorrelation function for rotational diffusion decays over much larger time scales than 1 ns.

4.3.6 Partitioning

One of the key ideas of the study was to investigate alcohol permeation into the lipid bilayer. Analysis of the alcohol partitioning into membranes proved to be a challenging task. However, simulations shed light on molecular interactions impossible to observe through experiments. These include the hard-to-quantify permeation phenomena. Determination of partition coefficients for ethanol inside the membrane was a main objective, which proved to be a challenging one. However, following certain obvious principles, we were able to obtain rough partitioning data. An example of a simulation starting point is given in Fig. 4.15 showing all the alcohols residing in the aqueous phase at time t = 0 ns. The follow-up is given in Fig. 4.16 showing efficient alcohol partitioning inside the membrane.

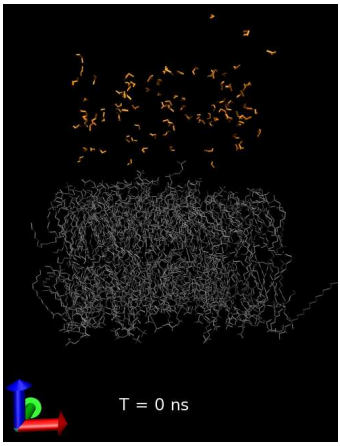

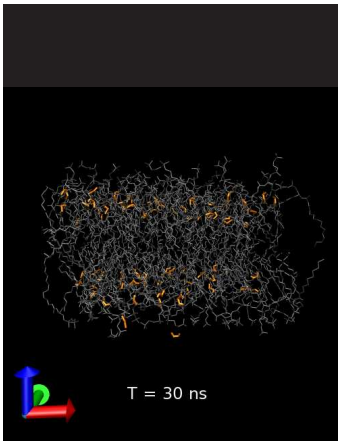

Figures 4.15. and 4.16. Simulation beginning, DPPC (gray) and ethanol (orange). Characteristic simulation snapshot (t = 30 ns) showing ethanol partitioning.

The partition coefficient can be determined as the ratio of the molar concentrations of the alcohols in lipid/water

$$K_p = \frac{X_{\text{lipid}}}{X_{\text{water}}}, \tag{4.1}$$

where

$$X_{\text{lipid}} = \frac{N_{\text{alcohol}}}{N_{\text{alcohol}} + N_{\text{lipid}}} \tag{4.2}$$

$$X_{\text{water}} = \frac{N_{\text{alcohol}}}{N_{\text{alcohol}} + N_{\text{water}}}. \tag{4.3}$$

For the partition coefficient lower limit estimates we get almost identical values for both lipids, however ethanol partitioning is greater than methanol as expected (see Table 4.3). The concentration of alcohol in the system corresponds to the second rectangle from the left in 4.17.

The problem with introducing partition coefficients in simulation studies lies in the solvation. Although the used amount of water molecules sufficiently solvates the lipids, it is not enough to create a bulk water surrounding for the alcohols. This means that the very mobile ethanol molecules entering and leaving the membrane are inadvertently pushed back into the membrane from the other side due to the periodic boundary conditions and small amount of solution in between. This causes the partition coefficients to be larger in simulation than in real life.

Figure 4.17 shows the tendency of the partition coefficient to decrease with increasing alcohol (ethanol) concentration. Error estimates are given as rectangles. The decreasing value is easily understood, as the affinity of the alcohols for the membrane goes down once a saturation, or maximum occupancy is reached. The partitioning seems to reach a plateu-like state with concentrations around 0.1 mol/l and above.

The observed tendency in Fig. 4.17 is consistent with experiments [146]. We may hazard a guess as to what mechanism/mechanisms the alcohol molecules use in order to transit through the bilayer. It seems the most favourable position for an alcohol molecule is right below the headgroup of the lipid molecule. This position is maintained by an elaborate hydrogen bond network between the charged lipid headgroup and the polar alcohol molecule. In order to be mobile, the alcohol molecule needs to break through the network of hydrogen bonding and penetrate a very nonpolar region of the lipid system.

	DPPC-EtOH	**DPPC-MeOH**	**POPC-EtOH**	**POPC-MeOH**
K_p	> 40	> 27	> 40	> 26

Table 4.3. Partition coefficient estimates for max. 90 alcohols in the system.

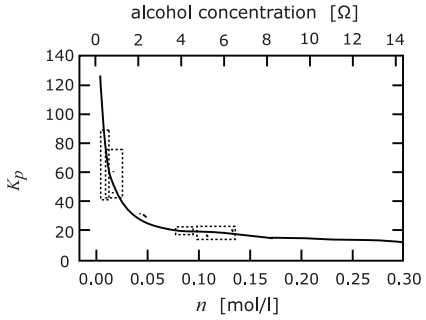

Figure 4.17. Partition coefficients of ethanol in DPPC+ethanol systems with varying ethanol concentration.

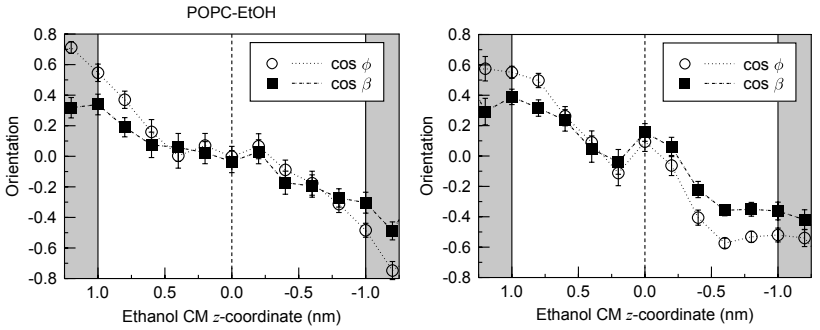

Figures 4.18. and 4.19. Orientation of ethanol inside DPPC. Orientation of ethanol inside POPC bilayer.

This is more easily done for the ethanol molecule which has a nonpolar methyl group whereas the methanol molecule is by that group smaller and thus contains an effectively much smaller nonpolar portion. Ethanol molecular orientation through the bilayer is described in Fig. 4.18 for the DPPC bilayer and in Fig. 4.19 for POPC. The angles ϕ and β are the bilayer normal to the vectors from ethanol group CH_3 to O and CH_2 to O. It can be deduced that the ethanols tend to be more specifically oriented in the lipid head group region, however their transport through the layer being facilitated by the change in charge environment provided through rotation of the molecule. This kind of molecular orientation study is unique to simulations and provides valuable information in the understanding of the interactions taking place between the solute alcohol and the biological membrane.

Comparison to experiments

The partitioning analysis completed above is here briefly compared to related experiments. The challenge here is that also in experiments the definition of partition coefficients is manifold and ambiguous. As in simulations, the system setup affects the results explicitly. Therefore even unique species depict different behavior in terms of results fromdifferent studies.

New studies on partitioning emerge periodically. In an NMR study published recently, Koenig and Gawrisch introduce a method to study physiologically relevant concentrations of ethanol in the presence of excess water [94]. They observe that only 4% of ethanol at a time is bound to phosphatidylcholine structures. These results may imply that the high partition coefficients and bound ethanol estimates we obtained are over the top values. Comparison to our results, however, is very difficult given the large amount of water present in the experiments.

One particular collaboration has yet to be introduced. This is the work done on partitioning by Amy Rowat and co-workers in Denmark. They have studied the enthalpy change upon titration of water-lipidethanol suspension into aqueous ethanol solution by isothermal titration calorimetry. Fig. 4.20 a) an enthalpogram, where the integrated area of each peak gives the enthalpy of injection, ΔH. This is repeated for various ethanol concentrations giving the plot (Figure 4.20) part b. The point at which there is no net heat exchange is called the *null* point, and the difference between this point and the amount of ethanol in the lipid-water-ethanol suspension yields an estimate of the partition coefficient K_p.

The effect of lipid saturation on ethanol partition coefficients was studied. The results are summarized in Table 4.4.

The results indicate a strong dependence on lipid saturation, namely the partitioning of ethanol into a bilayer is significantly greater for unsaturated lipids (here DOPC cf. POPC, PDPC in our simulations). So far this outcome is not corroborated by our results, but computational studies are underway to further investigate this matter. Preliminary results for ethanol in PDPC suggest that the partitioning coefficient indeed increases rather substantially for increasing unsaturation.

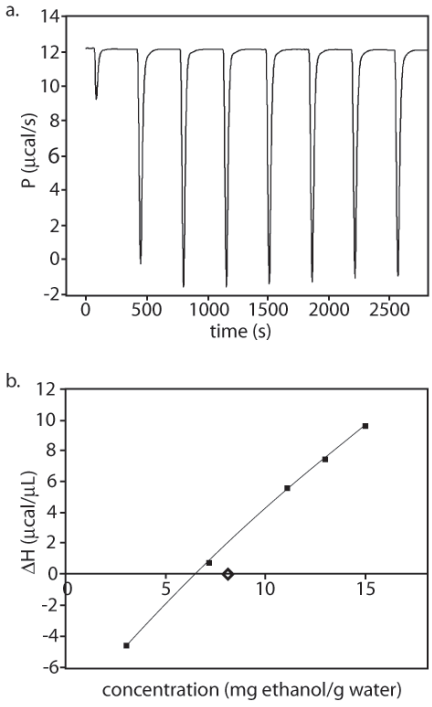

Figure 4.20. DOPC-water-ethanol by ITC [70].

	DOPC	DMPC
K_p	71 ± 10	15 ± 2

Table 4.4. Partition coefficients by ITC studies.

4.3.7 Pressure profiles

The concept of pressure profiles was introduced in Section 2.2.5. The local pressure of a system can be investigated by adding the local (negative) kinetic and configurational stress tensors to give $P = -\sigma_K - \sigma_C$ [127]. A lateral pressure profile $\Pi(z)$ is then the difference between the normal and the lateral components of the pressure tensor. Given the z-axis is in the direction of the normal to the bilayer surface we have $P_N = P_{zz}$ and $P_L = ½(P_{xx} + P_{yy})$ and the lateral pressure profile thus reads

$$\Pi(z) = P_L - P_N. \tag{4.4}$$

In equilibrium the integrated lateral pressure profile across the membrane should be zero. This ensures the mechanical stability of the membrane. The local variations, however, result from the interplay of forces that may vary spatially. Three different interaction regimes may be highlighted, namely two repulsive and one attractive contribution.

One repulsive contribution arises from the polar, hydrophilic headgroups' electrostatic and steric interactions, an attractive contribution from the interfacial energy between the water and the hydrocarbon phase aiming at minimizing surface area, and finally the second repulsive term arising from the steric interactions of the hydrocarbon chains. Implementation for lipid bilayers is carried out by dividing the system into thin slices and calculating the local pressure tensor in each compartment as described in [147–149]. For more details please see e.g. [127].

The pressure profile studies concluded for the alcohol-solute systems revealed that the partitioning of alcohol into the bilayer clearly modifies the local pressure of the membrane. Figure 4.21 shows how the addition of ethanol in DPPC and PDPC bilayers levels off the first positive and negative peaks in the lipid headgroup region. This corresponds to a more even local pressure around the headgroups in the presence of alcohol. While the local pressure arises from molecular interactions, and these interactions are dependent on molecular position we can draw the conclusion that the alcohols in fact wash out some structure on the level of the entire membrane. It is clear from Fig. 4.21 that the characteristic peaks are still there, i.e. the fundamental bilayer constitution is not disrupted, but the alcohols definitely affect the surroundings of the headgroup atoms in a way that influences their interactions with neighboring molecules.

A clarifying example may be in place. Take the interaction rising from the water and the hydrocarbon phases meeting at the lipid/water interface. The interactions at this boundary aim at minimizing membrane surface area and corresponding energy. Now in the pressure profile of a pure bilayer we see strong peaks revealing high local pressure changes. This means that it is energetically favorable for the bilayer to maintain a high degree of local structure in order to minimize the interaction boundary. On addition of alcohol into the system this structure is compromised as is seen from the pressure profile through smaller local pressure differences. This realization is in good agreement with e.g. area per headgroup studies (see Sec. 4.3.1) where it was found that the alcohols to a small extent do indeed fluidize the membrane through permeation.

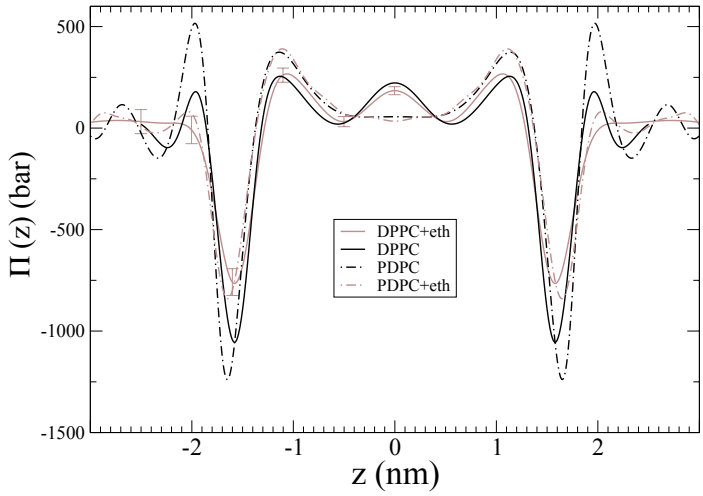

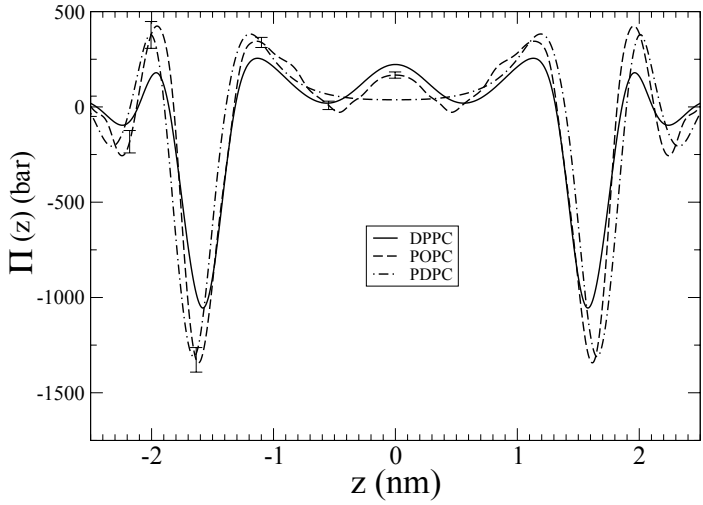

Figures 4.21. and 4.22. Pressure profiles indicating changes due to addition of ethanol solute. Pressure profiles of pure lipids with different degree of saturation [127].

For comparison, the effect of lipid saturation on pressure profiles is given in Fig. 4.22. An interesting study has also been done by Carrillo- Tripp and Feller [150] who study polyunsaturated lipid bilayers with embedded protein by a NVT-enseble. This differs from our NpT -studies on PDPC bilayers most in that the pressure profile responds to environment changes differently when it is restricted by constant area (as in the case of [150]) than by overall system pressure. In a nutshell, the changes we observe in the pressure profiles are equally small but opposite to those discovered

through constant volume simulations. This result is in good agreement with respect to the chosen simulation method as discussed in [127].

The changes in the lateral pressure profile due to ethanol are significant and suggest that the lateral pressure profile could be the mechanism by which anesthetics affect membrane protein functionality, as suggested by Cantor [51, 82–84, 151]. However, since we do not have proteins in our model this matter remains to be clarified.

4.4 Conclusions

Alcohol and lipid systems have been previously studied by experimental methods such as NMR [81, 91–94, 152, 153], X-ray [87], micropipette aspiration [54, 101, 102] and volumetric analyses [49, 154]. Barry and Gawrisch find through ^{2}H NMR studies that ethanol has a disordering effect on lipids and that there are similarities in ethanol and water interaction with lipids therefore suggesting strong influence of hydrogen bonding [92]. Also Feller et al. name hydrogen bond formation as the main source of hydrophilic interaction between ethanol and POPC bilayers [81]. Their studies are based on nuclear Overhauser enhancement spectroscopy as well as molecular dynamics simulations. Holte and Gawrisch state that ethanol resides with highest probability at the lipid water interface near the lipid glycerol backbone and upper methylene portions [93]. These observations are based on two-dimensional NOESY NMR studies. Results of Klemm and Williams also indicate that alcohol alters the organization of water and that with respect to lipids, ethanol is interacting near the carbonyl domain [153]. In differential scanning calorimetry and X-ray studies it has likewise been shown that above the melting temperature of the lipid, ethanol produces structural changes in bilayers [87]. All of these studies are supported by our elaborate findings. The fact that the simulation results have been found to be in line with related experimental studies for hydrogen bonding and ordering of hydrocarbon chains, for example, supports the idea that the present approach can be applied to provide more detailed insight into alcoholinduced effects in lipid membranes.

Significant results include that the hydrogen bonding capability of ethanol clearly makes it a more potent player in interacting with the lipid membrane than methanol. The effect it has in fluidizing the membrane and washing out of structure is largely the same irrespective of lipid saturation. This has the immediate consequence that the effect of alcohol in natural membranes that vary in lipid composition can be expected to be in line with the results obtained here.

About the mechanism of alcohol (anesthetic) action it can be said, that it involves heavy partitioning into the membrane and short-lived hydrogen bonding with lipid molecules. Polarity of the molecule aids it in penetrating the bilayer but also in moving inside the bilayer laterally. Ethanols have the ability to change lipid leaflets inside the membrane without entering through the "bulk" water phase outside. Lipid unsaturation was qualitatively shown to increase alcohol partitioning inside the membrane.

Perhaps the most relevant question for the future is the influence of alcohol on the functionality of proteins embedded in membranes. Studies by R. Cantor [51, 82–84, 151, 155] suggest that anesthetics such as alcohols may change the lateral pressure profile exerted by the membrane on the proteins, as is clearly the case based on our findings. The implications on altering structure and consequently also the function of membrane proteins is evident. This intriguing idea calls for more detailed investigation. Work along these lines is currently in progress.

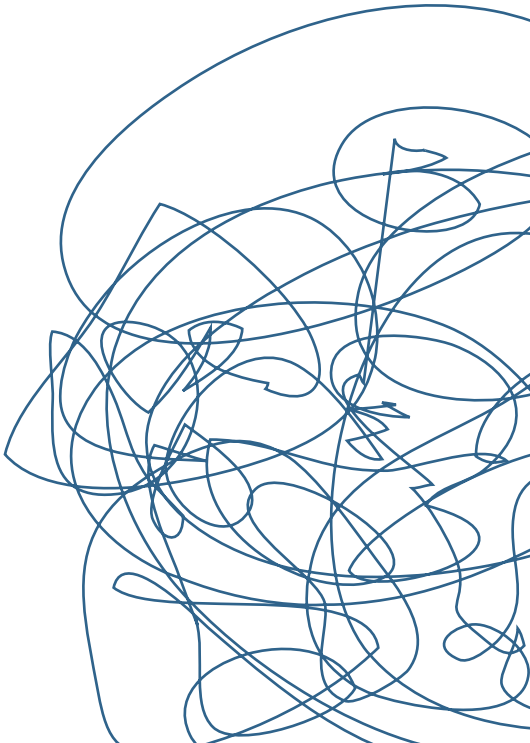

Part II

Chapter 5

Colloids and Transport

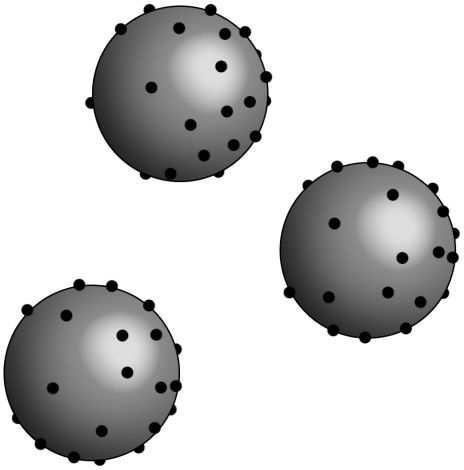

5.1 Introduction

A colloid, particle or dispersion, is characterized by constituting one or two different phase components. Colloidal particles, typically in the size regime of one nanometer to one micrometer are large enough to be observed by optical techniques. In physics, colloids are an interesting model system for atoms and molecules. Their well-defined size, shape and charge characteristics are easily exploited for simulation purposes in computational soft condensed matter science. Simple model systems can be created using colloidal particles as example species. This is also why colloidal particles were chosen for this study, as described in Chapter 7.

Colloids and particles in the colloidal regime can be tuned, manipulated and transported under a variety of external stimuli. External fields include the obvious electric and magnetic fields but also confinement, gravity, temperature, shear flow and optical tweezers can be viewed as fields. A full description of all of these is outside the scope of this thesis, attention being devoted to the electric field, temperature and gravity. This chapter describes the effects of chosen external fields on biologically relevant systems and colloids.

Simple experiments led to the discovery of important electrokinetic phenomena a long way back. One interesting observation took place around 600 B.C., when Thales of Miletus in Turkey noticed rubbed amber could attract small fluff particles. The charged amber generated an electric field which polarized the fluff [156]. The effect became known as dielectrophoresis or DEP in 1951 by the suggestion of H. A. Pohl [157]. It is a technique of great importance to the experimental community ranging from the traditional materials science to the biological sciences. However, at the same time it is a method that has developed fairly hidden from the eyes of theoretists, not to mention computational scientists, and is therefore the main subject of interest in the coming chapters. Another significant historical mark in electrokinetics took place in the 1920s when electrorotation was performed on dog blood cells. The experiment resulted in a frequencyindependent value for the capacity of the cell membrane [158].

5.2 Colloids

Colloids are ubiquitous in every-day life. They are constituents of paint, make-up and several foodstuffs. Mayonnaise, butter and milk are examples of colloidal suspensions. My personal food-stuff favorite is ice-cream, a suspension classifiable as both colloidal dispersion and emulsion but also as a foam. It is an example of a soft solid that contains small ice crystals (about 50 μm in size), and air bubbles (about 100–200 μm) up to 50 % of the total volume within a continuous matrix of unfrozen emulsion (sugar water) [159]. Ice-cream is an example of a largely polydisperse suspension difficult to describe by simple model systems, nevertheless well demonstrating the wide range of colloidal systems out there.

These curious particles have received a great deal of attention in the past. Several Nobel laureates' work has concentrated on colloids including Theodor Svedberg (1926 Nobel in chemistry) for disperse systems and Jean Perrin (1926 Nobel in physics) for his work on the discontinuous structure of matter, and especially for his discovery of sedimentation equilibrium.

A technologically important aspect of colloids is the tunability of their properties in e.g. magnetic and optical colloids. Materials can be designed from colloids for specific applications. This is much aided by the increased understanding of underlying interparticle interactions that has been gained through model system studies. Synthetic colloids can be found in paints, foams and pastes.

A typical component of a colloid has one dimension in the range of 1 nm to 1 μm with high surface to volume ratio. On a microscopic scale a colloidal

system is heterogeneous, although macroscopically seems homogeneous (ice-cream is "smooth" to the eye). This means that in a system comprising of several species the size difference between the largest and smallest can be significant. A colloidal particle also need not be round. It can assume any shape that is energetically feasible with respect to the surroundings. Often this means reducing surface area, resulting in round, oblate or prolate spheroidal particles.

Colloid particles in dispersions undergo Brownian motion. This means, that the particles will bump into one another periodically but randomly. Whether a dispersion is stable or prone to aggregation is determined by the magnitude of the attractive and repulsive interaction forces. The attractive forces between two particles are called van der Waals interactions, resulting from attractions between electric dipoles. Repulsive interactions are often due to like charges or steric effects [159].

A model of a colloid possessing an electric double layer is given in Fig. 5.1. A system of charged colloids can manifest a so-called diffuse double layer. Counter and co-ions in immediate contact with a surface are said to be located in the Stern layer forming a molecular capacitor. Figure 5.2 shows two models and corresponding electric potential profiles. The Gouy-Chapman model (Fig. 5.2 l.h.s.) underemphasizes the structure of the double layer. This is corrected in the Stern representation where the ions closest to the electrode are confined to a rigid Helmholtz plane [160]. A close-up of the Helmholtz plane is given in Fig. 5.3.

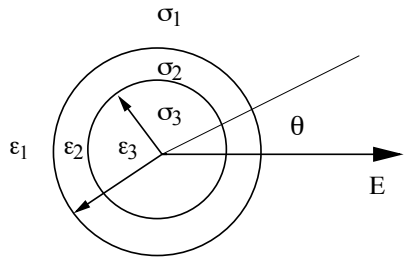

Figure 5.1. Model of a colloidal particle and three regions with different permittivities ε and conductivities σ.

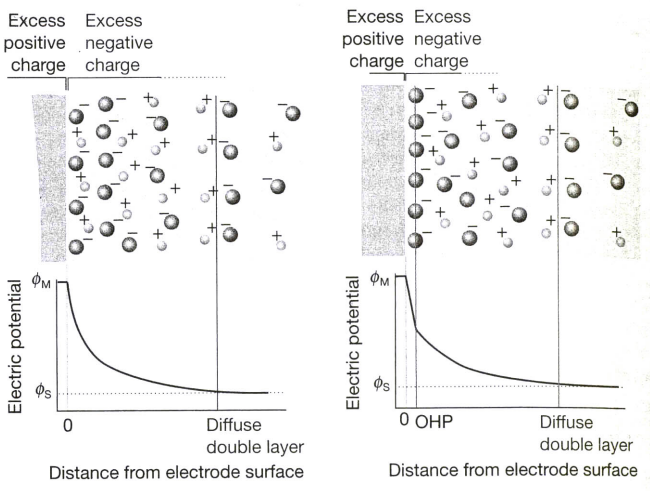

Figure 5.2. Gouy-Chapman (left) and Stern models of the electrical double layer [160].

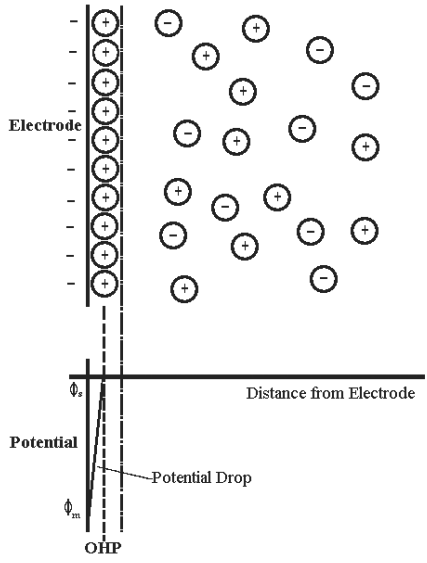

Figure 5.3. Helmholtz plane of the Stern model.

An example system could be a large, charged macroion that attracts charged ions from solution creating on its surface a layer of oppositely charged particles effectively shielding the macroparticle charge from the surroundings. Typically the microions see the macroion surface as a flat charged wall (infinite plane electrode) due to their great difference in size.

5.3 Electrokinetics

The science of electrical charges moving in liquid media is called electrokinetics. It studies particle motion which is the direct result of applied electric fields. Electrokinetics covers subjects such as electrophoresis, dielectrophoresis, electro-osmosis, and electrorotation. More about the former two can be found in the next section. Particles can be by nature charged, neutral or polarizable. However, most particles have electrical and magnetic properties associated with their shape or material resulting in non-zero interaction forces. The smaller the particle, the more visible the effect of the external field.

The action of an external electric or magnetic field is to exert forces and/or torques on those particles (less than approximately 10^{-3} meters in diameter). The mechanics and dynamics induced by these forces and torques is called electromechanics or electrokinetics. The electric or magnetic field may be imposed by external means (via electrodes, magnetic pole pieces, etc.) or by other nearby charged, polarized, or magnetized particles [161].

When considering systems at a very small scale, say well below micron, the electro-magnetic effects become increasingly pronounced. Such systems require special treatment in terms of applicable theory as well as experimental techniques, and the study of these processes is consequently termed *nanoelectromechanics* [162]. Most of our work is, in fact, done in this regime, however I will refrain from using the term "nano" explicitly. In the sub-micron particle size range also effects due to thermal gradients, hydrodynamics and sedimentation become important [163].

5.4 DEP vs. electrophoresis

A particle carrying electric charge experiences a force exerted by an external electric field. This is utilized in the method called electrophoresis. In dielectrophoresis, a neutral but polarizable particle is subjected to an inhomogeneous electric field that causes the particle to become polarized as shown in Fig. 5.4. (Partial) charges are distributed on the particle surface unevenly and a charge gradient is formed. This detail separates the phenomenon from conventional electrophoresis, where particles are actually charged. A non-uniform external electric field applies a force which sets the particle in motion.

The major advantage of DEP with respect to electrophoresis is that it can be used to manipulate all kinds of particles, not only charged species.

Then again, the disadvantage of DEP is that the polarization forces are typically weak. For DEP phenomena AC fields anywhere between 10 Hz and 100 MHz can be employed [164].

Successful manipulation of particles requires balancing the forces due to viscosity, buoyancy and hydrodynamics with the DEP-force [165]. To ensure large enough DEP-forces, the devices are set to produce large field gradients. Field gradients of the order of 10^9-10^{10} V/m^2 can be achieved with field strengths around 10^5 V/m [166]. For trapping of small, well below micron sized particles, the gradient is obtained by introducing microdevices with very small electrode separation. Curiously, DEP is the electric analog of magnetophoresis, in which metals collect at the poles of a magnet. Because magnetic monopoles do not exist, there is no magnetic analog to electrophoresis [167].

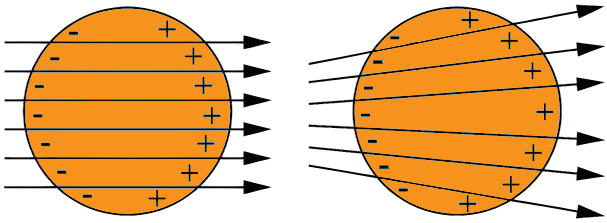

Figure 5.4. Inhomogeneous field moves particles in DEP.

5.5 Hydrodynamics

The motion of a particle in a fluid is affected by the motions of other particles, largely due to conservation of momentum. This is characterized by the hydrodynamic interactions between the colloidal particles mediated by the solvent. Further, even a single particle in a fluid medium experiences a viscous resistance due to external forces that decreases its acceleration and sets a finite critical velocity. The resistive force, or hydrodynamic drag F_H is linear with respect to particle velocity and dependent on particle shape, with the following criteria: Particle velocity is the instantaneous velocity relative to the fluid, the particle is small, the fluid sufficiently viscous and the motion is slow [168]. For a small sphere of radius a moving with a relative velocity U through a fluid of viscosity η, the hydrodynamic drag is given by the Stokes relation

$$F_H = -6\pi\eta a U . \tag{5.1}$$

The shape dependence of the above relation implies that already a two-colloid case calls for special treatment of the drag force. Particles consisting of a few globular subunits are not very well described by slender body approximations. Studies on the translational resistance of hydrodynamic friction on various shaped objects has been reported by several authors [169–173].

Fluid heating is a topic to consider in experimental small scale devices [174]. Significantly increased fluid flow can cause excess forces on the particle as well as drift [166], the possibility for which should be carefully evaluated for light weight particles. Inevitable power dissipation must be accepted as long as convective currents are being avoided [175]. Motion of the suspending liquid can even be used in conjunction with the DEP-force, or have its effect eliminated by choosing appropriate (AC) frequencies [176].

5.6 Brownian motion

The effect of changing the temperature of a system is changing the thermal force affecting the motion of the particles. The random motion of particles in response to temperature is called Brownian motion, in honor of botanist Robert Brown (1773–1858) who first documented this jittery motion in pollen grains.

In all systems with non-zero temperature (i.e. *all* systems) particles have thermal energy and undergo respective thermal motion. Particles dispersed in liquid medium experience the thermal impacts of the solvent particles.

The principal non-deterministic force acting on the particles is the diffusion force driven by Brownian motion [165]. This motion is often not desired in experiments nor simulations, because of its random nature and "damping" effect on the desired translational motion, therefore better known as noise. Noise is a result of the Brownian motion being a stochastic process with zero (or close to zero) time-average. The resulting random displacement of particles follows ideally a Gaussian profile with a (one dimensional) mean squared displacement given by

$$|\Delta x|^2 = 2Dt, \tag{5.2}$$

where D is the diffusion coefficient for a colloidal particle in a fluid that can be written

$$D = \frac{k_B T}{6\pi\eta a},$$

(5.3)

also known as the Stokes-Einstein relation, one of the fruits of 1905, the same "miraculous" (crazy) year Einstein discovered the photoelectric effect.

As already stated, a particle undergoing Brownian motion bounces around due to thermal fluctuations. It has no memory of its trajectory, and therefore cannot trace back the route it took in moving from point A to point B. It is an example of a stochastic process with no correlations between successive particle positions. This can be described through a first-order Markov process, a mathematical scheme that exactly fits Brownian motion. A Markov chain of states satisfies the following two conditions:

1. **The outcome of each trial depends only upon the immediately preceeding trial**
2. **Each trial belongs to a finite set of possible outcomes** [24].

A general description of the system development in time can be given through a phenomenological Master Equation

$$\frac{dP_k}{dt} = \sum W_{kl} P_l - W_{lk} P_k,$$

(5.4)

where P_k gives the probability of the system being in state k, and W_{kl} is a matrix of transition rate constants. The Fokker-Planck equation is a linear approximation of the Master Equation that describes the time evolution of the probability density function $\rho(x, t)$ of a particle:

$$\frac{\rho(x,t)}{t} = \Gamma \frac{}{x}\left(\frac{F(x,t)}{x} + k_B T \frac{}{x}\right)\rho(x,t).$$

(5.5)

The first use of the Fokker-Planck equation was the statistical description of Brownian motion which brings us to the fluctuation-dissipation theory, see e.g. [177]. Alternatively, a common means to describe Brownian motion is in term of the Langevin equation [24], using terms for viscous (friction) and thermal noise forces. This approach also readily results in Eq. 5.3 for the diffusion coefficient.

The effect of Brownian motion is especially notable in dielectrophoresis, which is used for particle separation, where the course of the particle is being manipulated by changing the direction and magnitude of the applied electric field. With decreasing particle size, thermal noise of the surrounding medium becomes important to the transport dynamics. The force on a particle due to Brownian motion increases as the particle volume decreases.

Due to a rapid improvement in experimental methods, namely lithographically manufactured micro-electrodes, it is possible to achieve increased electrical field gradients sufficient to move most particle sizes and types. It is not yet known what is the small size limit of particles that can be efficiently transported or separated. However, studies have shown that even for single macromolecules, the DEP collection overrides the randomizing effect of Brownian motion [165].

5.7 Sedimentation

The gravitational field acting on a particle in solution is called sedimentation. It is basically the phenomenon of an uneven suspension setting in response to gravity. This is easily demonstrated when earth is added to a container filled with water see Fig. 5.5. The container is shaken and then let to rest. After a while all the soil will have travelled through the water down to the bottom, i.e. deposited. In a mixture of liquid and granular solid the two phases have different densities resulting in gravity driving one phase relative to the other [178].

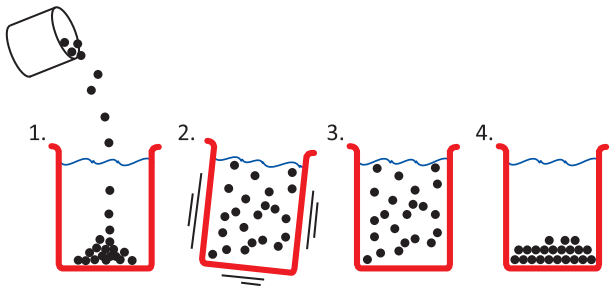

Figure 5.5. The process of sedimentation of solid in a liquid.

The gravitational "buoyancy" force acting on a particle is $F_g = g(\rho_{colloid} - \rho_{water})V_{colloid}$ where g is the acceleration due to gravity. For a very small particle this force is easily overcome by more potent forces,

e.g. due to electric interactions. On increasing the particle mass, however, sedimentation becomes an important phenomenon to control. One would not desire for common colloidal emulsion such as milk or beauty cream to phase separate after all. Esa Kuusela and co-workers have studied this phenomenon with non-Brownian particles in order to investigate pure sedimentation [179]. In other colloid simulation studies the gravitational force is often neglected, however it remains an important topic for experimentalists.

5.8 Biological motivation

Most biological, i.e. carbon-containing, non-synthetic systems are either charged or polarizable, and can be manipulated by external fields. Suitably sized bioparticles include DNA, viruses, bacteria, and red blood cells. All of these lie in the colloid regime, i.e. nano- to micrometer range.

Pohl was the first to demonstrate in 1966 the use of an external electric field in separating living biological cells [180]. More novel uses of DEP include electrofusion, automated processing of living cells and collecting and positioning DNA [161]. DEP can be considered a competitive alternative to the more conventional methods of cell concentration and separation, such as centrifugation, filtration, fluorescence activated cell sorting, or optical tweezers.

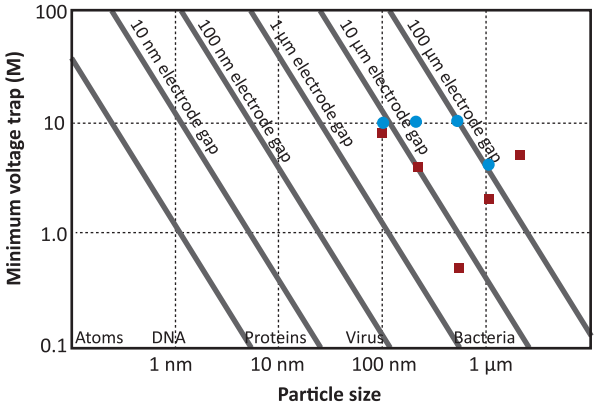

Figure 5.6. The dielectrophoretic force scales with particle and electrode size.

For isolating and analyzing a wide range of particle types, namely cells, bacteria, viruses, DNA and proteins, the basic DEP method is probably unique. The scaling of the dielectrophoretic force with particle size and electrode

size allows for separation and trapping of species ranging from nm to μm length scales, see Fig. 5.6 where data points are taken from [1]. After selective isolation and recovery by DEP, cells remain viable for further analysis, processing or cell therapy. DEP can also be operated under sterile conditions. Although the ability to selectively isolate cells without harming them is important for many biomedical applications, DEP can also be used to destroy selected target cells. The applicability of this function lies in selectively destroying specific cell types in a mixture of cells [181]. Due to operating directly on unlabeled cells in their natural state, DEP eliminates the expense, labor and time of labeling and tagging, as well as the development and validation of such labels and tags.

DEP can be used to detect changes in cell morphology. The main characteristics of a cell that determine its DEP properties are cell volume, total plasma membrane area, the endoplasmic reticulum, the nuclear size, cytoplasmic ion content and ion mobility, as well as the membrane's permeability to ions [182]. Changes in these characteristics provide the most commonly used marker for detecting tumor cells. The transformation from a healthy cell to a pathogen is characterized by atypical cell morphologies. These include altered cell diameter, unusual peripheral or internal membrane structure and modified nuclear appearance. Charged, or partially charged species in different cell compartments take different amounts of time to respond to an applied electric field. Thus cellular morphology and composition affect the cell's DEP-response [182].

5.9 Malaria affects cell electric response

Malaria is an infectious disease caused by the unicellular *Plasmodium* parasites. The resulting high fevers can be lethal when left untreated. The species *Plasmodium falciparum* is responsible for most infections leading to death. It is estimated to kill around two million people each year, and the parasite causing malaria is gaining resistance to the most commonly used drugs, chloroquine and fansidar [183]. Malaria is most prevalent in rural areas of warm climate developing countries, therefore a high impact in diagnostics is given to reusable instruments that are transportable, robust, automatized and cheap. Gascoyne and co-workers have suggested using DEP in a micro-total analysis system (μTAS) from sample collection to molecular detection that would satisfy the fore-mentioned criteria [184, 185].

It has been shown that the electrical conductivity of the erythrocyte cell membrane increases sharply on becoming hosts to malarial parasites as shown in Fig. 5.7. This is suggested to bear relation to new membrane per-

[1] http://nano.ece.uci.edu/papers/singlemolecule.pdf Aug 30, 2006

meation pathways, peroxidation damage and changes in membrane fluidity, all due to the cell being infected [184].

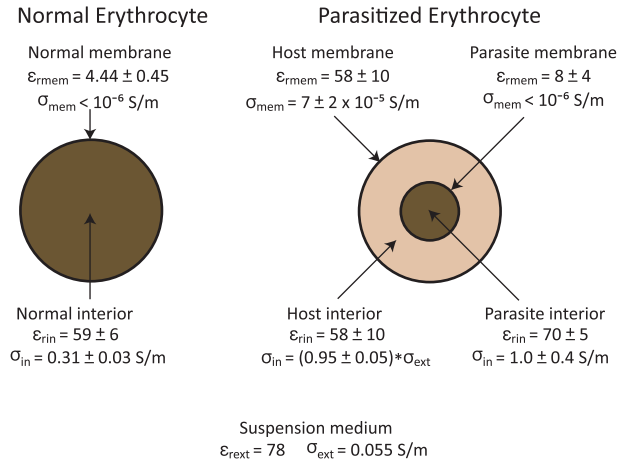

Figure 5.7. Mean dielectric parameters for normal and infected cells (modified from [184]).

Gascoyne et al. [184] studied the DEP levitation and trapping responses of normal and parasitized cells. They obtained the frequency dependent cell collection responses and analyzed these using a shell model [186]. They found that the contrasting behavior of the normal vs. the infected cell arose from differences in retaining cytoplasmic ions. This had the direct consequence that when placed in low conductivity, isotonic medium, the cytoplasmic conductivity of the infected cell fell to that of the medium in about 10 minutes. Normal cells were able to maintain their high cytoplasmic conductivity. The mechanism of ion loss may involve parasitic expression of membrane pores, lipid peroxidation and fluidity changes of the host cell membranes. A substantial review of parasite–membrane interactions can be found in [187].

Effective treatment requires knowledge of the specific malaria species causing the infection. The same microscopic method that was used 100 years ago is still often the only possibility for disease detection. It requires a skilled technician or pathologist to identify mixed infections or low infection levels, not to mention achieving the limit of sensitivity. Better and faster detection and analysis devices using DEP would benefit the infected, and facilitate basic malaria research.

5.10 Versatility of DEP

One of the central methods of modern electrokinetics is dielectrophoresis. Recent studies attest the versatility of DEP in the manipulation of carbon nanotubes [188, 189], DNA [190] and biological microorganisms [164, 174], as well as the assembly of nanowires [191] and biosensor arrays [192]. A nanoscopic force microscope technique based on DEP was also recently introduced [193]. The relevance of DEP methods to more complex integrated microscopic analysis and assembly devices [194], so-called "lab-on-a-chip" devices, is evident.

To summarize, dielectrophoretic technologies are an attractive tool with wide-reaching applications in cell separation, manipulation, and characterization with evident biological and biotechnological significance.

Controlled cell separation, trapping and cell destruction can be achieved with this powerful technique. The length scale of systems that can be operated through DEP ranges from the molecular scale all the way to microorganisms, such as bacteria. Tumor as well as parasite infested cells can be detected and manipulated. DEP has the potential of becoming a fast, powerful, inexpensive and easy-to-use tool in medicine and biotechnological research. The more traditional materials science and (soft) condensed matter research communities have a powerful, versatile experimental technique at hand. With in-depth research into the properties of DEP we can enhance its applicability even further.

Chapter 6

DEP Theory

Now let us turn to a more detailed picture of colloids in fields. This chapter provides an overview of the theory relevant to the simulation model building in the next chapter.

6.1 Sphere in an electric field

Place a particle in an electrical field $\mathbf{E}$. It will experience a lateral force $\mathrm{F_E,lat}$ [167, 195, 196] given by

$$\mathbf{F_{E,lat}} = q\mathbf{E} + (\mathbf{p}\cdot\nabla)\mathbf{E} + \frac{1}{6}\nabla\left(\mathbf{Q} : \nabla\mathbf{E}\right) + \ldots \tag{6.1}$$

where q is the net charge of the particle, $\mathbf{p}$ the dipole moment and $\mathbf{Q}$ is the particle's induced quadrupole moment with the operation : representing two dot products on dyadic tensors [196]. The first term describes the Coulombic interaction between the particle and the electric field. Clearly, this vanishes for uncharged particles or particles in an alternating field with zero time average, $\langle E\rangle$ = 0. The second term arises from the coupling of the field with particle polarization. This term vanishes only if the field is spatially homogeneous, i.e. $\nabla\mathrm{E}$ = 0. Finally, the quadrupole and higher order terms are negligible for moderately inhomogeneous electric fields [167].

Now take a dielectric sphere in a uniform electric field. The field is related to the electrostatic potential through the gradient, i.e. $\mathbf{E} = -\nabla\phi$. Conversely, the electric potential is given in terms of the electric field strength E as

$$\phi_0 = E_0 x = Er\cos\theta. \tag{6.2}$$

Outside of the sphere the potential is $\phi_1 = \phi_0(1 - f_{CM}a^3/r^3)$and inside $\phi_2 = \phi_0(1 - f_{CM})$ respectively. Here f_{CM} is the Clausius-Mossotti factor (see 6.4) and a is the radius of the dielectric sphere. The Clausius- Mossotti charge polarization factor describes the electrical polarization of the particle with respect to its suspending medium [185].

Given the permittivities of the medium ε_1 and particle ε_2, and requiring

continuity at the interface of the two, we get

$$\varepsilon_1 \left(\frac{\phi_1}{r}\right)_{r=a} = \varepsilon_2 \left(\frac{\phi_2}{r}\right)_{r=a}.$$

(6.3)

Substituting the potentials ϕ_1 and ϕ_2 into the above we get the expression for the Clausius-Mossotti factor as

$$f_{CM} = \frac{\varepsilon_2 - \varepsilon_1}{\varepsilon_2 + 2\varepsilon_1}.$$

(6.4)

We can compare to the classical relation of the dielectric constant and molecular polarizability γ_{mol}, also called the Clausius-Mossotti equation

$$\gamma_{mol} = \frac{3}{4\pi N}\frac{\varepsilon - 1}{\varepsilon + 2},$$

(6.5)

where N is the number of molecules and $\frac{\varepsilon - 1}{\varepsilon + 2}$ is roughly proportional to the density of the substance, which Mossotti (in 1850) and Clausius (in 1879) established independently [197]. This relation holds best for low values of the dielectric constant, and for dilute substances such as gases.

In an electric field that is time independent but nonhomogeneous (i.e. $\nabla \mathrm{E} \neq 0$) the force acting on a perfectly insulating particle is

$$\mathbf{F} = 2\pi a_1^3 f_{CM}(_{1,2})\nabla \mathbf{E}^2.$$

(6.6)

One special case is worth mentioning. In the case of the metallic sphere, the particle permittivity "2 goes to infinity ($\varepsilon_2 \to \infty$). According to the general expression for the dielectric force, $\mathbf{F} = (\mathbf{p} \cdot \nabla)\mathbf{E}$, only the dipole moment of the particle p and the gradient of the field are needed to obtain the dielectric force. For a conducting sphere in a perfectly insulating medium of permittivity ε_1, the dipole is equal to $4\pi a^3 \varepsilon^1$ and one gets for the force acting on the particle the expression [198]

$$\mathbf{F} = 2\pi a_1^3 \nabla \mathbf{E}^2.$$

(6.7)

6.2 Non-zero conductivity case

For particles with non-zero conductivities in non-zero conductivity media the force expression becomes more complicated. A material's conductance is given by

$$G = \frac{\sigma A}{d},$$

(6.8)

where σ is the conductivity, A the area and d the thickness. For example, the conductance of a biological membrane reflects its net transport of ionic species through pores, ion carriers, channels and pumps [199].

The capacitance of a flat biological membrane of typical composition is around $9\ \mathrm{mF/m^2}$ [199] and is expressed as

$$C = \frac{\varepsilon_0 \varepsilon A}{d}$$

(6.9)

The complex permittivity of a material depends on its dielectric constant and electrical conductivity. For example, the complex dielectric properties of aqueous media are dominated by dipoles and ionic conductivity, so the components of the fluid permittivity ε_1^* are the bulk medium permittivity and conductivity. Those of latex microspheres arise from the electronic polarizability of the polymer from which they are made of, and those of living cells from interfacial polarization of ions at the cell membrane surface [167].

The general complex permittivity is given by $\varepsilon^* = \varepsilon - i(\sigma/\omega), i = \sqrt{-1}$ [165], where $\omega = 2\pi f$ is the angular frequency. This holds for an isotropic homogeneous dielectric. The Clausius-Mossotti factor can be rewritten as

$$f_{CM}^* = \frac{\varepsilon_2^* - \varepsilon_1^*}{\varepsilon_2^* + 2\varepsilon_1^*}.$$

(6.10)

The conductivity of a colloidal particle consists of three parts, one bulk and two surface components. Surface effects are due to the movement of charge in the diffuse double layer, and the Stern layer conductance [200]. For simple latex spheres the bulk component is approximately zero and the surface conductivity approximately equal to $2K_s/a$, where K_s is the surface conductance due to the electrical double layer and directly proportional to

the surface charge density, and a the particle radius [175]. The charge double layer effects become more prominent for small particles at low conductivities. Therefore e.g. the DEP-properties of DNA molecules in solution are independent of the sub-molecule scale base sequence, since they are controlled by the molecular charge double layer and surface conductivity effects [167].

The real and imaginary components of f^*_{CM} couple with the components of the applied electrical field to create the DEP-force [185]. Implemented for a varying (AC) electric field, and the polarization of a particle being frequency dependent one obtains the time-averaged DEP force as [161]

$$\langle F_{DEP} \rangle = 2\pi a_1^3 Re[f^*_{CM}] \nabla E^2_{rms}. \tag{6.11}$$

This is the force described by the point-dipole model in which higherorder terms (cf. Eq. 6.1) are neglected. For particle sizes close to the device size, the quadrupolar and higher order terms must again be included [201]. The point-dipole model works well for single particles, dilute solutions and for systems of particles with sizes significantly smaller that the characteristic size of the device.

6.2.1 Cross-over frequency

The AC field can be chosen to accommodate the needs of the experiment. DEP can be used to manipulate either single particles or efficiently move or trap several like particles. Kadaksham et al. have shown [166] that close to the cross-over frequency (see below) yeast cells can be manipulated individually, but at other frequencies the cells readily form chains which move toward the electrode edges. The cross-over frequency spectrum can be used as an indication of a species' dielectric response to changes in e.g. conductivity of the medium or pH [162].

The frequency at which the DEP-force changes sign is called the cross-over frequency. It is also characterized by the Clausius-Mossotti factor being equal to zero. This is due to the fact that by definition, the real part of the complex Clausius-Mossotti factor (6.10) obtains values between -0.5 and 1.0 [166]. At negative $\mathrm{Re}[f^*_{CM}]$ values the DEP-force opposes the field gradient, i.e. particles collect at low field regions.

At positive values the DEP force and the gradient of the electric field are in the same direction, and consequently particles collect in the regions of high electric field. Thus, at the cross-over frequency also the Clausius-Mossotti factor changes sign.

6.3 Charge interactions

The electrostatic force acting on polarized particles depends on two length scales in addition to particle size. These are the characteristic length describing the extent of the spatial nonuniformity of the field and the distance between particles. When several particles are present in a system, the particles interact with one another in addition to coupling to the field. Effects due to charge images must be considered. This is true for colloids and live cells alike.

When two charged particles approach one another their mutual polarization interaction yields a change in their dipole moments. The induced mutual polarization interaction has been shown to play a crucial role in the DEP spectrum and cross-over frequency [202]. These correlation effects cannot, therefore, be ignored in the study of DEP. Take the interaction of a point charge and a point dipole. The separation between the dipole charges is much smaller than the distance at which the dipole is being observed and that from the viewpoint of the point charge the partial charges of the dipole seem to merge and cancel as the distance increases. The potential energy of this interaction is [160]

$$V = -\frac{p_1 q_2}{4\pi_0 r^2}. \tag{6.12}$$

The point-dipole approximation excludes many-body and multipolar interactions and thus errs considerably for more complicated interacting systems. This was also studied by Huang et al. by comparing the results obtained by the point-dipole model to those obtained by the multiple image approach [202].

Already the interaction of two polar molecules calls for refinement to the potential above. For the simplest case of two parallel dipoles one can write

$$V = -\frac{p_1 p_2 f(\theta)}{4\pi_0 r^3}, \qquad f(\theta) = 1 - 3\cos^2\theta. \tag{6.13}$$

However, a polar molecule with dipole moment p_1 can induce a dipole p_2* in a neighboring polarizable molecule. The interaction of a dipole with an induced dipole does not average to zero because the latter's orientation follows the former's [160]. Also the case of a particle being located in a strong electric field gradient or near a field null call for the application of multipolar moments [196]. This can be achieved by considering the dipole–

induced dipole (DID) model [203]. This multiple image method includes the effect of neighboring dipole moments, i.e. the creation of image dipoles. The formation of multiple images leads to an infinite series of image dipoles.

Huang et al. provide an analytical treatment of the matter in [200], where they construct a sum of dipole moments inside each particle and derive the expressions for the dipole factors. These, in turn, can be used to modify the DEP-force description (6.11) obtained previously. They find that when two polarizable particles approach one another, their mutual polarization gives rise to an interaction that changes the dipole moments of each of the individual particles. Numerical results provide the DEP crossover frequency as a function of medium conductivity for two particles at different separation and an isolated particle for comparison. The multiple image effect leads to a redshift in f_{CF} in a longitudinal and blueshift in a transverse field case. As the ratio r/D (particle separation to diameter) increases, the crossover spectrum approaches that of the isolated particle. Therefore the multipole images are important to take into account when the particles are touching or very close to one another. Several other results can be found in [200] all evidencing the strength of the spectral representation theory in providing detailed information and comparison between longitudinal and transverse field cases.

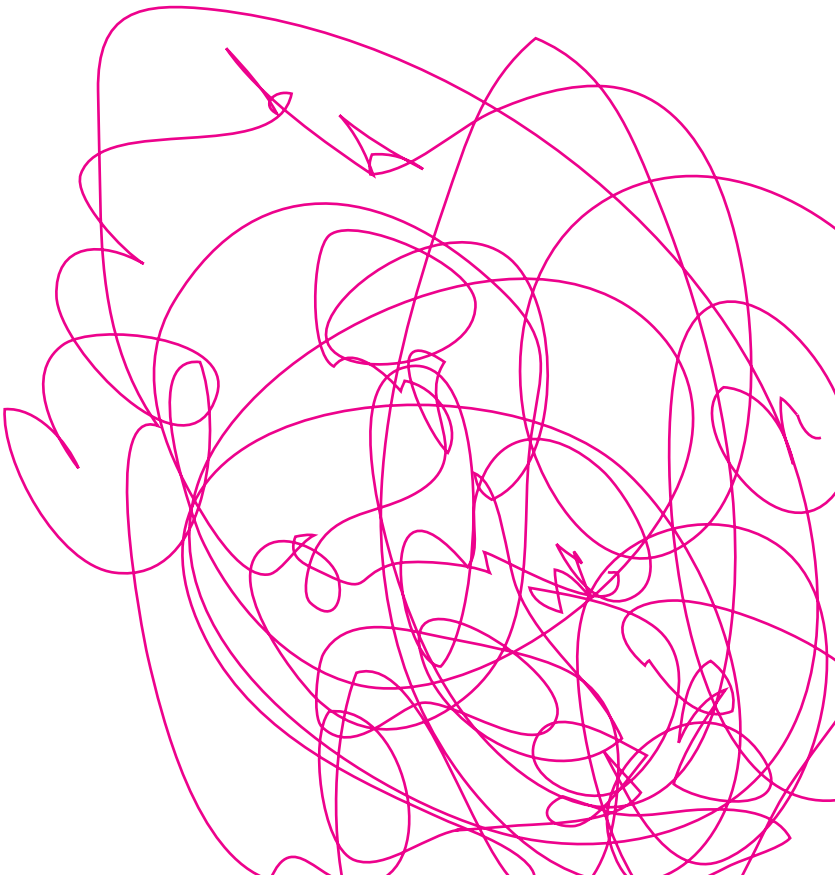

Chapter 7

Modeling Dielectrophoresis

7.1 Introduction

This chapter is based on publications III and IV (see p. 135) with research performed in collaboration with Emppu Salonen, Ilpo Vattulainen and Mikko Karttunen. Here are described the model and simulations that have been carried out to investigate the dielectrophoretic properties of colloidal particles and the use of molecular dynamics in the study of DEP. There is reason to point out that prior to the work discussed here there have been no computational model studies of DEP.

7.2 Model

The simulation system is shown in Fig. 7.1. A spherical particle in a dielectric medium will experience a force given by the coupling of the particle's induced dipole moment p and the electric field E as

$$\mathbf{F}_{DEP} = (\mathbf{p} \cdot \nabla)\mathbf{E}, \tag{7.1}$$

where $\mathbf{p} = \alpha_p \mathbf{E}$, i.e. the induced dipole moment is directly proportional to the electric field times total effective polarizability. The DEP force becomes

$$\mathbf{F}_{DEP} = \frac{1}{2}\alpha_p \nabla \mathbf{E}^2. \tag{7.2}$$

In order to transport sub-micrometer size colloids, the required large field gradient was obtained using a spherically symmetric DC electric

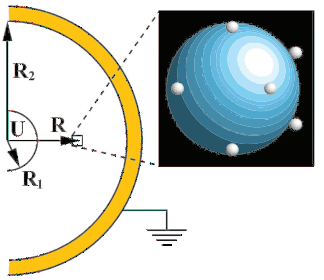

Figure 7.1. Particle polarized by an inhomogeneous field of a spherical capacitor.

$$E(R) = E_0 \left(\frac{R_0}{R} \right)^2 \hat{e}_R,$$

(7.3)

where E_0 is the electric field strength at the initial radial position R_0 of the colloid, and $\hat{e}_R$ is the radial unit vector. R_0 is also the characteristic length of the field, namely 1500 [1] as used in all the studies described in the following sections. The arising DEP force can be further written as

$$F_{DEP} = -2\alpha_p \frac{E_0^2}{R_0} \left(\frac{R_0}{R} \right)^5 \hat{e}_R.$$

(7.4)

Depending on the direction of the force, a distinction between positive and negative dielectrophoresis is made. If a particle is more polarizable than the medium, it will be attracted in the direction of higher field strength, resulting in positive DEP. The opposite case of a particle being less polarizable and subject to repulsion from the high field strength region, is called negative DEP. Thus, in the presence of a non-uniform electric field, the particles will move. These effects are not dependent on the polarity of the field, which makes them unique for DEP with respect to electrophoresis.

The choice of colloids in this computer simulation was based on their well-defined size, shape and interactions. As a generic, coarse-grained model for a polarizable particle we considered a charged spherical macroion, on which N_i small microions, are electrostatically bound. The microions carry a charge q = +2e each, and the macroion charge was set to $Q = -N_i q$. Thus the macroion-microion complexes or "colloids" are charge-neutral, as is the whole simulation system since $Q + N_i q = 0$.

Excluded volume interactions between all particles are modeled using a shifted repulsive Lennard-Jones potential, here called the WCA-potential [204]:

[1] For definition of σ, see eq. (7.5).

$$\Phi_{WCA} = 4\left[\left(\frac{\sigma}{r_{ij} - r_0}\right)^{12} - \left(\frac{\sigma}{r_{ij} - r_0}\right)^{6} + 1/4\right].$$

(7.5)

where $r_{ij} = |r_j - r_i|$ is the center to center distance between the interacting particles i and j. This formalism depicts a slight modification to the classical system of N molecules in a volume V whose total potential energy is written as a sum of spherically symmetric 6-12–type Lennard-Jones pair potentials. Here σ represents the sum of the solute and solvent radii, and since the size disparity between macroion and other particles is large, the range of the potential would be too big for the small particles in the system. This defect in the potential is corrected by shifting along the radial direction by r0 as proposed in [205]. The shifting of the potential was equal to ε. The WCA-potential is truncated at $r_{ij} = r_0 + 2^{1/6}$. The hard-core radius r0 was assigned a non-zero value equal to 4.5σ only in interaction pairs involving macroions.

The characteristic parameters and " of the potential Φ_{WCA} were chosen as the basic units of length and energy respectively. The unit of time is then $\tau = \sigma\sqrt{m/\varepsilon}$. Number density and temperature can also be represented in dimension free form as

$$\rho^* = N/V\sigma^3 = \rho\sigma^3$$

(7.6)

$$T^* = (\beta)^{-1},$$

(7.7)

where $\beta = 1/(k_B T)$.

Electrostatic interactions were calculated directly from Coulomb's law using a constant value of the relative permittivity of the medium ε_r, given by

$$\frac{1}{4\pi_{0r}} = 56\sigma/e^2,$$

(7.8)

where ε_0 is the vacuum permittivity. This formulation also ensures staying in the regime of strong Coulomb coupling, meaning in this case that the microions stay bound on the macroion surface.

The model being applied at the nanoscale it is intuitive to compare the DEP force to the thermal force,

$$F_{thermal} = \frac{k_B T}{2a_0},$$

(7.9)

where $a_0 \approx r_0 + \sigma/2$ is the effective radius of the colloid. The ratio of the two forces is then

$$\Theta = \frac{F_{thermal}}{F_{DEP}} = \frac{k_B T}{\alpha_p a_0 \left|\nabla E^2\right|}.$$

(7.10)

At small values of the DEP force dominates whereas for large Θ the thermal motion becomes increasingly important. Theta-values were obtained through simulations.

For the used field strength and temperature, the magnitude of the thermal noise to DEP force Θ varied from 0.07 to 40. However, for a given simulation this value changed according to radial position of the particle in the electric field (due to $F_{DEP} \propto R^{-5}$, see Eq. 7.4). In the next sections the simulations are discussed in more detail.

7.3 One-colloid case

7.3.1 Simulation set-up

Classical MD simulations were used to simulate the dielectrophoretic behavior of a single charge-neutral nano-sized colloidal particle. The cubic simulation cell had a side length of $L_0 = 35\sigma$, the effective particle radii being 5σ for the macroion and $\sigma/2$ for the solvent and microion particles. (We have in mind the radius of the macroion to be of the order of 1 nm.) Solvent number density was chosen as $\rho_s = 0.3\sigma^{-3}$ as depicted in the MD electrophoresis study of Tanaka and Grosberg [206] excluding the volume occupied by the other particles. The solvent and microion particles were assigned a mass equal to $1m$, and the macroion the mass of bulk solvent corresponding to its volume, i.e. $155m$ ($1m \approx 30\ amu$). Thus the simulation cell mass density was uniform. In the absence of the field, the microions distribute evenly on the macroion surface. This is due to the mutual repulsion of the likecharged microions. When the external field is applied, the redistribution of the microions yields the polarization effect of the colloid.

For the DEP force the polarizability α_p was calculated as follows. The colloid was allowed to polarize in a selected electric field strength. The system was then quenched to a low temperature in order to obtain the minimum energy state. The dipole moment $p = \Sigma_i q_i r_i$ was linearly proportional to the electric field strength, as can be seen from Fig. 7.2 where the later-used electric field strengths are highlighted. A linear fit gave for the polarizability $\alpha_p = 4.94 \pm 0.16 e^2\sigma^2/\varepsilon$. The remaining volume in the simulation box was filled with the neutral solvent particles up to the chosen number density.

The field was further tested by changing the polarity from $+100V$ to $-100V$ corresponding to $|E_0| = 0.96\varepsilon/e\sigma$. The colloid was expected to move in the direction of higher field strength despite the polarity, which was observed, see Fig. 7.3. This result validated the use of the current model distinctly for DEP.

The system was then thermalized for a period of 85τ at the desired temperature, ranging from $T = 0.03 - 2.4\varepsilon/k_B$ corresponding to 10 – 720 K, by coupling to the Berendsen thermostat [115]. For the production runs the thermostat coupling was retained only within a distance of 1 from the simulation cell borders. This allowed for the neutralization of the dissipated heat that resulted from the work done by the electric field on the colloid as suggested in [206], where it was also proven that this action did not produce anomalous hydrodynamics. The current system depicted negligible Joule heating, nevertheless the border thermostat was left in place.

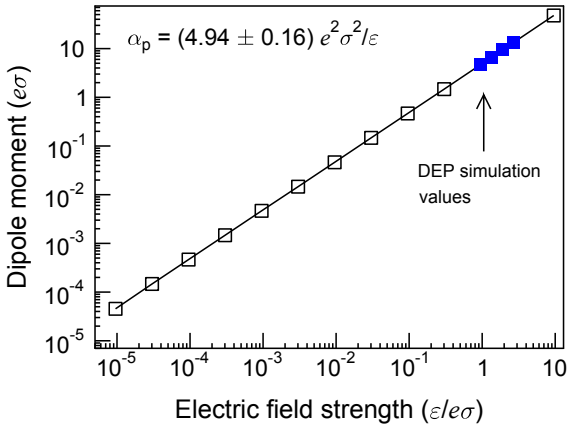

Figure 7.2. Induced dipole moment p as a function of the electric field strength E.

The equations of motion were integrated using the velocity Verlet algorithm [110] with time steps between 0.002τ and 0.004τ depending on temperature. The total simulation time was 5785τ. The DEP force was varied through choice of field strength, $E_0 = 0.96,\ 1.35,\ 1.91$ and $2.70\ \varepsilon/e\sigma$, giving as the ratios of the DEP force approximately 1 : 2 : 4 : 8. To handle the particle movement in the non-homogeneous field geometry, an electric field frame of reference was created with a periodic solvent particle shifting [207]. For each electric field strength and temperature combination a set of 20-80 simulations was carried out in order to obtain reliable statistics.

Finite-size effect

The balance between finite-size effects and computational efficiency was obtained after testing simulation cell sizes between 20σ and 42.5σ and the respective amount of solvent particles ranging from 2239 to 22728. During the tests the temperature was kept at $0.03\ \varepsilon/k_B$ in order to minimize statistical fluctuations.

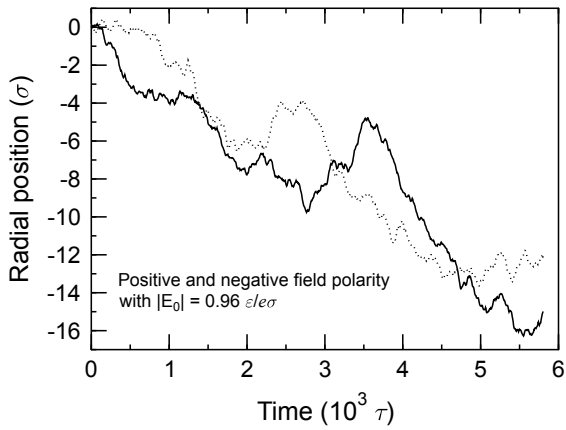

Figure 7.3. Colloid displacement in two different field polarities, solid (dotted) line positive (negative) polarity case.

The low-density fluid used here seemed to produce the effect that the average colloid radial displacements $\langle \Delta R \rangle$ increased with decreasing L_0, see Fig. 7.4. This is in contrast to the known relation of hydrodynamic friction $\eta \propto L_0^{-1}$ [208, 209], however also observed by Tanaka and Grosberg [206]. Calculation of the Schmidt number further convinced us that the friction experienced by the colloid was in fact strongly dependent on system size and the number of solvent particles.

Based on careful consideration of the above and the fact that the simula-

tion system did not conserve momentum (temperature coupling needed) the system size was set at $L_0 = 35\sigma$. The resulting colloid displacements were larger than for a similar system of more solvent particles, however all the reported simulations were carried out for the same system size parameters and thus all observed effects are in agreement relative to one another. A systematic comparison to experiments was not the aim of this study but the verification of the DEP model itself.

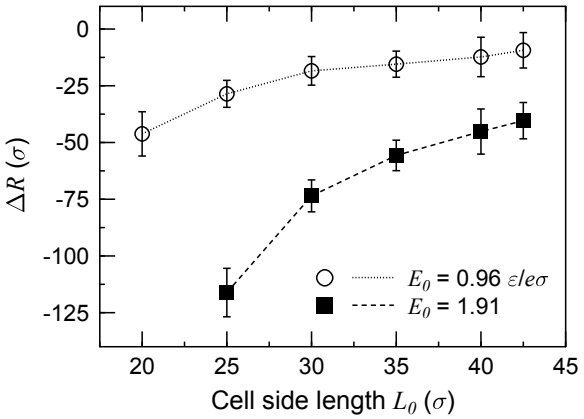

Figure 7.4. Radial displacements as a function of cell size.

7.3.2 Results

The main results of this study were the colloid radial displacements. The average radial displacement over a time interval Δt is

$$\langle \Delta R \rangle = \frac{F_{DEP}}{\xi} \Delta t, \tag{7.11}$$

where ξ is the friction factor of the solvent. Figure 7.5 shows average colloid radial displacements at the end of the simulations for three different temperatures (10 – 300 K). As the radial position of the colloid changes, so does the magnitude of the electric field and its gradient in the nonhomogenous field configuration. The figure also shows the increase of the colloid Brownian motion with increased temperature and the subsequent decrease in average colloid radial displacement. The temperature dependence was investigated further, see Fig. 7.6. This brings us to the question whether the DEP force for a given polarization is the same at different temperatures. The solvent particle collisions with the microions generate fluctuation in the dipole moment of the colloid. However, such collisions were proven never

to cause microion loss from the surface and consequent drastic changes in the charge environment. Instead the dipole moment of a given simulation system fluctuated around the value obtained for the minimum energy configuration after quenching.

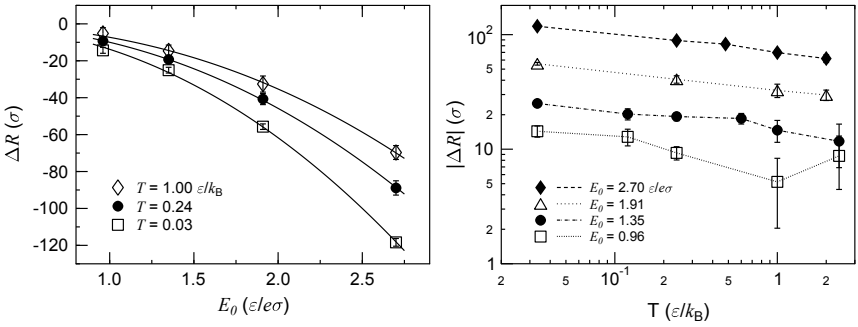

Figures 7.5. and 7.6. *Average colloid radial displacements. Absolute values of radial displacements as a function of temperature.*

The direction of the colloid movement was governed by the fact that the colloid was more polarizable than the medium, resulting in positive DEP, i.e. particle movement towards higher field strength. Morgan et al. defined particle DEP mobility μDEP in [174]. We have obtained a general relation with respect to our simulation parameters as

$$\mu_{DEP} = \frac{\alpha_p}{2\xi},$$

(7.12)

which is related to the particle average velocity due to the field

$$\langle v_{DEP} \rangle = \mu_{DEP} \nabla E^2.$$

(7.13)

This was calculated from particle trajectories and the average values of ∇E^2 over a chosen time interval from the beginning of the simulations giving the mobilities as shown in Figures 7.7 and 7.8.

The data for all E_0 at a given temperature was consistent, although only selected field strengths are shown. For lower E_0 the DEP movement is less pronounced and the increase of noise is evident, as can be seen from the error bars of the $E_0 = 0.96\varepsilon/e\sigma$ case (Fig. 7.7) and the $E_0 = 1.35\varepsilon/e\sigma$ case (Fig. 7.8).

The fact that the mobility changes with time implies that also the friction factor ξ is prone to this variation. This indicates the coupling of the motion of the colloid with the solvent velocity field. Due to the non-equilibrium behavior of the colloid further analysis of this effect is difficult. However one can assume that the characteristic time scale for the evolution of this transport phenomenon is temperature dependent.

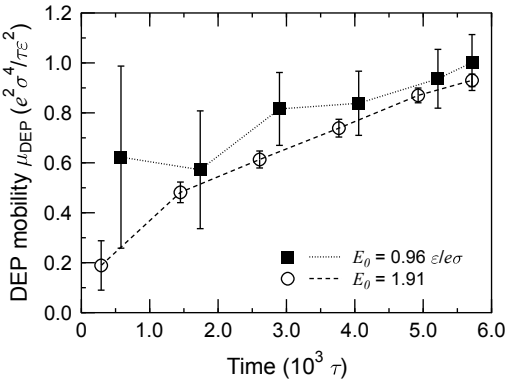

Figure 7.7. Colloid mobility at T = 0.03 "/kB = 10 K.

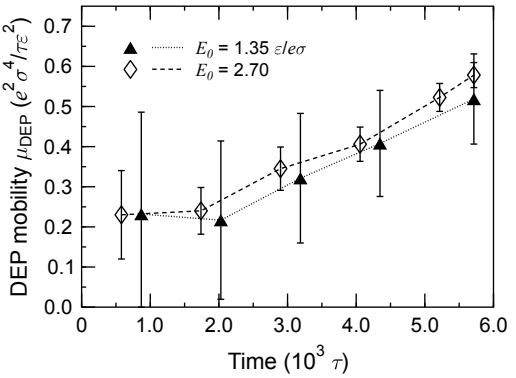

Figure 7.8. Colloid mobility at T = 1.0 "/kB = 300 K.

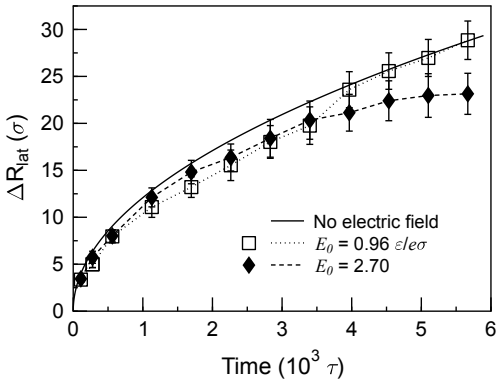

Figure 7.9. Lateral displacements at T = 1.0 "/kB = 300 K.

The colloid motion was further studied using displacements R_{lat} in the y-z plane. This refers to the colloid movement perpendicular to the electric field gradient, i.e. deviations from the driving DEP force direction. Results are shown in Fig. 7.9. Particle movement in this plane is a challenge to the accuracy of particle manipulation by DEP.

The solid line in Fig. 7.9 refers to the diffusion prediction at zero field $\Delta R_{lat}(t) = \sqrt{4Dt}$. High field strength cases clearly deviate from this prediction indicating a steering effect of the field gradient on the colloid. Perhaps also the coupling of the particle motion to the abovementioned solvent velocity field suppresses the lateral motion. This seems to take place during the course of the simulation through lowering of the natural solvent friction factor and subsequent loss of the equilibrium nature of the particle motion.

7.4 Two-colloid case

In experimental studies several particles are normally transported, separated or trapped at a time. As manipulated particles drift into close proximity of one another, their mutual interactions lead to modifications in their electric polarization and the DEP force affecting them. Such changes may result in enhanced trapping efficiencies at non-dilute conditions. This would be beneficial from the electrokinetics point of view if it were a means to overcome the large thermal noise associated with small (nanoscale) particle motion.

7.4.1 Simulation set-up

Molecular dynamics simulations were used to study the aggregation and DEP transport of a dimer comprising two spherical colloids. Each macroion carried a charge equal to $Q = -N_i q$ where $q = +2e$ is the microion valence. Three different macroion sizes were employed with the hard-core radii r0 =4.5, 16.9 and 29.6 with the number of microions on the surface increasing correspondingly, $N_i = 10,\ 100$ and 300. This resulted in similar microion densities on the macroion surface. Overall charge-neutrality was strictly enforced.

The influence of colloid–colloid interactions on dipole moments was investigated in the absence of solvent. The microions were allowed to move freely on the surface of the two macroions fixed in space at a distance D apart. The energy minimum was investigated by quenching with the Berendsen thermostat. Figure 7.10 shows the dipole moments as the colloid separation is varied with $N_i = 10$ (open squares), $N_i = 100$ (filled circles) and $N_i = 300$ (open diamonds). The solid line is the analytical prediction in the continuum limit [200].

For large N_i and large colloid the results are in best agreement with the theoretical prediction (solid line). The worsening of this agreement for smaller systems is due to the pronounced discrete nature of the microion distribution and highlights the fact that continuum theories are not applicable in the nanoscale. Yet it is rather remarkable how well the continuum description predicts at least the qualitative behavior down to very small scales. The inset shows the total attractive force between the two colloids of the dimer with $N_i = 10$, solid line being the pure dipole-dipole contribution to the electrostatic force. The same trend in results was observed for the case of the dimer being aligned perpendicular to the field.

The colloidal dimer with $r_0 = 4.5$ and $N_i = 10$ was then immersed in a solvent of explicit neutral particles of density $\rho_s = 0.3\sigma^{-3}$ as in the one-colloid case. A cubic simulation cell with a side length of 45 was used, the solvent then comprising about 27000 particles.

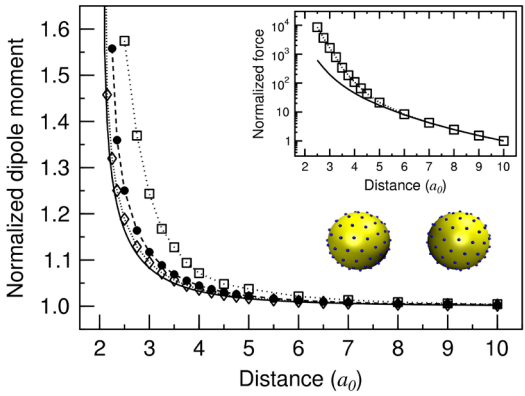

Figure 7.10. Dipole moments for colloids parallel to field.

Test simulations with a larger number of solvent particles showed that already this system size resulted in minimal finite-size effects.

The electric field strengths used were $E_0 = 0.68, 0.96, 1.35, 1.91$ and $2.7\varepsilon/e\sigma$. For each combination of E_0 and system temperature $0.03\varepsilon/k_B \leq T \leq 1.0\varepsilon/k_B$, 50–160 independent DEP simulations of length 5785τ were carried out.

7.4.2 Results

The DEP force on a dimer is larger than on a single nanocolloid. Also, the frictional force on the dimer is larger. An estimate of the ratio of the frictional force of a dimer to that of a single colloid, ξ_2/ξ_1 is given by Swanson et al. [170]. For the dimer aligned in parallel with the field $\xi_2^{\parallel}/\xi_1 \approx 1.29$ and for the perpendicularly aligned dimer $\xi_2^{\perp}/\xi_1 \approx 1.43$. A simple estimate for the dimer DEP displacement ΔR_2 in terms of the single colloid displacement ΔR_1 can then be obtained as

$$\Delta R_2 \approx \frac{F_2(R_0)}{F_1(R_0)} \left(\frac{\xi_1}{\xi_2^{\parallel}} \right) \Delta R_1, \tag{7.14}$$

since the dimer is mostly aligned parallel to the field. Not taking into account the spacial variance of the field, Fi(R0) is here the initial DEP force on the i-particle colloid system.

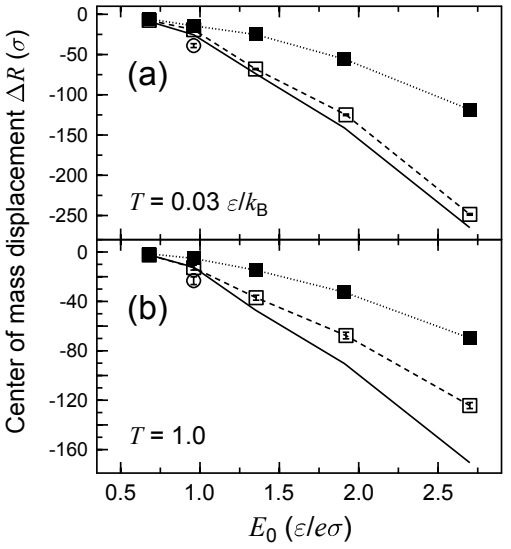

Figure 7.11. Mean radial displacements at (a) $\mathrm{T} = 0.03\ \varepsilon/k_B = 10\ \mathrm{K}$ *and (b)* $\mathrm{T} = 1.0\ \varepsilon k_B = 300\ \mathrm{K}$ *for dimer (open) and monocolloid (solid square).*

Figure 7.11 shows the comparison of the mean radial displacements of the dimer with those of the single colloid case (cf. Sec. 7.3.2). The solid line is the prediction based on (7.14). For high field strengths the dimer (open squares) clearly travels further than the single colloid (solid squares) in the same simulation time. For low field strengths the difference is not that great. The open circles at $E_0 = 0.96\varepsilon/\mathrm{e}\sigma$ represent a case where the dimer polarization was split into two separate states. The fraction of simulations with larger polarization was well below 50% for both temperatures. In some rare cases the dimer would change polarization during the course of the simulation. To summarize, Fig. 7.11 shows that the DEP force acting on the dimer sufficiently outweighs the increase in solvent-based friction. Therefore aggregation of single colloids to form dimer, or more complex structures seems feasible for obtaining more efficient DEP transport.

Through the increase in the friction factor, rotation of the dimer will decrease the efficiency of DEP. This is most likely to occur at higher temperatures. Besides the increase in the friction factor from parallel to perpendicular alignment with respect to the field, the dipole moment of the rotating dimer changes according to the change in microion distribution in response to the field. The external electric field exerts on the rotating dimer an electrostatic torque

$$\Gamma = p_2(R,\theta) \times E(R),$$

(7.15)

where p2, the dimer dipole moment, depends on the radial position R as well as the orientation angle . The characteristic time scale of rotation can be shorter than that needed for reorientation of the microions. This affects the actual values of the dipole moment. Figure 7.12 shows the values of the torque at $E_0 = 1.91\varepsilon/e\sigma$ and $1464\sigma \le R \le 1539\sigma$.

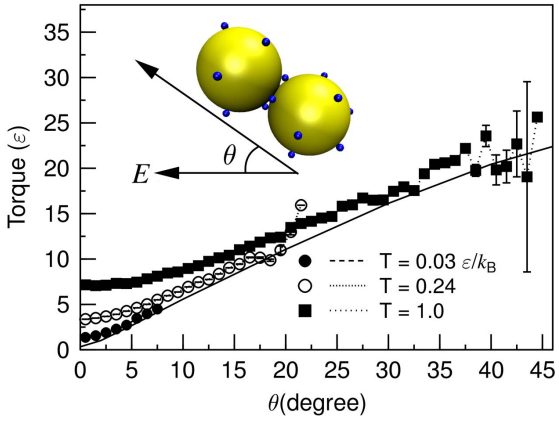

Figure 7.12. Torque on the dimer as a function of orientation.

For low temperatures the dimer rotations are slow and result in a smaller torque (solid circles in Fig. 7.12). In simulations at the lowest temperature, the dimer is not observed to deviate much from being aligned parallel with the field. With increasing temperature, the fluctuations in the microion distribution on the colloids result in higher Γ-values even for small angles.

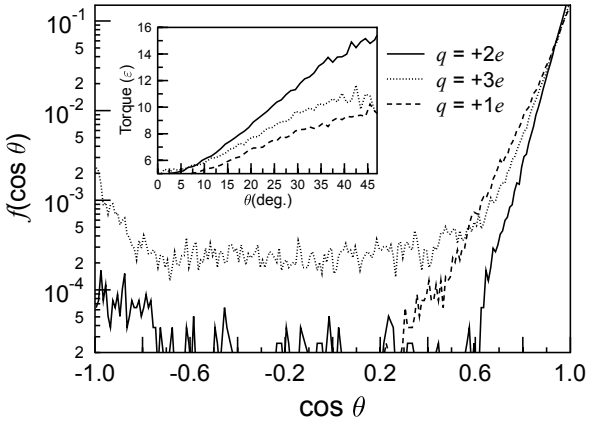

Figure 7.13. Dimer orientations with respect to E-field.

To further test the microion distribution effects on dimer rotation, microion valences of $q = +1e$ and $q = +3e$ were used. The orientational distributions of the dimers is shown in Figure 7.13, with the inset showing the torque for different microion valencies at $E_0 = 1.35\varepsilon/e\sigma$ and $T = 1.0\varepsilon/k_B$. The orientations are biased toward $cos\theta = 1.0$ due to the starting configuration of the dimer parallel to the field. The distribution shows that the 2-valence case rotates less than the two other. This is also indicated by the differences in the Γ-values.

7.5 Conclusions

The above studies show that the current DEP model is valid for studying single molecule and dimer behavior under non-uniform external electric fields. The model incorporates a non-conducting solvent which enables capturing the gross hydrodynamics and has experimental relevance to e.g. reverse micelles [210] and reverse phase emulsions [211]. Studies show particle coupling to the external field, the correlation of this coupling with particle shape, and the impact on particle mobility. Particle motion is also coupled to the velocity field that changes with temperature, creating challenges for the overall manipulation of particles by DEP.

Aggregation is shown in the dimer case to be an efficient way to increase the DEP force. The subsequent increase in solvent-based friction is not sufficient to counter this effect. Dimer rotation increases with temperature, and affects the dipole moment that couples to the electric field. However, controlled aggregation can be a tool for accurate particle manipulation in external electric fields.

For small particles the thermal effects are important. Soft-matter systems are generally susceptible to change by thermal energies of the order of k_BT. In DEP, however, these can be overcome by careful choice of system parameters, and for very small particles the enhanced DEP due to aggregation can be a part of the answer. Colloids in the nano-regime can be efficiently manipulated by dielectrophoresis. The fact that the particle motion in a non-homogeneous electric field is a non-equilibrium process does not make it a less suitable method for experimental use. This simply poses a challenge for unveiling the theoretical background behind the observed phenomena.

Several questions remain to be answered by theory and computational studies, namely the effect of co- and counter-ions in solution, the temperature dependence of the coupling to the solvent velocity field, and many-particle aggregation phenomena, just to name a few. Work will continue also in

model development in order to better tackle these questions.

In the meanwhile, the experimental community has surged in using dielectrophoresis for new techniques and applications. Bacterial genetics and flow-through devices could be the next important fields in DEP. Physical separation of particles with respect to their dielectric properties is efficient and inexpensive using DEP together with a flow-through device [212, 213]. Flores-Rodriguez and Markx used this method in a recent study with barium titanate particles [214]. Castellarnau et al. have recently examined the use of DEP to distinguish between wildtype bacterial cells and their mutant derivatives with a modified phenotype. Hunt and Westervelt developed dielectrophoresis tweezers for single cell manipulation with a wide range of possible applications in *in vitro* fertilization, cell-cell interaction, cell adhesion, embryology, microbiology, stem cell research as well as single cell transfection [215].

Summary and Outlook

The intriguing phenomena taking place at the biological cell boundary call for detailed experimental as well as theoretical and computational considerations. The cell membrane plays a crucial role in determining the size, shape and electrical characteristics of the cell. These are also the attributes that take part in controlling cell interactions with the environment and substance transport to and from the cell.

It was found that the complexity of the biological membrane is yet to be thoroughly revealed. Transport of small solutes into the cell take place through several possible pathways. A well-known interaction is through protein channels in the membrane. Experimental and computational evidence support the hypothesis that small solutes also interact directly with the lipid molecules in the bilayer that protect the cell interior. The exact mechanism of these interactions may be manyfold but involve hydrogen bonding and conformational as well as pressure changes. These changes manifest themselves in the structural properties of the membrane such as area per lipid.

Further studies include two– to many-component bilayers and the effect of ethanol as well as concentration studies involving the unsaturated PDPC bilayer. Other solutes and anesthetic studies are likewise underway. Great emphasis is also put on the study of pressure profiles for various systems and the refinement of underlying simulation and analysis tools. Coarse grained molecular dynamics was used to tackle dielectrophoresis of colloidal soft-matter particles. Individual colloids as well as dimer formations were studied in an external electric field produced via spherical capacitor geometry. Particle polarization coupled to the external field and subsequent movement was evidenced. Thermal effects were quantified as well as the impact on results of different dipole strengths and the influence of dimer geometry with respect to the field. Dielectrophoresis was found to be an efficient way to transport particles even in the very small size regime. Our study of nanocolloids proved the technique applicable even to nanoscale system sizes and offered evidence that the effect could be enhanced by aggregation of particles. The molecular dynamics method turned out to be reliable and fast. Results were compared to existing theory. DEP transport and manipulation such as trapping can be applied to a variety of biologically relevant species as well.

The future possibilities are manifold. DEP studies for different particle shapes and further aggregation phenomena are underway. Technical development of the simulation protocol to incorporate AC fields and ionic solutions would create a wide range of new possibilities.

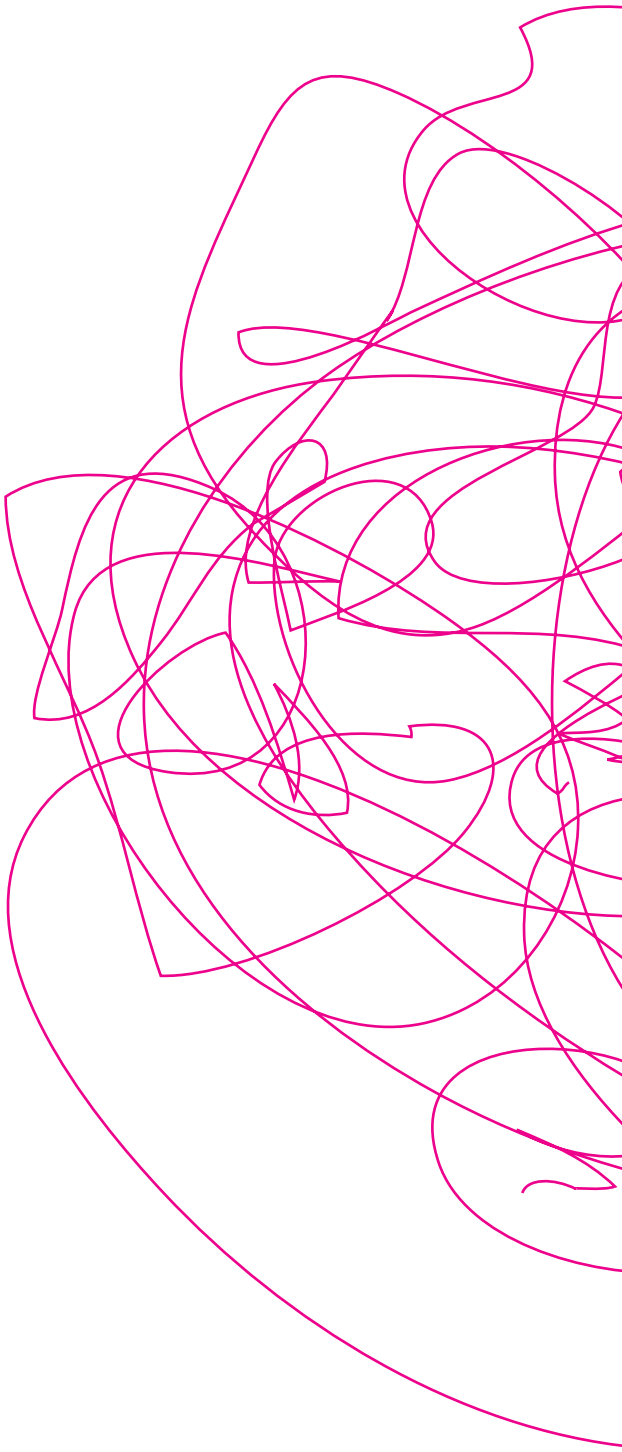

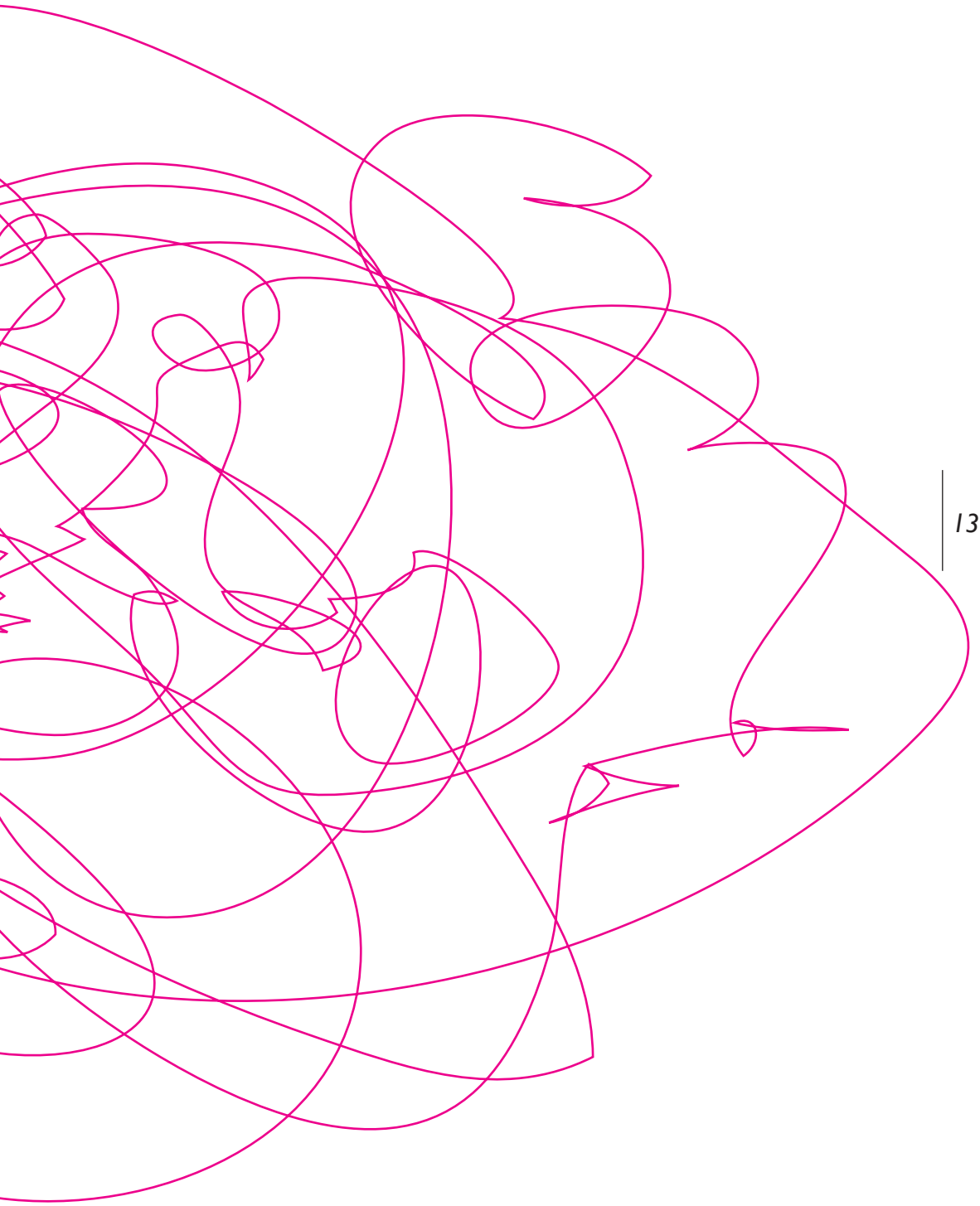

List of Publications

The thesis is based on the following publications:

I

M. Patra, E. Salonen, E. Terama, I. Vattulainen, R. Faller, B.W. Lee, J. Holopainen and M. Karttunen, *Under the influence of alcohol: The effect of ethanol and methanol on lipid bilayers,* Biophys J 90, 1121- 1135 (2006). (Part I)

II

E. Terama, S. Ollila, M. Patra, A. Rowat, C. Trandum, P. Westh, E. Salonen, M. Karttunen and I. Vattulainen, *Influence of ethanol on lipid membranes: From lateral pressure profiles to dynamics and partitioning,* to be submitted. (Part I)

III

E. Salonen, E. Terama, I. Vattulainen and M. Karttunen, *Dielectrophoresis of nanocolloids: A molecular dynamics study,* Eur. Phys. J. E 18, 133-142 (2005). (Part II)

IV

E. Salonen, E. Terama, I. Vattulainen and M. Karttunen, *Enhanced dielectrophoresis of nanocolloids by dimer formation,* submitted to Phys. Rev. Lett. (Part II)

The author has participated in the planning, execution and write-up of the above publications. In publication I the author did a large part of the analysis and participated in drawing the conclusions for the manuscript. Publication II is a follow-up of publication I for which the author has done system set-up, simulations, part of analysis and written the publication. In publications III and IV the author has actively participated in all stages from model development to writing, and has contributed to the final products equally with co-author E. Salonen.

Bibliography

[1] P. L. Yeagle, editor, The structure of biological membranes, CRC press, Boca Raton, FL, 2nd edition, 2005.

[2] K. Simons and W. L. C. Vaz, Annu. Rev. Biophys. Biomol. Struct. 33, 269 (2004).

[3] M. Edidin, Nature Rev. Mol. Cell. Bio 4, 414 (2003).

[4] M. Edidin, Annu. Rev. Biophys. Biomol. Struct. 32, 257 (2003).

[5] D. A. Brown and E. London, Annu. Rev. Cell Dev. Biol. 14, 111 (1998).

[6] M. Bloom, E. Evans, and O. G. Mouritsen, Quarterly Rev. of Biophysics 24, 293 (1991).

[7] R. B. Gennis, Biomembranes. Molecular Structure and Function, Springer Advanced Texts in Chemistry, Springer, New York, NY, 1989.

[8] S. J. Singer, Annu. Rev. Physiol. 66, 1 (2004).

[9] S. J. Singer and G. L. Nicolson, Science 175, 720 (1972).

[10] O. G. Mouritsen, Life – as a matter of fat, Springer, Berlin, 2005.

[11] K. Simons and E. Ikonen, Nature 387, 569 (1997).

[12] B. Alberts, D. Bray, J. Lewis, M. Raff, K. Roberts, and J. D. Watson, Molecular Biology of The Cell, Garland, 3rd edition, 1994. 133

[13] A. Guichet, T. Wucherpfennig, V. Dudu, S. Etter, M. Wilsch-Bräuniger, A. Hellwig, M. Gonz´alez- Gait´an, W. B. Huttner, and A. A. Schmidt, EMBO J. 21, 1661 (2002).

[14] T. P. W. McMullen, R. N. A. H. Lewis, and R. N. McElhaney, Curr. Opin. Coll. Interf. Sci. 8, 459 (2004).

[15] H. T. McMahon and J. L. Gallop, Nature 438, 14 (2005).

[16] A. Ottova and H. T. Tien, Bioelectrochemistry 56, 171 (2002).

[17] R. Koynova and M. Caffrey, Chem. Phys. Lipids 115, 107 (2002).

[18] S. Tristram-Nagle and J. F. Nagle, Chem. Phys. Lipids 127, 3 (2004).

[19] S. C. Chen, J. M. Sturtevant, and B. J. Gaffney, Proc. Natl. Acad. Sci 77, 5060 (1980).

[20] A. Seelig and J. Seelig, Biochemistry 16, 45 (1977).

[21] M. B. Sankaram and T. E. Thompson, Proc. Natl. Acad. Sci. USA 88, 8686 (1991).

[22] R. F. M. de Almeida, A. Fedorov, and M. Prieto, Biophys. J. 85, 2406 (2003).

[23] K. Gawrisch, The structure of biological membranes, chapter 4, pp. 147–171, CRC Press, Boca Raton, FL, 2nd edition, 2005.

[24] A. D. Leach, Molecular Modeling: Principles and applications, Addison-Wesley Longman, Edinburgh, 1996.

[25] J. H. Davis, Biochim. Biophys. Acta 737, 117 (1983).

[26] R. W. Pastor, R. M. Venable, and S. E. Feller, Acc. Chem. Res. 35, 438 (2002).

[27] I. Vattulainen and M. Karttunen, Computational Nanotechnology, American Scientific Publishers, Stevenson Ranch, CA, 2004.

[28] N. W. Ashcroft and N. D. Mermin, Solid state physics, Hold-Saunders, 1:st edition, 1976.

[29] E. A. Evans, R. Waugh, and L. Melnik, Biophys. J. 16, 585 (1976).

[30] G. Gompper and M. Schick, Self-Assembling Amphiphilic Systems, Academic Press, London, 1995.

[31] E. Evans and W. Rawicz, Phys. Rev. Lett. 64, 2094 (1990).

[32] S. A. Safran, Statistical thermodynamics of surfaces, interfaces and membranes, Addison-Wesley, Reading, MA, 1994.

[33] I. Vattulainen and O. G. Mouritsen, Diffusion in condensed matter, chapter 12, pp. 473–511, Springer, Berlin, 2005.

[34] H. C. Berg, Random walks in biology, Princeton University Press, Princeton, 1993.

[35] P. Hänggi, P. Talkner, and M. Borkovec, Rev. Mod. Phys. 62, 251 (1990).

[36] J. Mart´i and F. S. Csajka, Europhys. Lett. 61, 409 (2003).

[37] E. Hessel, A. Herrmann, P. Müller, P. P. M. Schnetkamp, and K.-P. Hofmann, Eur. J. Biochem. 267, 1473 (2000).

[38] S. König, T. M. Bayerl, G. Coddens, D. Richter, and E. Sackmann, Biophys. J. 68, 1871 (1995).

[39] C. Hofsäss, E. Lindahl, and O. Edholm, Biophys. J. 84, 2192 (2003).

[40] A. Filippov, G. Orädd, and G. Lindblom, Biophys. J. 84, 3079 (2003).

[41] A. Filippov, G. Orädd, and G. Lindblom, Langmuir 19, 6397 (2003).

[42] E. Lindahl and O. Edholm, J. Chem. Phys. 115, 4938 (2001).

[43] P. Niemelä, M. T. Hyvönen, and I. Vattulainen, Biophys. J. 87, 2976 (2004).

[44] S. J. Marrink and H. J. C. Berendsen, J. Phys. Chem. 100, 16729 (1996).

[45] D. Bemporad, J. W. Essex, and C. Luttmann, J. Phys. Chem. B 108, 4875 (2004).

[46] S. T. Burns and M. G. Khaledi, J. Pharma. Sci. 91, 1601 (2002).

[47] E. S. Rowe, Biochim. et Biophys. Acta 813, 321 (1985).

[48] E. S. Rowe, Biochemistry 22, 3299 (1983).

[49] P. Westh, C. Trandum, and Y. Koga, Biophys. Chem. 89, 53 (2001).

[50] D. Bassolino-Klimas, H. E. Alper, and T. R. Stouch, J. Am. Chem. Soc. 117, 4118 (1995).

[51] R. S. Cantor, J. Phys. Chem. B 105, 7550 (2001).

[52] D. R. Carl and S. E. Feller, Langmuir 19, 8560 (2003).

[53] S. Mitragotri, M. E. Johnson, D. Blanckschtein, and R. Langer, Biophys. J. 77, 1268 (1999).

[54] H. V. Ly and M. L. Longo, Biophys. J. 87, 1013 (2004).

[55] J. T. H. Connor, Science 304, 54 (2004).

[56] B. Antkowiak, Naturwissenschaften 88, 201 (2001).

[57] L. J. Mullins, Chem. Rev. 54, 289 (1954).

[58] P. Seeman, Pharmacol. Rev. 24, 583 (1972).

[59] J. H. Chin and D. B. Goldstein, Science 196, 684 (1977).

[60] T. H. Stanley, BUMC Proc. 13, 7 (2000).

[61] J.-M. Alakoskela, Interactions in lipid-water interface assessed by fluorescence spectroscopy, PhD thesis, University of Helsinki, Helsinki, Finland, 2006.

[62] P. L. Silvestrelli and M. Parrinello, J. Chem. Phys. 111, 3572 (1999).

[63] K. P. C. Vollhardt and N. E. Schore, Organic Chemistry, Freeman, 5th edition, 2005.

[64] S. S. Zumdahl, Chemistry, Houghton Mifflin, Boston, 4th edition, 1997.

[65] S. Patterson, The St. Petersburg Times 59 (2001).

[66] J. W. Moore, C. L. Stanitski, and P. C. Jurs, Chemistry, Brooks/Cole, Belmont, CA, 2nd edition, 2005.

[67] Y. F. Yano, Colloid Interface Sci. 284, 255 (2005).

[68] T. Takamuku, K. Saisho, S. Nozawa, and T. Yamaguchi, J. Mol. Liquids 119, 133 (2005).

[69] M. Patra, E. Salonen, E. Terama, I. Vattulainen, R. Faller, B. W. Lee, J. Holopainen, and M. Karttunen, Biophys. J. 90, 1121 (2006).

[70] E. Terama, S. Ollila, M. Patra, A. Rowat, C. Trandum, P. Westh, E. Salonen, M. Karttunen, and I. Vattulainen, Influence of Ethanol on Lipid Membranes: From Lateral Pressure Profiles to Dynamics and Partitioning, to be submitted, 2006.

[71] P. Buchanan, N. Aldiwan, A. K. Soper, J. L. Creek, and C. A. Koh, Chem. Phys. Lett. 415, 89 (2005).

[72] J. J. C. Mansure, A. D. Panek, L. M. Crowe, and J. H. Crowe, Biochim. Biophys. Acta 1191, 309 (1994).

[73] N. P. Franks and W. R. Lieb, Nature 274, 339 (1978).

[74] V. C. Abadji, D. E. Raines, L. A. Dalton, and K. W. Miller, Biochim. Biophys. Acta 1194, 25 (1994).

[75] W. R. Klemm, Alcohol 7, 49 (1990).

[76] C. P. Cartwright, F. J. Veazey, and A. H. Rose, J. Gen. Microbiol. 133, 857 (1987).

[77] K. Tu, M. Tarek, M. L. Klein, and D. Scharf, Biophys. J. 75, 2123 (1998).

[78] L. Koubi, M. Tarek, M. L. Klein, and D. Scharf, Biophys. J. 78, 800 (2000).

[79] L. Koubi, M. Tarek, S. Bandyopadhyay, M. L. Klein, and D. Scharf, Biophys. J. 81, 3339 (2001).

[80] C. Ho and C. D. Stubbs, Biochemistry 36, 10630 (1997).

[81] S. E. Feller, C. A. Brown, D. T. Nizza, and K. Gawrisch, Biophys. J. 82, 1396 (2002).

[82] R. Cantor, Biophys. J. 36, 2339 (1997).

[83] R. S. Cantor, J. Phys. Chem. B 101, 1723 (1997).

[84] R. S. Cantor, Biophys. J. 76, 2625 (1999).

[85] N. P. Franks and W. R. Lieb, Science 254, 427 (1991).

[86] R. G. Eckenhoff and J. S. Johansson, Pharmacol. Rev. 49, 343 (1997).

[87] E. Wachtel, N. Borochov, D. Bach, and I. R. Miller, Chem. Phys. Lipids 92, 127 (1998).

[88] S. J. Slater, C. Ho, F. J. Taddeo, M. B. Kelly, and C. D. Stubbs, Biochemistry 32, 3714 (1993).

[89] F. Zhang and E. Rowe, Biochemistry 31, 2005 (1992).

[90] Z. Zhou, B. G. Sayer, D. W. Hughes, R. E. Stark, and R. M. Epand, Biophys. J. 76, 387 (1999).

[91] J. A. Barry and K. Gawrisch, Biochemistry 33, 8082 (1994).

[92] J. A. Barry and K. Gawrisch, Biochemistry 34, 8852 (1995).

[93] L. L. Holte and K. Gawrisch, Biochemistry 36, 4669 (1997).

[94] B. W. Koenig and K. Gawrisch, J. Phys. Chem. B 109, 7540 (2005).

[95] C. A. Rutkowski, L. M. Williams, T. H. Haines, and H. Z. Cummins, Biochemistry 30, 5688 (1991).

[96] F. Hallett, J. Marsh, B. Nickel, and J. Wood, Biophys. J. 64, 435 (1993).
[97] B. König, H. Strey, and K. Gawrisch, Biophys. J. 73, 1954 (1997).

[98] H. V. Ly, Effect of short-chain alcohols on elasticity, stability and phase transition of lipid membranes, PhD thesis, University of California at Davis, Davis, California, USA, 2003.

[99] W. Rawicz, K. C. Olbrich, T. McIntosh, D. Needham, and E. Evans, Biophys. J. 79, 328 (2000).

[100] D. Needham and R. Nunn, Biophys. J. 58, 997 (1990).

[101] H. V. Ly, D. E. Block, and M. L. Longo, Langmuir 18, 8988 (2002).

[102] K. J. Tierney, D. E. Block, and M. L. Longo, Biophys. J. 89, 2481 (2005).

[103] T. Wiseman, S. Williston, J. F. Brandts, and L. N. Lin, Anal. Biochem. 179, 131 (1989).

[104] A. C. Rowat, P. L. Hansen, and J. H. Ipsen, Europhys. Lett. 67, 144 (2004).

[105] A. C. Rowat, J. Brask, T. Sparrman, K. J. Jensen, G. Lindblom, and J. H. Ipsen, Eur. Biophys. J. 33, 300(2004).

[106] R. J. Clarke and C. Lüpfert, Biophys. J. 76, 2614 (1999).

[107] M. Boström, W. Kunz, and B. W. Ninham, Langmuir 21, 2619 (2005).

[108] D. Frenkel and B. Smit, Understanding molecular simulation: From algorithms to applications, 2nd edition, Academic Press, San Diego, 2nd edition, 2002.

[109 L. C. Allen and A. M. Karo, Rev. Mod. Phys. 32, 275 (1960).

[110] M. P. Allen and D. J. Tildesley, Computer Simulation of Liquids, Oxford University Press, Oxford, 1987.

[111] A. D. MacKerell Jr., Computational Biochemistry and Biophysics, chapter 2, pp. 7–38, Marcel Dekker, Inc., New York, 2001.

[112] T. Schlick, Molecular Modeling and Simulation, Springer, New York, 2002.

[113] R. Khare, A. K. Sum, S. K. Nath, and J. de Pablo, J. Phys. Chem. B 108, 10071 (2004).

[114] D. Rigby, Fluid Phase Equilib. 217, 77 (2004).

[115] H. J. C. Berendsen, J. P. M. Postma, W. F. van Gunsteren, A. DiNola, and J. R. Haak, J. Chem. Phys. 81, 3684 (1984).

[116] S. Nose, Molecular Physics 52, 255 (1984).

[117] W. G. Hoover, Phys. Rev. A 31, 1695 (1985).

[118] M. Parrinello and A. Rahman, J. Appl. Phys. 52, 7182 (1981).

[119] O. M. Becker and M. Watanabe, Computational Biochemistry and Biophysics, chapter 3, pp. 39–67, Marcel Dekker, Inc., New York, 2001.

[120] H. J. C. Berendsen, D. van der Spoel, and R. van Drunen, Comp. Phys. Comm. 91, 43 (1995).

[121] E. Lindahl, B. Hess, and D. van der Spoel, J. Mol. Mod. 7, 306 (2001).

[122] T. A. Darden, Computational Biochemistry and Biophysics, chapter 5, Marcel Dekker, Inc., New York, NY, 2001.

[123] D. A. Case, T. E. Cheatham III, T. Darden, H. Gohlke, R. Luo, K. M. Merz Jr., A. Onufriev, C. Simmerling, B. Wang, and R. J. Woods, J. Comp. Chem. 26, 1668 (2005).

[124] I. Vattulainen and M. Karttunen, Handbook of Theoretical and Computational Nanotechnology, chapter 29, American Scientific Publishers, Stevenson Ranch, CA, USA, 2nd edition, 2006.

[125] M. Patra, M. Karttunen, M. T. Hyvönen, E. Falck, and I. Vattulainen, J. Phys. Chem. B 108, 4485 (2004).

[126] E. Falck, M. Patra, M. Karttunen, M. T. Hyvönen, and I. Vattulainen, Biophys. J. 87, 1076 (2004).

[127] S. Ollila, M. T. Hyvönen, and I. Vattulainen, Polyunsaturation in lipid membranes - dynamic properties and lateral pressure profiles, Submitted to J. Phys. Chem. B, 2006.

[128] O. Berger, O. Edholm, and F. Jahnig, Biophys. J. 72, 2002 (1997).

[129] D. P. Tieleman and H. J. C. Berendsen, J. Chem. Phys. 105, 4871 (1996).

[130] H. J. C. Berendsen, J. P. M. Postma, and W. F. van Gunsteren, Intermolecular Forces, Their Origin and Determination, Clarendon Press, Oxford, UK, 1981.

[131] U. Essman, L. Perela, M. L. Berkowitz, H. L. T. Darden, and L. G. Pedersen, J. Chem. Phys. 103, 8577 (1995).

[132] M. Patra, M. Karttunen, M. Hyvönen, E. Falck, P. Lindqvist, and I. Vattulainen, Biophys. J. 84, 3636 (2003).

[133] S. W. Chiu, E. Jakobsson, S. Subramanian, and H. L. Scott, Biophys. J. 77, 2462 (1999).

[134] M. Pasenkiewicz-Gierula, T. R´og, J. Grochowski, P. Serda, R. Czarnecki, T. Librowski, and S. Lochy´nski, Biophys. J. 85, 1428 (2003).

[135] G. Pabst, M. Rappolt, H. Amenitsch, S. Bernstorff, and P. Laggner, Langmuir 16, 8994 (2000).

[136] G. Pabst, M. Rappolt, H. Amenitsch, and P. Laggner, Phys. Rev. E 62, 4000 (2000).

[137] A. N. Dickey and R. Faller, J. Polym. Sci. Part B: Polym. Phys. 43, 1025 (2005).

[138] A. Seelig and J. Seelig, Biochemistry 13, 4839 (1974).

[139] M. Aratono, T. Toyomasu, M. Villeneuve, Y. Uchizono, T. Takiue, K. Motomoura, and N. Ikeda, J. Colloid Interface Sci. 191, 146 (1997).

[140] S. König, W. Pfeiffer, T. Bayerl, D. Richter, and E. Sackmann, J. Phys. (France) 2, 1589 (1992).

[141] U. Essmann and M. L. Berkowitz, Biophys. J. 76, 2081 (1999).

[142] P. F. F. Almeida, W. L. C. Vaz, and T. E. Thompson, Biochemistry 31, 6739 (1992).

[143] E. Falck, M. Patra, M. Karttunen, M. T. Hyvönen, and I. Vattulainen, Biophys. J. 89, 745 (2005).

[144] R. A. Böckmann, A. Hac, T. Heimburg, and H. Grubmüller, Biophys. J. 85, 1647 (2003).

[145] P. B. Moore, C. F. Lopez, and M. Klein, Biophys. J. 81, 2484 (2001).

[146] M. M. Sarasua, K. R. Faught, S. L. Steedman, M. D. Gordin, and M. K. Washington, Alcohol. Clin. Exp. Res. 13, 698 (1989).

[147] E. Lindahl and O. Edholm, J. Chem. Phys. 113, 3882 (2000).

[148] J. Gullingsrud and K. Schulten, preprint submitted to Biophys. J. (2004).

[149] J. Sonne, F. Y. Hansen, and G. H. Peters, J. Chem. Phys. 122, 124903 (2005).

[150] M. Carrillo-Tripp and S. E. Feller, Biochemistry 44,
10164 (2005).

[151] R. S. Cantor, Biophys. J. 80, 2284 (2001).

[152] W. R. Klemm, Alcohol 15, 249 (1998).

[153] W. R. Klemm and H. J. Williams, Alcohol 13, 133 (1996).

[154] P. Westh and C. Trandum, J. Phys. Chem. B 104, 11334 (2000).

[155] R. S. Cantor, Biochemistry 42, 11891 (2003).

[156] P. J. Burke, Encyclopedia of Nanoscience and Nanotechnology, chapter Nanodielectrophoresis: Electronic Nanotweezers, pp. 1–19, American Scientific Publishers, Stevenson Ranch, CA, USA, 2003.

[157] H. A. Pohl, J. Appl. Phys. 22, 869 (1951).

[158] H. Fricke, Phys. Rev. 26, 682 (1925).

[159] I. W. Hamley, Introduction to Soft Matter, John Wiley & Sons, Inc., Chichester, UK, 2000.

[160] P. W. Atkins, Physical Chemistry, Oxford University Press, Oxford, 5 edition, 1994.

[161] T. B. Jones, Electromechanics of particles, Cambridge Univ. Press, Cambridge, 1995.

[162] M. P. Hughes, Nanoelectromechanics in Engineering and Biology, CRC Press, Boca Raton, USA, 2003.

[163] T. Müller, A. Gerardino, T. Schnelle, S. G. Shirley, F. Bordoni, G. D. Gasperis, R. Leoni, and G. Fuhr, J. Phys. D: Appl. Phys. 29, 340 (1996).

[164] G. H. Markx, Y. Huang, X. Zhou, and R. Pethig, Microbiology 140, 585 (1994).

[165] A. Ramos, H. Morgan, N. G. Green, and A. Castellanos, J. Phys. D 31, 2338 (1998).

[166] J. Kadaksham, P. Singh, and N. Aubry, Electrophoresis 26, 3738 (2005).

[167] P. R. C. Gascoyne and J. Vykoukal, Electrophoresis 23, 1973 (2002).

[168] S. Kim and S. J. Karrila, Microhydrodynamics: Principles and selected applications, Butterworth-Heinemann series in Chemical Engineering, Butterworth-Heinemann, 1:st edition, 1991.

[169] S. Wakiya, J. Phys. Soc. Japan 22, 1101 (1967).

[170] E. Swanson, D. C. Teller, and C. de Ha¨en, J. Chem. Phys. 68, 5097 (1978).

[171] E. Swanson, D. C. Teller, and C. de Ha¨en, J. Chem. Phys. 72, 1623 (1980).

[172] J. B. Hubbard and J. F. Douglas, Phy. Rev. E 47, R2983 (1993).

[173] J. F. Douglas, H.-X. Zhou, and J. B. Hubbard, Phys. Rev. E 49, 5319 (1994).

[174] H. Morgan, M. P. Hughes, and N. G. Green, Biophys. J. 77, 516 (1999).

[175] N. G. Green and H. Morgan, J. Phys. D: Appl. Phys. 30, L41 (1997).

[176] N. G. Green and H. Morgan, J. Phys. D: Appl. Phys. 31, L25 (1998).

[177] J. Weber, Phys. Rev. 101, 1620 (1956).

[178] E. Kuusela, Steady-State Sedimentation of Non-Brownian Particles with Finite Reynolds Number, PhD thesis, Helsinki Unviersity of Technology, 2005.

[179] E. Kuusela, J. M. Lahtinen, and T. Ala-Nissila, Phys. Rev. Lett. 90, 094502 (2003).

[180] H. A. Pohl and I. Hawk, Science 152, 647 (1966).

[181] A. Menachery and R. Pethig, IEE Proc. Nanobiotechnol. 152, 145 (2005).

[182] P. R. C. Gascoyne, Cell Dielectric Properties as Diagnostic Markers for Tumor Cell Isolation, chapter 53, pp. 1–4, noidea, 2000.

[183] D. Butler, Nature 386, 535 (1997).

[184] P. Gascoyne, C. Mahidol, M. Ruchirawat, J. Satayavivad, P. Watcharasit, and F. F. Becker, Lab. Chip 2, 70 (2002).

[185] P. Gascoyne, J. Satayavivad, and M. Ruchirawat, Acta Tropica 89, 357 (2004).

[186] P. Marszalek, J. J. Zielinsky, M. Fikus, and T. Y. Tsong, Biophys. J. 59, 982 (1991).

[187] K. Kirk, Physiol. Rev. 81, 495 (2001).

[188] R. H. M. Chan, C. K. M. Fung, and W. J. Li, Nanotechnology 15, S672 (2004).

[189] J. Kim and C. Han, Nanotechnology 16, 2245 (2005).

[190] S. Tuukkanen, A. Kuzyk, J. J. Toppari, V. P. Hytönen, T. Ihalainen, and P. Törmä, Appl. Phys. Lett. 87, 1 (2005).

[191] K. D. Hermanson, S. O. Lumsdon, J. P. Williams, E. W. Kaler, and O. D. Velev, Science 294, 1082 (2001).

[192] D. S. Gray, J. L. Tan, J. Voldman, and C. S. Chen, Biosens. Bioelectr. 19, 1765 (2004).

[193] B. P. Lynch, A. M. Hilton, C. H. Doerge, and G. J. Simpson, Langmuir 21, 1436 (2005).

[194] D. R. Reyes, D. Iossifidis, P. Auroux, and A. Manz, Anal. Chem. 74, 2623 (2002).

[195] X. Wang, X.-B. Wang, and P. R. C. Gascoyne, J. Electrostatics 39, 277 (1997).

[196] T. B. Jones and M. Washizu, J. Electrostat. 37, 121 (1996).

[197] J. D. Jackson, Classical Electrodynamics, John Wiley, New York, 2nd edition, 1975.

[198] L. Benguigui and I. J. Lin, J. Appl. Phys. 53, 1141 (1982).

[199] K. Ratanachoo, P. R. C. Gascoyne, and M. Ruchirawat, Biochim. Biophys. Acta 1564, 449 (2002).

[200] J. P. Huang, M. Karttunen, K. W. Yu, and L. Dong, Phys. Rev. E 67, 021403 (2003).

[201] N. Aubry and P. Singh, Europhys. Lett. 74, 623 (2006).

[202] J. P. Huang, M. Karttunen, K. W. Yu, L. Dong, and G. Q. Gu, Phys. Rev. E 69, 051402 (2004).

[203] K. W. Yu and J. T. K. Wan, Comp. Phys. Comm. 129, 177 (2000).

[204] J. D. Weeks, D. Chandler, and H. C. Andersen, J. Chem. Phys. 54, 5237 (1971).

[205] B. B. Laird and J. L. Skinner, J. Chem. Phys. 90, 3274 (1989).

[206] M. Tanaka and A. Y. Grosberg, Eur. Phys. J. E 7, 371 (2002).

[207] E. Salonen, E. Terama, I. Vattulainen, and M. Karttunen, Eur. Phys. J. E 18, 133 (2005).

[208] I.-C. Yeh and G. Hummer, Biophys. J. 86, 681 (2004).

[209] B. Dunweg and K. Kremer, J. Chem. Phys. 99, 6983 (1993).

[210] M. Hakoda, K. Nakamura, A. Enomoto, and T. Hoshino, J. Chem. Eng. Japan 29, 300 (1996).

[211] N. Flores-Rodriguez, Z. Bryning, and G. H. Markx, IEE Proc. Nanobiotechnol. 152, 137 (2005).

[212] L. J. Yang, P. P. Banada, M. R. Chatni, K. S. Lim, A. K. Bhunia, M. Ladisch, and R. Bashir, Lab. Chip 6, 896 (2006).

[213] X. Liu, J. L. Spencer, A. B. Kaiser, and W. M. Arnold, Curr. Appl. Phys. 6, 427 (2006).

[214] N. Flores-Rodriguez and G. H. Markx, J. Phys. D: Appl. Phys. 39, 3356 (2006).

[215] T. P. Hunt and R. M. Westervelt, Biomed. microdevices 8, 227 (2006).